MONTE CARLO SIMULATIONS OF AMPHIPHILES: A SYSTEMATIC STUDY

MARTIN KENWARD

Monte Carlo Simulations of Amphiphiles: A Systematic Study.

by

© Martin Kenward
B.Sc. Hons.

A thesis submitted to the
School of Graduate Studies
in partial fulfillment of the
requirements for the degree of
Master of Science.

Department of Physics and Physical Oceanography
Memorial University of Newfoundland

February 5, 2001

ST. JOHN'S NEWFOUNDLAND

Abstract

The study of amphiphilic molecules and their behaviour in solution is encompassed in a broad array of disciplines. The utility and prevalence of these molecules in our everyday lives and in a wide array of practical applications have stimulated a great deal of effort to understand their properties. Moreover the interesting behaviour of amphiphilic molecules in solution has received much attention. One specific example is the formation of macromolecular aggregates composed of many amphiphilic molecules and often referred to as micelles.

In this thesis we examine systems of self–assembling amphiphilic molecules using Monte Carlo simulations. Aggregates of amphiphilic molecules in solution are not monodisperse; there is a broad distribution of aggregate sizes. This distribution has characteristic properties and contains information about the free energy of the system and other properties. Qualitative comparisons are made between a predicted form of the aggregate size distribution, a model for the free energy of aggregates and the results from the simulations. Direct comparisons between the Monte Carlo results and results from experiment are not carried out.

We carry out a systematic examination of the aggregation of amphiphiles. This examination is based on a variation of the molecular weight, the temperature (or so–called reduced interaction parameters) and various other parameters. An examination of the aggregate composition, morphology and the critical micelle concentration is also carried out.

Contents

Abstract ii

Acknowledgements vi

List of Abbreviations and Symbols vii

List of Tables ix

List of Figures xv

1 Introduction 1

1.1 An Introduction to Amphiphilic Molecules 1

1.2 Amphiphilic Molecules in Solution 3

1.2.1 The Hydrophobic Effect 6

1.3 Micelles and Other Morphologies 7

1.4 Scope of Thesis 9

2 Statistical Thermodynamics of Self-Assembly 11

2.1 Introduction and Review of Statistical Mechanics 12

2.2 Statistical Mechanics of Clusters 13

2.2.1 Mayer's Cluster Expansion and Cluster Integrals 13

2.3 Physical Clusters and Equilibrium Size Distributions 15
2.4 Modeling the Free energy of Micelle Systems 21
2.4.1 The Goldstein Model 22

3 Monte Carlo: Introduction and Application **27**
3.1 Statistical Mechanics and the Partition Function 27
3.2 The Partition Function: The Monte Carlo Way 28
3.2.1 Simple Sampling 29
3.2.2 Importance Sampling 30
3.3 Autocorrelation Times and Equilibrium 33
3.4 Simulating Self–Assembly: The Monte Carlo Way 36
3.4.1 Amphiphiles: The Coarse–Grained Description 37
3.4.2 The Lattice Model 39
3.4.3 Modeling the Interactions 40
3.5 Monte Carlo Moves 43
3.5.1 Reptation 43
3.5.2 Kink–Filp 44
3.5.3 Crank–Shaft 45
3.5.4 Brownian Motion 45
3.6 Model Autocorrelation Functions and Times 46
3.6.1 Chain Extraction 49
3.6.2 Chain Exchange 50
3.6.3 End–to–End 50
3.6.4 Diffusion 51
3.7 Monte Carlo Simulations: A Practical Algorithm 52

4 A Systematic Study of Self–Assembly **55**

4.1 Introduction to Model Systems of Interest 55

4.1.1 Model Systems: An Overview 56

4.1.2 Relaxation Times and Equilibrium 58

4.2 Micelle Composition 62

4.3 Size Distributions 67

4.3.1 General Discussion 68

4.3.2 Calculated Size Distributions 69

4.4 The Critical Micelle Concentration (CMC) 86

4.4.1 CMC versus Interaction Parameter ϵ_{ts} 88

4.4.2 X_{cmc} versus Chain Length Z_{st} 90

4.5 Aggregate Shape and the Size Distribution 92

4.5.1 Aggregate Shape/Morphology 93

4.5.2 Aggregate Scaling and Density Profiles 107

5 Concluding Remarks **115**

5.1 Review and Further Discussion of Results 115

5.2 Further Studies and Modifications Using This Model 120

Bibliography **122**

Appendix A **A-1**

A.1 Accompanying CD–ROM A-1

A.2 Tables of completed simulations A-1

Acknowledgements

I would like to thank my supervisor Dr. Mark Whitmore for: his skillful help, knowledge and encouragement throughout the course of this work and for helping me refine ideas, which have become the contents of this thesis. I would also like to thank: the school of Graduate Studies, the Department of Physics and Physical Oceanography and Dr. Whitmore for financial support. I also extend my gratitude to those who have helped me in any way throughout the course of my studies.

I also wish to acknowledge the assistance in the way of computing resources made available by the nationwide computing initiative C3.ca Inc. for providing generous assistance in the way of numerous high performance computing sites across the country. Specifically I would like to acknowledge the use of resources at: Memorial University of Newfoundland, Université de Montréal, Université Laval, University of Calgary and the University of Alberta.

List of Abbreviations and Symbols

ε_{ts}	Reduced interaction parameter between tail–group and solvent.
ε_{hs}	Reduced interaction parameter between head–group and solvent.
ε_{th}	Reduced interaction parameter between tail–group and head–group.
Z_s	Total length of the amphiphile (monomer units).
Z_{st}	Length of tail–group of the amphiphile (monomer units).
Z_{sh}	Length of head–group of the amphiphile (monomer units).
N_s	Number of amphiphiles used in simulation.
φ_s	Volume fraction of amphiphile.
$\mathcal{Q}$	Canonical partition function.
Ξ	Grand Canonical partition function.
$\mathcal{H}$	Hamiltonian.
X_{tot}	Total mole fraction of amphiphile.
X_{cmc}	Critical micelle concentration (mole fraction).
X_n	Mole fraction of aggregates of size n.
z	Lattice co–ordination number.
Δ_n	Total free energy of an aggregate of n molecules.
δ_n	Free energy per molecule in an aggregate of size n.
$\langle R_i^2 \rangle^{\frac{1}{2}}$	Average principle radii of gyration in the direction i.

continued overleaf

τ_{max}	Maximum number of relaxation times.
μ_n	Chemical potential of an aggregate of size n.
μ_n°	Standard chemical potential of an aggregate of size n.
α_s	Asphericity parameter.

List of Tables

4.1 Table of simulations contained in this section along with the Figure number in which the size distributions are shown. 70

4.2 Table of scaling parameter d and associated parameters. 114

A.1 Table of completed Monte Carlo simulations for molecules with lengths $4 \leq Z_s \leq 10$. A-2

A.2 Table of completed Monte Carlo simulations for molecules with lengths $10 \leq Z_s \leq 14$. A-3

A.3 Table of completed Monte Carlo simulations for molecules with lengths $14 \leq Z_s \leq 25$. A-4

List of Figures

1.1 Schematic diagram of two typical short chain surfactant molecules. 2

1.1(a) Sodium n–alkyl sulphates. 2

1.1(b) n–alkyl polyoxyethelene ethers. 2

1.2 Phase diagram for a three component system of CTAB, hexanol and water [132]. L_1 denotes a micelle phase (water rich); L_2 denotes an inverse micelle phase (hexanol rich); D and E are lamellar and hexagonal liquid crystalline phase respectively [132]. 4

1.3 Schematic representation of the variation of physical properties of a sodium dodecyl sulphate (SDS) and water solution. (Sodium n–alkyl sulphate with $n = 12$). 5

1.4 Free energy of transfer of hydrocarbons from pure liquid water to pure liquid hydrocarbon for alkanes, alkenes and ω–alkadienes as a function of the number of carbon atoms in the chain (reproduced from Tanford [122]). 7

1.5 Various possible morphologies of aggregates: spheres, cylinders and bilayers. The minimum dimensions of the aggregates are on the order of $2Z_s$. . 8

2.1 Clusters of three particles, corresponding to the terms $f_{1,2}f_{1,3}$, $f_{1,2}f_{2,3}$, $f_{1,3}f_{2,3}$ and $f_{1,2}f_{1,3}f_{2,3}$ respectively. 15

2.2 Diagram of assumed aggregate composition. 22

2.3 Assumed density profile of spherical aggregates in the Goldstein model. . . 23

3.1 Illustration of a typical model coarse grained molecule used in this thesis, with $Z_s = 10$, $Z_{sh} = 4$ and $Z_{st} = 6$, the head– and tail–groups are blue and red respectively. 39

3.2 Illustration of reptation motion. 44

3.3 Illustration of kink–flip motion. 44

3.4 Illustration of crank–shaft motion. 45

3.5 Illustration of Brownian motion. 46

3.6 Two possible mechanisms for micelle growth. 48

4.1 Schematic phase diagram for a dilute solution of amphiphiles and solvent. (Reproduced from DeGiorgio [17]). 57

4.2 Logarithm of the diffusion and autocorrelation time(s) for a h_2 system of $N_s = 2000$ symmetric molecules with $Z_s = 14$, $Z_{sh} = Z_{st} = 7$ and a volume fraction of $\phi_s = 2.50\%$. 59

4.3 Logarithm of the diffusion and autocorrelation time(s) for a h_2 system of $N_s = 2000$ asymmetric molecules of length $Z_s = 5$, $Z_{st} = 3$ and a total volume fraction of $\phi_s = 5.14\%$. 60

4.4 Snapshot from simulation for a system with $N_s = 2000$, $Z_s = 18$, $Z_{sh} = 4$, $Z_{st} = 14$ and $\phi_s = 4.9\%$. The unit of length is equal to a bond length. . . . 64

4.5 Directionally averaged density profiles and related distributions for a h_1 system with $N_s = 2000$, $Z_s = 18$, $Z_{sh} = 4$, $Z_{st} = 14$ and $\phi_s = 4.9\%$ for aggregates in the range of 69 to 83 molecules per aggregate and for $\varepsilon_{ts} = 0.45$. This is the same system as in Figure 4.4. The unit of length is equal to a bond length. 65

4.6 Directionally averaged density profiles and related distributions for a h_2 system with $N_s = 1000$, $Z_s = 14$, $Z_{st} = Z_{sh} = 7$ and $\phi_s = 2.5\%$ for aggregates in the range of 35 to 40 molecules per aggregate and for $\varepsilon_{ts} = 0.75$. The unit of length is equal to a bond length. 66

4.7 Size distribution, X_n, and free energy, δ_n, for a h_2 system with $N_s = 2000$ molecules with $Z_s = 5, Z_{st} = 3$ and a total volume fraction of $\phi_s = 5.14\%$. The size distributions correspond to the unfilled symbols and the free energy corresponds to the filled symbols. 69

4.8 Aggregate size distributions for a h_2 system with $N_s = 2000, Z_s = 5, Z_{st} = 3, Z_{sh} = 2$ and a total volume fraction of $\phi_s = 5.14\%$. 71

4.9 Surface aggregate size distribution for a system with $N_s = 2000$, $Z_s = 5, Z_{st} = 3, Z_{sh} = 2$ and a total volume fraction of $\phi_s = 5.14\%$. 72

4.10 Fitted curves for a h_2 system with $N_s = 2000$ molecules with $Z_s = 5, Z_{st} = 3$ and a total volume fraction of $\phi_s = 5.14\%$ 73

4.11 Variation of fitting parameters α, ξ and η with the interaction parameter ε_{ts}. This corresponds to the same system as in Figure 4.10. 74

4.12 Aggregate size distribution and fitted curves for a h_2 system with $N_s = 1000$ molecules with $Z_s = 6, Z_{st} = 4, \tau_{max} = 150$ and $\phi_s = 2.51\%$. 75

4.13 Aggregate size distributions and fitted curves for a h_1 system of 1000 molecules with $Z_s = 6, Z_{st} = 4$ and $\phi_s = 9.37\%$. 77

4.14 Aggregate size distributions and fitted curves for a h_2 system of $N_s = 1000$ molecules with $Z_s = 6, Z_{st} = 3$ and $\phi_s = 2.52\%$. 78

4.15 Snapshot of simulation for system with 1000 molecules with $Z_s = 6, Z_{st} = 3$, at $\varepsilon_{ts} = 1.10$ and a total volume fraction of $\phi_s = 2.52\%$. 79

4.16 Aggregate size distributions and fitted curves for a h_2 system of 500 molecules with $Z_s = 7, Z_{st} = 5$ and $\phi_s = 5.46\%$. 80

4.17 Aggregate size distribution and fitted curves for a h_1 system with N_s = 1000 molecules with $Z_s = 8, Z_{st} = 4$ and $\phi_s = 4.56\%$. 81

4.18 Non–micellar aggregate size distribution for a h_1 system of 1000 molecules with $Z_s = 10$, $Z_{st} = 2$ and $\phi_s = 8.00\%$. 82

4.19 Aggregate size distributions and fitted curves for a h_1 system of 1000 molecules with $Z_s = 15$, $Z_{st} = 10$, $\tau_{max} = 60$ and $\phi_s = 4.73\%$. 83

4.20 Aggregate size distributions and fitted curves for a h_2 system of 1000 molecules with $Z_s = 16$, $Z_{st} = 12$ and $\phi_s = 3.79\%$. 84

4.21 Aggregate size distributions and fitted curves for a h_2 system of $N_s = 1000$ molecules with $Z_s = 20, Z_{st} = 15$ and $\phi_s = 2.56\%$. 85

4.22 Logarithm of X_{cmc} as a function of ε_{ts} for molecules with $5 \leq Z_s \leq 9$ and various values of Z_{st} and Z_{sh}. The lines are shown as a guide to the eye. . 89

4.23 Logarithm of X_{cmc} as a function of ε_{ts} for molecules with lengths $Z_s = 10$ and various values of Z_{st}. 90

4.24 Logarithm of the CMC as a function of ε_{ts} for molecules in the range $11 \leq Z_s \leq 22$ with various values of Z_{st}. 91

4.25 Plot of the logarithm of X_{cmc} versus Z_{st}. 92

4.26 The shape distribution and asphericity parameter for a h_2 system with 2000 molecules of length $Z_s = 5, Z_{st} = 3$ and $\phi_s = 5.14\%$. 98

4.26(a) Principal radii of gyration versus aggregation number and Gaussian fit to distribution. 98

4.26(b) Asphericity parameter α_s versus aggregation number. 98

4.27 Gaussian + matching function fits using Eqn. (4.21) for a h_2 system with 2000 molecules of length $Z_s = 5, Z_{st} = 3$ and $\phi_s = 5.14\%$. 99

4.28 Variation of the peak in the aggregate size distribution as a function of the interaction parameter ε_{ts}. This is the same system as depicted in Figure 4.27. 100

4.29 Principal radii of gyration (for $\varepsilon_{ts} = 0.95$) and the aggregate size distributions for a h_1 system with $N_s = 1000$ molecules with $Z_s = 6$, $Z_{st} = 4$ and $\phi_s = 9.37\%$ 101

4.30 Gaussian + matching function fit to the distributions for a h_1 system of $N_s = 1000$ molecules with $Z_s = 6$, $Z_{st} = 4$ and a volume fraction of $\phi_s = 9.37\%$ 102

4.31 The principal radii, asphericity parameter and aggregate size distribution for a h_1 system of 1000 molecules with $Z_s = 10$, $Z_{st} = 6$, $\varepsilon_{ts} = 0.70$ and $\phi_s = 2.46\%$. 103

4.31(a) Principal radii of gyration versus aggregation number 103

4.31(b) Asphericity parameter α_s versus aggregation number 103

4.32 Gaussian + matching function fit to the distributions for a system of $N_s = 1000$ molecules with with $Z_s = 10$, $Z_{st} = 6$ and a volume fraction of $\phi_s = 2.46\%$ 104

4.33 The principal radii, asphericity and distributions for a h_2 system of $N_s = 2000$ molecules with $Z_s = 10$, $Z_{st} = 8$ and $\phi_s = 2.74$. 105

4.33(a) Principal radii for $\varepsilon_{ts} = 0.60$ and Gaussian + matching function fits to the distributions as functions of n. 105

4.33(b) Asphericity parameter versus aggregation number for $\varepsilon_{ts} = 0.60$. 105

4.34 Variation of the Gaussian peak in the distribution as a function of the interaction parameter ε_{ts} for a wide range of Z_s. 106

4.35 Log–log plot of R^2_{mean} as a function of n for a h_2 system of 2000 molecules with $Z_s = 5, Z_{st} = 3$ at a total volume fraction of $\phi_s = 5.14\%$. The unit of length is equal to the lattice constant. 108

4.36 Log–log plot of R^2_{mean} versus n for a h_2 system of 1000 molecules with $Z_s = 6$, $Z_{st} = 3$ and a volume fraction of $\phi_s = 2.52\%$. The unit of length is equal to the lattice constant. 109

4.37 Log–log plot of R^2_{mean} versus n for a h_2 system of 1000 molecules with $Z_s = 14$, $Z_{st} = 10$ and a volume fraction of $\phi_s = 2.72\%$. The unit of length is equal to the lattice constant. 110

4.38 Schematic behaviour of the model density profile in Eqn. (4.28) for some typical values of a and l. 111

4.39 Log–log plot of the squared radius of gyration as a function of the aggregation number n for value of $a = 1..2$ with $l = 0.2$. The slope of this line is approximately 0.50. 112

4.40 Behaviour of the density profile as a function of the parameter a with $l = 0.408$ corresponding to the system in Figure 4.6. Increasing a corresponds to increasing n. 113

Chapter 1

Introduction

"To accomplish great things, we must not only act, but also dream;

not only plan, but also believe."

Anatole France.

This chapter is devoted to a discussion of amphiphilic molecules, their composition, properties in solution and the methods used to study them. Amphiphilic molecules are studied in a broad range of disciplines including Physics, Chemistry and Chemical Engineering. These molecules exhibit a variety of behaviour in solution and have many desirable properties; for these reasons their study is currently an active field of research. In this thesis a systematic examination of the aggregation of amphiphilic molecules based on the variation of temperature/interactions, molecular weight and other properties is carried out.

1.1 An Introduction to Amphiphilic Molecules

The term amphiphilic originates from the Greek words "amphi" meaning of both kinds and "philos" meaning strong affinity or attraction. Webster's Online Dictionary [131] defines amphiphilic as:

amphiphilic: *(adj): circa* 1950: *of, relating to, or being a compound (as a surfactant) consisting of molecules having a (typically polar) water–soluble group attached to (a) water–insoluble hydrocarbon chain(s); also: being a molecule of such a compound.*

Hence, amphiphilic[1] has come to describe molecules composed of two distinct sections which exhibit opposing behaviour in solution. Typically one section is "hydrophobic" (water disliking) and referred to as the tail–group of the molecule. The second section is typically "hydrophilic" (water liking) and referred to as the head–group of the molecule. For brevity, the term amphiphile(s) will be used throughout this thesis to denote (an) amphiphilic molecule(s).

The typical composition of amphiphiles is the following: the tail–group is composed of one or more linear hydrocarbon chains (repeated CH_2's terminating in a CH_3) and the head–group is either an ionic or nonionic species. Although amphiphiles can have a wide variety of compositions the discussion here will be restricted to relatively short single chain amphiphiles. The model molecules studied in this thesis are most often compared with sodium n–alkyl sulphates and n–alkyl polyoxyethelene ethers [10, 105]. These molecules are depicted in Figure 1.1 and differ only in the composition of their head–groups.

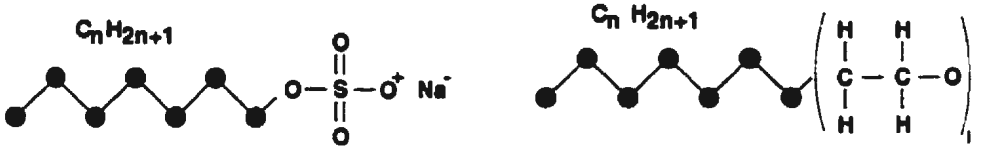

(a) Sodium n–alkyl sulphates. (b) n–alkyl polyoxyethelene ethers.

Figure 1.1: Schematic diagram of two typical short chain surfactant molecules.

Amphiphilic molecules can behave as surfactants, i.e., surface active agents. At very

[1]Evidently it was G. S. Hartley in 1936 [34] who first proposed the term *amphipathy* to describe these types of molecules to later be replaced by *amphiphiles*.

low concentrations they locate themselves at an air/water interface such that the tails lie above the water and the heads protrude into the water [26, 122]. As the concentration is increased the surface layer becomes saturated and the remaining molecules go preferentially into the bulk solvent [122, 26].

The available literature on amphiphiles is voluminous, some classic works can be found in references [8, 12, 14, 17, 22, 23, 26, 29, 34, 43, 49, 53, 58, 59, 76, 90, 122, 132, 134, 137]. Amphiphiles are found in many facets our everyday lives in the form of plastics, synthetic materials, detergents and cellular structures. The wide use, applicability and complex behaviour of amphiphiles have stimulated a great deal of effort to investigate their behaviour and properties.

One of the first studies of amphiphilic aggregation proper was carried out by Hartley [34] in a classic 1936 paper on the "Aqueous Behaviour of Paraffin Chain Salts". Hartley was also the first to suggest that aggregates formed by these molecules at low concentrations are spherical and coined the term 'micelle' meaning 'small bit' to describe them [34]. McBain [73] is accredited with first identifying these molecules as being composed of distinct opposing sections, i.e., a hydrophobic and hydrophilic section.

These early pioneering studies broke the ground for further examinations of amphiphilic systems. Although much knowledge has been gained about the behaviour and properties of amphiphiles, their study still comprises an active field of research. Many properties of these systems are still not well understood, including the morphology and morphological transitions of aggregates.

1.2 Amphiphilic Molecules in Solution

Amphiphiles, being simultaneously hydrophobic and hydrophilic, tend to exhibit ambivalent behaviour in solution. As a result, they adopt unique orientations, often assembling

to a decrease in entropy associated with the reordering of the water molecules. For other hydrocarbons the entropic contribution is much larger [122]. The free energy of transfer for many hydrocarbons is roughly proportional to the surface area of the molecules [42, 122].

There is a distinct dependence on the immiscibility of a hydrocarbon chain on its length, i.e., the number of carbons in the chain. Figure 1.4 shows a plot of the free energy of transfer $\mu_{HC} - \mu_W$ of several hydrocarbons from pure liquid water to pure liquid hydrocarbon at 25°C. The free energy of transfer has roughly a linear dependence on the number of carbon atoms in the chain. For more thorough discussions of the hydrophobic effect, the reader is asked to consult [42, 122].

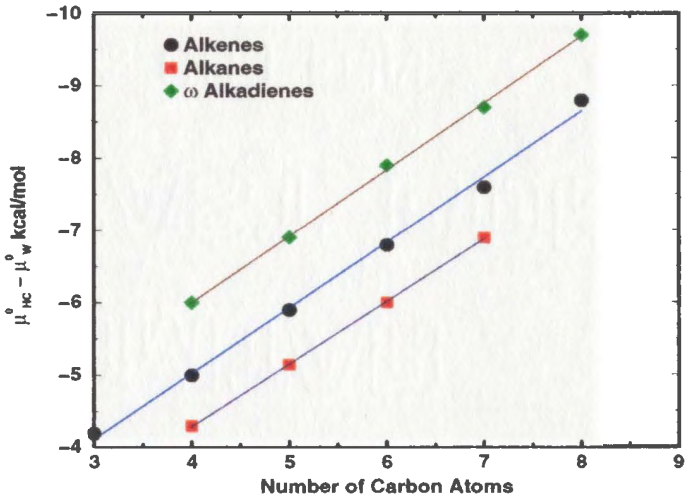

Figure 1.4: Free energy of transfer of hydrocarbons from pure liquid water to pure liquid hydrocarbon for alkanes, alkenes and ω–alkadienes as a function of the number of carbon atoms in the chain (reproduced from Tanford [122]).

1.3 Micelles and Other Morphologies

The morphology of an aggregate depends on many factors including the length of the amphiphile, number of tails, composition of the head–group, temperature, interactions and

The formation of aggregates is normally characterized by a relatively sharp transition in the observable properties of a system as a function of amphiphile concentration. This behaviour was originally observed by McBain [73] who studied the anomalous concentration dependence of the physical properties of soap (surfactant) solutions. Figure 1.3 shows a plot of various observables as a function of concentration. The vertical axis does not show any units or scale since it is only the qualitative behaviour of the various observables that is of interest. The CMC denotes the critical micelle concentration, i.e., the total amphiphile concentration at which micellization begins[2]. The onset of micellization also has a distinct temperature dependence.

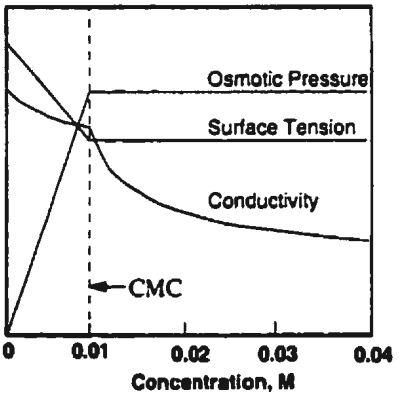

Figure 1.3: Schematic representation of the variation of physical properties of a sodium dodecyl sulphate (SDS) and water solution. (Sodium n–alkyl sulphate with $n = 12$).

Debye [16] was one of the first to report light scattering experiments which examined the variation of the weight average aggregation number as a function of concentration. These results indicated a strong correlation between the weight average aggregation number and concentration [16]. This in turn suggests a significant growth of each aggregate as a function of the concentration. Similar behaviour is observed as a function of temperature.

[2]The phrase 'critical micelle concentration' is somewhat of a misnomer since it does not correspond to a critical concentration of micelles; rather, it is a critical value of the total concentration.

The main driving force behind aggregation is the reduction in unfavourable solvent tail–group contacts. As a result, amphiphiles assemble themselves so as to minimize tail–solvent contact. The hydrophobic effect is the same effect which accounts for the low solubility of oil in water. The next section contains a brief description of the main properties of the hydrophobic effect.

1.2.1 The Hydrophobic Effect

McBain [73] originally attributed the association of hydrocarbon chains in water to a like–like attraction of the chains. The true nature of the hydrophobic effect is not a manifestation of a like–like attraction of hydrocarbons; rather, it is due mainly to the unique nature of water and its affinity to participate in hydrogen bonding [122]. It was Traube [125] who first qualitatively understood the true nature of the hydrophobic effect.

The hydrophobic effect results from the fact that bulk water is arranged such that each molecule participates on average in 3 to 3.5 hydrogen bonds [42, 122]. When a nonpolar solute (such as a hydrocarbon chain) is introduced into the water matrix the hydrogen bonding is disrupted. This forces the reorientation of the water molecules around the solute so as to maximize the number of hydrogen bonds, this is highly entropically unfavourable. This results in a low solubility of most nonpolar substances including hydrocarbons and fluorocarbons.

To illustrate this, consider the free energies of transfer of methane and n–butane to bulk water at 25°C which is about 14.5 kJ/mol and 24.5 kJ/mol respectively [42]. For n–butane this is divided as follows:

$$\Delta G = \Delta H - T\Delta S = -4.3 + 28.7 = +24.4 \text{ kJ/mol} \tag{1.1}$$

where ΔG, ΔH and ΔS correspond to the change in the Gibbs free energy, Helmholtz free energy and the entropy respectively. The low solubility of hydrocarbons is attributed

to a decrease in entropy associated with the reordering of the water molecules. For other hydrocarbons the entropic contribution is much larger [122]. The free energy of transfer for many hydrocarbons is roughly proportional to the surface area of the molecules [42, 122].

There is a distinct dependence on the immiscibility of a hydrocarbon chain on its length, i.e., the number of carbons in the chain. Figure 1.4 shows a plot of the free energy of transfer $\mu_{HC} - \mu_W$ of several hydrocarbons from pure liquid water to pure liquid hydrocarbon at 25°C. The free energy of transfer has roughly a linear dependence on the number of carbon atoms in the chain. For more thorough discussions of the hydrophobic effect, the reader is asked to consult [42, 122].

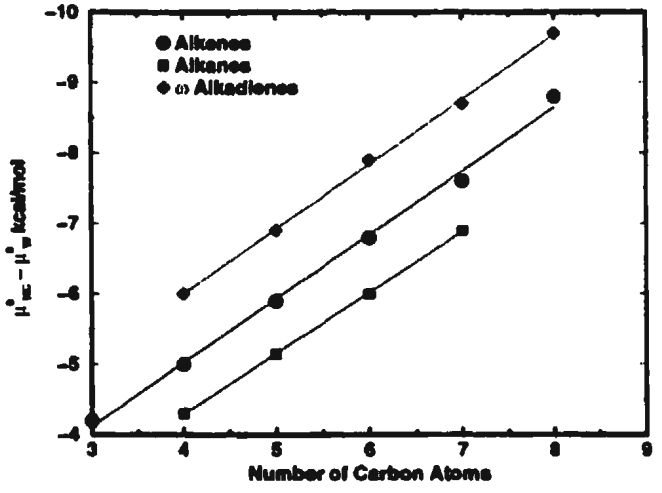

Figure 1.4: Free energy of transfer of hydrocarbons from pure liquid water to pure liquid hydrocarbon for alkanes, alkenes and ω–alkadienes as a function of the number of carbon atoms in the chain (reproduced from Tanford [122]).

1.3 Micelles and Other Morphologies

The morphology of an aggregate depends on many factors including the length of the amphiphile, number of tails, composition of the head–group, temperature, interactions and

total amphiphile concentration. There is a delicate balance between these factors which determines the morphology of the aggregate. Figure 1.5 illustrates three basic morphologies. There are many more exotic structures which can be formed; however, these are the simplest and easiest (geometrically) to examine [26, 42].

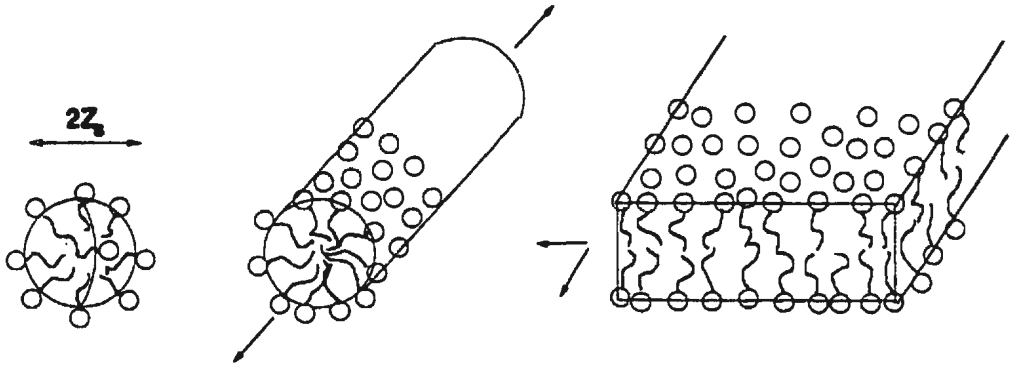

Figure 1.5: Various possible morphologies of aggregates: spheres, cylinders and bilayers. The minimum dimensions of the aggregates are on the order of $2Z_s$.

There is one important geometrical constraint on aggregates (under the proviso that there is negligible solvent penetration into the interior of the aggregates): one dimension of the aggregate cannot exceed $2Z_s$, where Z_s is the fully stretched length of the amphiphile. For a spherical micelle all three dimensions are on the order of Z_s whereas for an infinite cylinder two dimensions are on the order of Z_s and the other can be much larger than Z_s.

Systems of single chain amphiphiles at low concentrations typically assemble into spherical micelles, whereas amphiphiles with two parallel tail–chains such as lecithins tend to form lamellar structures or vesicles [8, 132]. Micellar shape is notoriously difficult to examine experimentally and there is still some debate as to the exact shape of aggregates under various conditions [26, 122, 132]. X–ray and light scattering techniques are often used to examine the shape of aggregates [26, 132]. The transition between different morphologies in some instances is still not well understood although some recent studies have

given some insight into these transitions [21, 26]. The growth and morphological transition of aggregates is most likely driven by one of several mechanisms as suggested by Eisenberg [21], the first being the favourable transfer of free molecules into aggregates and the second being the merger of two aggregates to form a compound aggregate.

The *a priori* assumed aggregate shape in the calculation of the free energy of the micelle systems is spherical because it allows a simple geometric interpretation and calculation of the free energy. The results from our Monte Carlo simulations suggest that aggregates are not perfect spheres but rather prolate spheroids with increasing eccentricity as a function of aggregation number. The results from the simulations can also be used to examine the morphological transition of aggregates.

Aggregates of amphiphiles in solution can exhibit a broad range of aggregate sizes, i.e., they are polydisperse, there is a continual exchange of amphiphiles with one another and with free amphiphiles in solution. As a result, micelles do not have a static identity. In order to describe micellar systems it is necessary to examine this characteristic distribution of aggregate sizes. This distribution is a sensitive function of solution conditions, amphiphile concentration and temperature.

From a theoretical perspective, treating micellar systems is quite challenging. There are many approaches used to examine these systems including self–consistent field theories [2, 31, 35, 40, 67, 68, 84, 96, 134], integral equation techniques [47, 52, 55, 69] and various other statistical mechanical approaches [8, 12, 14, 17, 42, 49, 75, 120].

1.4 Scope of Thesis

In this thesis, a combination of statistical mechanical methods and Monte Carlo simulations are used to examine the properties of aggregates including the characteristic aggregate size distribution and the critical micelle concentration. A systematic examination of the ag-

gregation of amphiphilic molecules using Monte Carlo simulations is carried out. This systematic study includes variations of molecular weight and temperature. Using these simulations, it is possible to examine the characteristic aggregate size distribution: moreover, it is possible to make qualitative comparisons between the results from the Monte Carlo simulations and a phenomenological model for the free energy of aggregates and for the predicted aggregate size distribution. The critical micelle concentration is also examined as functions of the length of the molecules and temperature.

An examination of the shape/morphology of aggregates is carried out. The results from the Monte Carlo simulations suggest that the shape of the aggregates depends quite markedly on temperature, total amphiphile concentration and amphiphile composition. A thorough examination of the interior composition of the aggregates in terms of their density profiles is also included. The scaling of the dimensions of the aggregates as a function of the aggregation number is also carried out, this leads to an interpretation of the behaviour of the density profiles as a function of the aggregation number.

Chapter 2

Statistical Thermodynamics of Self–Assembly

"Everything has beauty, but not everyone sees it."

Confucius

This chapter provides a description of aggregation from a statistical mechanical perspective. It includes a discussion of systems of fully interacting molecules based on the general formalism of Hill [36]. The main result will be the derivation of the characteristic aggregate size distribution (in the grand canonical ensemble) for a system of noninteracting clusters of molecules based on Hill's formalism [36]. This result provides the basis for comparison with the distribution of aggregate sizes obtained using the Monte Carlo simulations. A discussion of the Mayer cluster expansion is also included for illustrative purposes [36, 83]. The last section is devoted to a discussion and generalization of a phenomenological model for the free energy of aggregates originally derived by Goldstein for symmetric di–block amphiphiles [28].

2.1 Introduction and Review of Statistical Mechanics

This chapter begins with a very brief review of statistical mechanics. For more thorough reviews, the reader cannot do better than consult the following classic works [36, 64, 65, 106, 107, 123, 124]. This section is meant to review in short form some important concepts that will be used throughout this chapter.

Consider a system of N identical interacting particles in a volume V at a temperature T. The canonical partition function $\mathcal{Q}$ for this system is

$$\mathcal{Q} = \frac{1}{h^{3N}N!}\int d\Omega \exp(-\beta\mathcal{H}(\vec{\mathbf{x}}^N, \vec{\mathbf{p}}^N)) \tag{2.1}$$

where $d\Omega = d^N\vec{\mathbf{x}}d^N\vec{\mathbf{p}}$ and corresponds to an infinitesimal volume of the phase space for the system of N particles [1]. Assume that the Hamiltonian $\mathcal{H}$ has the form

$$\mathcal{H}(\vec{\mathbf{x}}^N, \vec{\mathbf{p}}^N) = \sum_{i=1}^{N}\frac{\vec{\mathbf{p}}_i^2}{2m} + V(\vec{\mathbf{x}}^N) \tag{2.2}$$

where $\vec{\mathbf{p}}_i$ is the momentum of an individual particle and $V(\vec{\mathbf{x}}^N)$ is the potential energy associated with a given configuration of the system.

With the Hamiltonian as defined in Eqn. (2.2) the integrals over momentum space are easily carried out and the partition function can be written as

$$\mathcal{Q} = \frac{1}{\Gamma^{3N}N!}\int d^N\vec{\mathbf{x}} \exp(-\beta V(\vec{\mathbf{x}}^N)) = \frac{\mathcal{Z}}{N!\Gamma^{3N}}, \tag{2.3}$$

where $\Gamma = \hbar/(2m\pi k_B T)^{\frac{1}{2}}$ and is referred to as the thermal wavelength, m is the mass of an individual particle, T is the thermodynamic temperature and $\hbar$ is Planck's constant divided by 2π. $\mathcal{Z}$ is the so–called configurational partition function and is defined as

$$\mathcal{Z} = \int d^N\vec{\mathbf{x}} \exp(-\beta V(\vec{\mathbf{x}}^N)) \tag{2.4}$$

[1] It should be noted that $\beta = \frac{1}{k_B T}$, where k_B is the Boltzmann constant and T is the thermodynamic temperature.

From the partition function it is then possible to calculate various properties of the system. One such property is the Helmholtz free energy $\mathcal{F}$ defined as

$$\mathcal{F} = -k_B T \ln(\mathcal{Q}) \tag{2.5}$$

It is also possible to calculate other quantities such as the chemical potential μ and the entropy $\mathcal{S}$ from the partition function. All intermolecular interactions and clusters of molecules are implicitly included in the partition function in Eqn. (2.3). It is convenient to rewrite the partition function in Eqn. (2.4) directly in terms of contributions from clusters.

2.2 Statistical Mechanics of Clusters

Two methods of including contributions from clusters in the partition function for a system are Mayer's cluster expansion [36, 83, 106] and the formalism developed by Hill [36, 37]. Both methods lead to representations of the partition function in terms of so–called aggregate partition functions. The method of Hill [37] is a formal but exact method of treating physical clusters and leads to a compact and elegant description of aggregates. Mayer's cluster expansion leads to a description of mathematical clusters whereas Hill's treatment leads to a description of physical clusters.

2.2.1 Mayer's Cluster Expansion and Cluster Integrals

This section focuses on Mayer's explicit representation of clusters in terms of the so–called aggregate (or cluster) partition functions [36, 83]. For a more complete derivation the reader is asked to consult [36, 83, 106]. This method is limited since it leads to a description of mathematical clusters and not true physical clusters and is limited to small molecules interacting via two body interactions; however, it does illustrate some important concepts.

Consider again the system as discussed in the first section of this chapter, N identical interacting particles in a volume V at temperature T. It is assumed that for small particles the potential energy $V(\vec{\mathbf{x}}_1, \ldots \vec{\mathbf{x}}_N)$ can be written as a sum of pair potentials such that

$$V(\vec{\mathbf{x}}_1, \ldots \vec{\mathbf{x}}_N) = \sum_{1 \le i < j \le N} u(r_{ij}) \tag{2.6}$$

where $u(r_{ij})$ is the interaction potential between two particles i and j as a function of the distance r_{ij} between them. It is useful to introduce the function f_{ij} defined as

$$f_{ij} = e^{-u(r_{ij})\beta} - 1 \tag{2.7}$$

It is then possible to write the integrand of the partition function in Eqn. (2.3) as

$$\exp(-V(\vec{\mathbf{x}}_1, \ldots \vec{\mathbf{x}}_N)\beta) = \prod_{1 \le i < j \le N} (1 + f_{ij}) \tag{2.8}$$

The products in the above equation can then be written as

$$\exp(-V(\vec{\mathbf{x}}_1, \ldots \vec{\mathbf{x}}_N)\beta) = 1 + \sum_{1 \le i < j \le N} f_{ij} + \sum_{1 \le i < j \le N} \sum_{1 \le k < l \le N} f_{ij} f_{kl} + \ldots \tag{2.9}$$

The above expression is often referred to as the cluster expansion. If the particles are treated as noninteracting, i.e., $u(r_{ij}) = 0$ and $f_{ij} = 0 \ \forall \ i, j$, then the configurational integral can be evaluated trivially. This corresponds to treating the system as an ideal gas.

In order to interpret the cluster expansion it is useful to consider a diagram which depicts the various possible clusters in terms of the f_{ij}'s. Figure 2.1 shows a representation of all possible clusters of three particles. A cluster is any two or more particles that are connected as in the cluster diagram.

It is useful to introduce the cluster sums $S_{i,j,k,\ldots}$ defined as the sum of all terms f_{ij} in which particles $i, j, k, \ldots$ are connected. For clusters of three particles the cluster sum $S_{1,2,3}$ is

$$S_{1,2,3} = f_{1,2} f_{1,3} + f_{1,2} f_{2,3} + f_{1,3} f_{2,3} + f_{1,2} f_{1,3} f_{2,3} \tag{2.10}$$

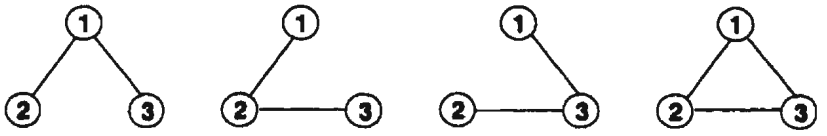

Figure 2.1: Clusters of three particles, corresponding to the terms $f_{1,2}f_{1,3}$, $f_{1,2}f_{2,3}$, $f_{1,3}f_{2,3}$ and $f_{1,2}f_{1,3}f_{2,3}$ respectively.

The cluster integrals q_j [36] are defined as

$$q_j = \frac{1}{j!V}\int\cdots\int S_{1,2,3,\ldots j}d\vec{\mathbf{x}}_1\ldots d\vec{\mathbf{x}}_j \tag{2.11}$$

where j is the size of the cluster, i.e., the number of particles in the cluster. It is possible to rewrite the total partition function in Eqn. (2.1) for the system in terms of these cluster partition functions [83, 106]. This leads to an interpretation of mathematical clusters [83, 36]. In the next section we examine a method to obtain an expression for the distribution of physical clusters in terms of cluster partition functions.

2.3 Physical Clusters and Equilibrium Size Distributions

This section describes a formal approach to obtain the equilibrium size distribution. This method was first suggested by Hill [36, 37] and leads to a formal but exact description of physical clusters unlike the mathematical clusters which result from Mayer's cluster expansion. This method will allow the calculation of the equilibrium numbers of clusters.

Consider a system composed of N molecules in a volume V at temperature T. The grand canonical partition function for this system is

$$\Xi = \sum_{N\geq 0} \mathcal{Q}_N \lambda^N \tag{2.12}$$

where $\lambda = e^{\mu\beta}$ is defined as the absolute activity and μ is the chemical potential of a single molecule.

Intermolecular interactions and clusters of molecules are implicitly represented in the partition function. To facilitate an explicit discussion of clusters it is necessary to write the partition function in Eqn. (2.12) in terms of so called aggregate (or cluster) partition functions similar to those of the last section. The method in this section is general and can be applied to any physical system of interest. Consider the system to be composed of N_n clusters of size n. It is then possible to rewrite the partition function as

$$\Xi = \sum_{\{\mathbf{N}\}} \left(\prod_n \lambda_n^{N_n} \right) \mathcal{Q}_{\{\mathbf{N}\}} \tag{2.13}$$

where $\{\mathbf{N}\} = N_1, N_2, \ldots$ and denotes a set of clusters such that $\sum_{n=1}^{\infty} nN_n = N$. The partition function $\mathcal{Q}_{\{\mathbf{N}\}}$ is defined as the partition function of the set of clusters $\{\mathbf{N}\}$. N_n is the number of clusters of size n and λ_n is the absolute activity of a cluster of size n such that

$$\lambda_n = \exp(\mu_n \beta) \tag{2.14}$$

where μ_n is defined as the chemical potential of an aggregate of n molecules. The N_n's of this section will be seen to correspond to actual physical cluster numbers and, in fact, it will possible to obtain the actual equilibrium number of physical clusters. Since these clusters are in equilibrium with each other the chemical potentials must satisfy

$$\mu_n = n\mu_1 \quad \rightarrow \quad \lambda_n = \lambda_1^n \qquad n = 1, 2, 3, \ldots \tag{2.15}$$

Using this relationship it is possible to write the total partition function for the system as

$$\Xi = \sum_{\{\mathbf{N}\}} \lambda_1^{\sum_n nN_n} \mathcal{Q}_{\{\mathbf{N}\}} \tag{2.16}$$

The partition function in Eqn. (2.16) is an explicit representation of physical clusters of molecules. The implicit representation in Eqn. (2.12) and the explicit representation in

Eqn. (2.16) must be identical so that

$$\begin{aligned} \Xi &= \sum_{N\geq 0} \mathcal{Q}_N \lambda^N \\ &= \sum_{\{\mathbf{N}\}} \lambda_1^{\sum_n n N_n} \mathcal{Q}_{\{\mathbf{N}\}} \end{aligned} \tag{2.17}$$

and it is possible to write

$$\begin{aligned} \Xi &= 1 + \lambda \mathcal{Q}_1 + \lambda^2 \mathcal{Q}_2 + \dots \\ &= 1 + \lambda_1 \mathcal{Q}_{100\dots} + \lambda_1^2 \mathcal{Q}_{200\dots} + \lambda_2 \mathcal{Q}_{010\dots} + \dots \end{aligned} \tag{2.18}$$

The partition functions can then be written as

$$\begin{aligned} \mathcal{Q}_1 &= \mathcal{Q}_{100\dots} \\ \mathcal{Q}_2 &= \mathcal{Q}_{200\dots} + \mathcal{Q}_{010\dots} \\ \mathcal{Q}_3 &= \mathcal{Q}_{300\dots} + \mathcal{Q}_{110\dots} + \mathcal{Q}_{001\dots} \\ \vdots &= \vdots \end{aligned} \tag{2.19}$$

where the aggregate partition functions $\mathcal{Q}_{ijk\dots}$ refer to the partition function for i aggregates of size 1, j aggregates of size 2, k aggregates of size 3 and so forth.

Using this representation of the partition function, it is possible to derive an expression for the distribution of aggregate sizes. The equilibrium number of clusters $\bar{N}_n$ of size n can be obtained from the basic thermodynamic relationship

$$\bar{N}_n = \lambda_n \frac{\partial \ln \Xi}{\partial \lambda_n} \tag{2.20}$$

Using $\lambda_n = \lambda^n$, i.e., $\lambda_1 = \lambda, \lambda_2 = \lambda^2, \dots$ the equilibrium numbers of clusters $\bar{N}_n$ are

$$\begin{aligned} \bar{N}_1 &= \lambda \mathcal{Q}_{100\dots} + \lambda^2 (2\mathcal{Q}_{200\dots} - \mathcal{Q}_{100\dots}^2) + \dots \\ \vdots &= \vdots \qquad\qquad \vdots \\ \bar{N}_n &= \lambda^n \mathcal{Q}_{000\dots1} + \lambda^{n+1} (\mathcal{Q}_{100\dots1} - \mathcal{Q}_{100\dots}\mathcal{Q}_{000\dots1}) + \dots \end{aligned} \tag{2.21}$$

The equilibrium quotients of aggregates can then be written as

$$\frac{\bar{N}_1^n}{\bar{N}_n} = \frac{\mathcal{Q}_{100\ldots}^n}{\mathcal{Q}_{00\ldots1}} \left(1 + \lambda \left[\frac{2n\mathcal{Q}_{200\ldots}}{\mathcal{Q}_{100\ldots}} - (n-1)\mathcal{Q}_{100\ldots} - \frac{\mathcal{Q}_{100\ldots1}}{\mathcal{Q}_{000\ldots1}}\right] + \ldots\right) \tag{2.22}$$

In mole fractions the equilibrium quotients are

$$\frac{X_1^n}{X_n} = \frac{N}{(nN)^n} \frac{\mathcal{Q}_{100\ldots}^n}{\mathcal{Q}_{00\ldots1}} \left(1 + \lambda \left[\frac{2n\mathcal{Q}_{200\ldots}}{\mathcal{Q}_{100\ldots}} - (n-1)\mathcal{Q}_{100\ldots} - \frac{\mathcal{Q}_{100\ldots1}}{\mathcal{Q}_{000\ldots1}}\right] + \ldots\right) \tag{2.23}$$

Mole fractions are used because they are the predominant units used in the literature, and because this will facilitate a comparison with the Monte Carlo model.

If the system is composed of noninteracting clusters of various sizes, it is possible to simplify the above expression. In this case, the aggregate partition functions can be simplified according to

$$\mathcal{Q}_{00\ldots0i0\ldots0j0\ldots} = \left(\frac{1}{N!}\mathcal{Q}_{00\ldots010\ldots}^i\right)\left(\mathcal{Q}_{000\ldots0\ldots010\ldots}^j\right) \tag{2.24}$$

The above result is applicable for all possible combinations and permutations of i, j and for any other possible aggregate partition function. Using the relationship in Eqn. (2.24) the equilibrium quotients can be simplified since all terms except the leading term will cancel, the quotient then becomes

$$\frac{X_1^n}{X_n} = \frac{N}{(nN)^n} \frac{\mathcal{Q}_{100\ldots}^n}{\mathcal{Q}_{000\ldots1}} \tag{2.25}$$

The individual $\bar{N}_n$'s can then be written as

$$\begin{aligned} \bar{N}_1 &= \lambda_1 \mathcal{Q}_{100\ldots} \\ \vdots &= \vdots \qquad\qquad \vdots \\ \bar{N}_n &= \lambda_n \mathcal{Q}_{000\ldots1} \end{aligned} \tag{2.26}$$

Using the $\bar{N}_n$'s as in Eqn. (2.26), it is possible to write

$$\bar{N}_n = \lambda_n \mathcal{Q}_{000\ldots1}$$

$$\begin{aligned} \ln(\tilde{N}_n) &= \ln(e^{\mu_n \beta} \mathcal{Q}_{000\ldots1}) \\ \ln(\tilde{N}_n) &= \mu_n \beta + \ln(\mathcal{Q}_{000\ldots1}) \end{aligned} \tag{2.27}$$

The chemical potentials μ_n can be written as

$$\mu_n = k_B T \left(\ln(\tilde{N}_n) - \ln(\mathcal{Q}_{000\ldots1}) \right) \qquad \forall\, n \tag{2.28}$$

This can be expressed in terms of mole fractions as

$$\begin{aligned} \mu_n &= k_B T \left(\ln(\tilde{N}_n) - \ln(\mathcal{Q}_{000\ldots1}) \right) \\ &= k_B T \left(\ln(\tilde{N}_n) + \ln(V \rho_{solvent}) - \ln(V \rho_{solvent}) - \ln(\mathcal{Q}_{000\ldots1}) \right) \\ &= k_B T \left(\ln\left(\frac{\tilde{N}_n}{V \rho_{solvent}} \right) - \ln\left(\frac{\mathcal{Q}_{000\ldots1}}{V \rho_{solvent}} \right) \right) \\ &= k_B T \left(\ln\left(\frac{\tilde{N}_n}{V} \right) + \ln\left(\frac{\rho_{tot}}{\rho_{solvent}} \right) - \ln\left(\rho_{tot} \right) - \ln\left(\frac{\mathcal{Q}_{000\ldots1}}{\rho_{solvent} V} \right) \right) \\ &= k_B T \left(\ln\left(\frac{X_n}{n} \right) + \ln\left(\frac{\rho_{tot}}{\rho_{solvent}} \right) - \ln\left(\frac{\mathcal{Q}_{000\ldots1}}{V \rho_{solvent}} \right) \right) \end{aligned} \tag{2.29}$$

where $\rho_{solvent}$ is the solvent density, and

$$\rho_{tot} = \frac{N_{solvent} + N}{V} = \rho_{solvent} + \sum_n n \rho_n \tag{2.30}$$

and where ρ_{tot} is the total density, and $X_n = \frac{n\rho_n}{\rho_{tot}}$ is the mole fraction of molecules in aggregates of size n and $\rho_n = (N_n / nV)$. It is now convenient to define the standard chemical potential on the number density scale $\mu_n^{\circ,\rho}$ as

$$\mu_n^{\circ,\rho} = -k_B T \ln\left(\frac{\mathcal{Q}_{000\ldots1}}{V \rho_{solvent}} \right) \tag{2.31}$$

i.e., the last term in Eqn. (2.29). The chemical potential on the mole fraction scale μ_n° [26] is defined as

$$\begin{aligned} \mu_n^{\circ} &= \mu_n^{\circ,\rho} + k_B T \ln\left(\frac{\rho_{tot}}{\rho_{solvent}} \right) \\ &= \mu_n^{\circ,\rho} + k_B T \ln\left(\frac{\phi_{tot}}{\phi_{solvent}} \right) \end{aligned} \tag{2.32}$$

If it assumed that $\rho_{tot} \approx \rho_{solvent}$, then μ_n° does not depend on ρ_{tot}. The chemical potential μ_n can then be written as

$$\mu_n = \mu_n^\circ + k_B T \ln\left(\frac{X_n}{n}\right) \tag{2.33}$$

As noted by Goldstein [28] this expression is such that the standard chemical potential μ_n° contains contributions arising from interactions between the clusters and the solvent, internal interactions in the cluster, and entropic contributions other than the translational entropy of mixing. The second term in Eqn. (2.33), $k_B T \ln\left(\frac{X_n}{n}\right)$ contains contributions from the translation entropy of mixing. This becomes more transparent if one derives the above relationship starting from the free energy for the system as in the method discussed in Goldstein [28].

Since $\mu_n = n\mu_1$ it is possible to write that

$$\mu_n^\circ + k_B T \ln\left(\frac{X_n}{n}\right) = n(\mu_1^\circ + k_B T \ln(X_1)) \tag{2.34}$$

Upon rearranging this expression, it is possible to write the equilibrium size distribution of molecules as

$$X_n = n X_1^n \exp(-\beta(\mu_n^\circ - n\mu_1^\circ)) \tag{2.35}$$

Eqn. (2.35) is self–consistent in the sense that

$$X_{tot} = \sum_{n=1}^{\infty} X_n \tag{2.36}$$

where X_{tot} is the total mole fraction of amphiphile in the system.

The expression in Eqn. (2.35) is the size distribution for a system of noninteracting clusters of molecules in terms of mole fractions of aggregates. The term $\mu_n^\circ - n\mu_1^\circ$ in Eqn. (2.35) is the free energy difference associated with the aggregation of n molecules including: interactions between the aggregates and solution, internal contributions from the

aggregates and entropic contributions other than those associated with the loss of translational entropy due to the localization of the molecules [28]. This term can be written in a more compact form as

$$\beta\Delta_n = \beta(\mu_n^\circ - n\mu_1^\circ) \tag{2.37}$$

The expression for the size distribution then becomes

$$X_n = nX_1^n \exp(-\Delta_n\beta) \tag{2.38}$$

This represents the size distribution for physical clusters of molecules. The $\bar{N}_n$'s are necessarily positive numbers and can be interpreted as numbers of physical clusters [36]. For a more thorough discussion of physical clusters the reader is referred to [36].

2.4 Modeling the Free energy of Micelle Systems

The discussion so far has been rather general; the remainder of this chapter will examine systems composed of amphiphilic molecules. This section contains a derivation of the free energy Δ_n for a spherical aggregate of n amphiphilic molecules, i.e., $\mu_n^\circ - n\mu_1^\circ$ of Eqn. (2.37). The discussion will not focus on the use of the aggregate partition functions per se; rather, a phenomenological model for the free energy is developed. For an explicit discussion of the properties of the aggregate partition functions for amphiphilic molecules, the reader is referred to [26, 36].

The expressions for the free energy examined in this section were originally derived by Goldstein [28] for systems of symmetric di–block. These expressions will provide the context for the aggregate size distributions obtained from the Monte Carlo simulations. A derivation and discussion of the model for the free energy of aggregates of both symmetric and asymmetric molecules is included. Other forms for the free energy can be found in the following references [42, 68, 120, 135].

2.4.1 The Goldstein Model

In order to discuss the free energy of systems of amphiphilic molecules, it is first necessary to describe the structure of the molecules and the aggregates. The molecules have a total length of Z_s with the tails and heads composed of Z_{st} and Z_{sh} units respectively, such that $Z_s = Z_{st} + Z_{sh}$. In the Goldstein model, the aggregates (or clusters) are assumed to be composed of n molecules arranged such that the tails form a spherical core. It is further assumed that the core is dry, i.e., there is no solvent found in the interior of the core. This assumption implies the remaining tail/head/solvent interactions occur on the surface of the aggregate. The head–groups protrude into the solvent exterior to the core. This region is often referred to as the corona. Negligible penetration of the corona into the core of the aggregate is assumed. The assumed aggregate composition is depicted in Figure 2.2.

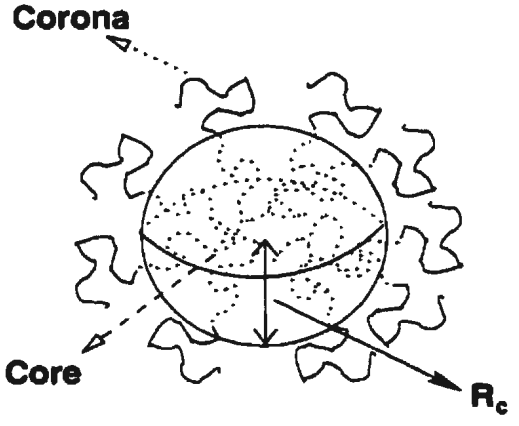

Figure 2.2: Diagram of assumed aggregate composition.

Under these assumptions the radius of the core, R_c, is

$$R_c = \left(\frac{3Z_{st}nv_o}{4\pi}\right)^{\frac{1}{3}} \tag{2.39}$$

where v_o is the volume of a monomer. This calculation implicitly assumes that the micelle is hard packed, i.e., the core is of uniform density equal to one up to the surface of the core, beyond which the density is zero, i.e.,

$$\rho_{core} = \begin{cases} 1 & r \leq R_c \\ 0 & r > R_c \end{cases} \tag{2.40}$$

It is also assumed (implicitly) that the head–groups lie exclusively outside the core and that this region is of uniform density. A schematic depiction of the assumed density profile for the corona and the core are shown in Figure 2.3.

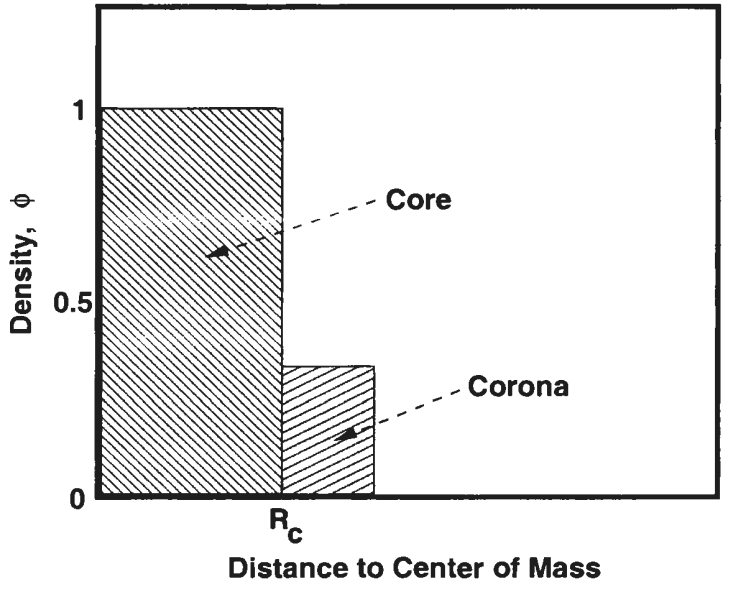

Figure 2.3: Assumed density profile of spherical aggregates in the Goldstein model.

To model the free energy of the aggregates, it is assumed that there are three separate contributions arising from: surface free energy, bulk free energy and an entropic contribution due to the elongation of the molecules. The free energy of an aggregate of n molecules is written as

$$\Delta_n = n(\delta_s + \delta_b + \delta_e) \tag{2.41}$$

where δ_s, δ_b and δ_e refer to the per molecule contributions from the residual tail–solvent and head–tail interactions, the bulk and the entropic terms respectively.

The surface term is assumed to be proportional to the surface area of the core, S_c, which is

$$S_c = 4\pi R_c^2 = 4\pi \left(\frac{nZ_{st}3v_o}{4\pi} \right)^{\frac{2}{3}} \tag{2.42}$$

where R_c is given by Eqn. (2.39). Denoting the surface free energy per unit area by τ, the total surface free energy of the aggregate can be written as

$$n\delta_s = S_c\tau = 4\pi \left(\frac{nZ_{st}3v_o}{4\pi} \right)^{\frac{2}{3}} \tau \tag{2.43}$$

It is convenient to the write this term as

$$n\delta_s = \gamma n^{\frac{2}{3}} \tag{2.44}$$

where $\gamma = \tau 4\pi (Z_{st}3v_o/4\pi)^{2/3}$.

The bulk term contribution to the free energy arises from the transfer of tail– and head–groups to the core and corona of the micelles respectively. This bulk term depends on the lengths of both the tail– and head–groups. It can be written as

$$n\delta_b = n(Z_{sh}h + Z_{st}h') \tag{2.45}$$

where h and h' are constants.

The last term in the free energy expression is the term associated with the elongation of the tail–groups of the molecules as the size of the aggregates increases. It is assumed [28] that the probability distribution function $P(r)$ for the end–to–end distance of a free chain is a Gaussian such that

$$P(r) \propto \exp\left(-\frac{3}{2} \left(\frac{r}{R_o} \right)^2 \right) \tag{2.46}$$

where $R_o = (Z_{st}b)^{1/2}$ is the average end–to–end distance of a random chain of Z_{st} units and where b is the effective segment length of a molecule. It is then possible to write the

entropy as a function of the length of the molecule as

$$S(r) = k_B \ln[P(r)] \tag{2.47}$$

so the change in free energy of n chains forming an aggregate is

$$\begin{aligned} n\delta_e &= -nk_BT\left[\ln(P(R_c)) - \ln(P(R_o))\right] \\ &= nk_BT\left[cn^{2/3}/{Z_{st}}^{1/3} - 3/2\right] \end{aligned} \tag{2.48}$$

where $c = \frac{3}{2}(\frac{3v_o}{4\pi b^3})^{2/3}$ and is a geometric factor of order unity [28].

As noted by Goldstein [28], this approximation for the stretching entropy of the chains is not particularly good for short chains, since they do not necessarily obey ideal random walk statistics; however, the important loss of configurational entropy as the chains elongate is emulated in this expression.

The full expression for the free energy of the aggregates is then

$$\begin{aligned} \Delta_n &= n(\delta_b + \delta_s + \delta_e) \\ &= n(Z_{sh}h + Z_{st}h') + \gamma n^{\frac{2}{3}} + nk_BT(cn^{2/3}/{Z_{st}}^{1/3} - 3/2) \end{aligned} \tag{2.49}$$

The free energy per molecule, δ_n, in an aggregate of size n is then

$$\delta_n = (Z_{sh}h + Z_{st}h') + \gamma n^{-\frac{1}{3}} + k_BT(cn^{2/3}/{Z_{st}}^{1/3} - 3/2) \tag{2.50}$$

This expression can be written more compactly as

$$\frac{\delta_n}{k_BT} = -\alpha + \xi n^{-\frac{1}{3}} + \eta n^{\frac{2}{3}} \tag{2.51}$$

with

$$\begin{aligned} \alpha &= -\frac{Z_{sh}h + Z_{st}h'}{k_BT} - \frac{3}{2} \\ \xi &= \frac{\gamma}{k_BT} \\ \eta &= \frac{c}{{Z_{st}}^{\frac{1}{3}}} \end{aligned} \tag{2.52}$$

This expression for the free energy can be inserted in Eqn. (2.38) in the previous section. The aggregate size distribution obtained in the previous section with the above expression for the free energy becomes

$$X_n = nX_1^n \exp\left(-n\left[-\alpha + \xi n^{-\frac{1}{3}} + \eta n^{\frac{2}{3}}\right]\right) \tag{2.53}$$

This expression will be used to examine the size distributions from the Monte Carlo simulations. A discussion of its properties and general behaviour is included in Chapter 4.

Chapter 3

Monte Carlo: Introduction and Application

"Who can believe what varies everyday, nor ever was, nor will be at stay?"

John Dryden (1631–1700)

Hind and Panther.

This chapter provides an introduction to the Monte Carlo method, its application in statistical mechanics and in the study of amphiphile self–assembly. The chapter begins with a review of the partition function and observables, followed by a general discussion of Monte Carlo. The remainder of the chapter is devoted to a discussion of Monte Carlo applied to the study of self–assembling amphiphilic systems.

3.1 Statistical Mechanics and the Partition Function

To quote Richard Tolman [124], "Statistical mechanics has the special function of providing reasonable methods for treating the behaviour of mechanical systems", so in essence the goal of statistical mechanics is to predict the behaviour of systems with many degrees

of freedom. For a macroscopic physical system the degrees of freedom are on the order of 10^{23}.

Consider the same system of N identical interacting particles, in a volume V at temperature T, as considered in the last chapter. If an analytical calculation of the partition function in Eqn. (2.3) were possible, all thermodynamic quantities would be obtainable therein.

Given an observable (or local operator) $\mathcal{A}(\vec{\mathbf{x}}^N, \vec{\mathbf{p}}^N)$ its thermal average value $\langle \mathcal{A} \rangle_T$ is calculated as

$$\langle \mathcal{A} \rangle_T = \frac{1}{\mathcal{Q}} \int d\Omega \mathcal{A}(\vec{\mathbf{x}}^N, \vec{\mathbf{p}}^N) \exp(-\beta \mathcal{H}(\vec{\mathbf{x}}^N, \vec{\mathbf{p}}^N)) \tag{3.1}$$

The explicit calculation of the partition function and thermal averages is possible for only the simplest of examples, such as a monatomic and diatomic ideal gas [11, 36, 64, 106]. In general, the evaluation of the partition function and associated observables is a highly nontrivial task, as a result it is often necessary to implement techniques such as Monte Carlo.

3.2 The Partition Function: The Monte Carlo Way

The available literature on the Monte Carlo method is voluminous. The interested reader is referred to references [1, 5, 6, 11] for a more general discussion of Monte Carlo applied to a variety of systems. The general Monte Carlo algorithm (applied to integrals over phase space) approximates the integrals in Eqn. (2.1) by a discretization of phase space. In this section two methods of integrating over phase space are examined. The first method is referred to as simple sampling Monte Carlo and involves randomly sampling states, i.e., sets of points in phase space. A second method is importance sampling Monte Carlo, of which a specific example is Metropolis Monte Carlo [86]. In this method states are

sampled based on a Markovian process. A thorough discussion and justification of the importance sampling method is included here to illustrate that it leads to results in the canonical ensemble [1].

3.2.1 Simple Sampling

As previously stated, the evaluation of the total partition function $\mathcal{Q}$ is in general a highly nontrivial task and it is necessary to resort to numerical techniques one such technique is simple sampling Monte Carlo. As the name implies, it is a 'simple' method by which to carry out the integration over the phase space of a system.

Using the partition function as defined in Eqn. (2.3), the thermal average of an observable $\mathcal{A}(\vec{\mathbf{x}}^N)$ can be written as

$$\langle \mathcal{A} \rangle_T = \frac{1}{\mathcal{Z}} \int d\Omega' \mathcal{A}(\vec{\mathbf{x}}^N) \exp(-\beta \mathcal{H}(\vec{\mathbf{x}}^N)) \tag{3.2}$$

where $d\Omega' = d^N\vec{\mathbf{x}}$ and $\mathcal{Z}$ is the configurational partition function as defined in Eqn. (2.4). The integral in Eqn. (3.2) can be written as a discrete sum over states in analogy to replacing integrals by discrete sums in one dimensional integration. The discrete analog of Eqn. (3.2) written as a sum over states is

$$\langle \mathcal{A} \rangle_T = \frac{\sum_{l=1}^{M} \mathcal{A}(\vec{\mathbf{x}}_l) \exp(-\beta \mathcal{H}(\vec{\mathbf{x}}_l))}{\sum_{l=1}^{M} \exp(-\beta \mathcal{H}(\vec{\mathbf{x}}_l))} \tag{3.3}$$

where M refers to the number of states and $\vec{\mathbf{x}}_l$ refers to a configuration of the N particles in the system or simply a state of the system.

Consider Eqn. (3.3), in the limit as $M \to \infty$, Eqn. (3.2) and, consequently, thermal averages in the canonical ensemble are obtained. It is not possible to sample an infinite number of states; moreover, it is not necessary to do so since states of high energy will contribute little to the sums in Eqn. (3.3). A "simple" alternative to sampling an infinite

[1] It should be noted that the term "Monte Carlo" is used to imply the stochastic nature of this technique.

number of states is to sample states randomly instead of at regular intervals [6]. This method is referred to as simple sampling.

Simple sampling Monte Carlo is somewhat more efficient than sampling states over a 'regular grid' in phase space [6]. The situation is not significantly improved since the number of states that must be sampled to obtain a decent thermal average is still not known. The main advantage of simple sampling is that one can ensure that the finite number of states which are sampled do not come from the same local region of phase space [6], i.e., this ensures that thermal averages are not taken over local regions of phase space.

3.2.2 Importance Sampling

As noted in the last paragraph, the method of simple sampling, although somewhat more effective than sampling states at regular intervals, is still a rather inefficient method to carry out the integrals over phase space. Even for a small system the number of available states is too numerous. A more efficient method of sampling states is needed. An alternative method is importance sampling; in the general sense importance sampling involves a controlled biasing of the points sampled to lie predominantly where the integrand (of the function being integrated) is largest. A specific example of importance sampling was suggested by Metropolis *et al.* [86].

The Metropolis algorithm will be discussed in terms of transitions between consecutive states or points in phase space. Metropolis *et al.* [86] suggested that, instead of choosing states randomly, it is more efficient to choose states $\vec{\mathbf{x}}_l$ weighted by a probability $P(\vec{\mathbf{x}}_l)$. If each state is weighted by $P(\vec{\mathbf{x}}_l)$, the thermal average $\langle \mathcal{A} \rangle_T$ can be written as

$$\langle \mathcal{A} \rangle_T = \frac{\sum_{l=1}^{M} \mathcal{A}(\vec{\mathbf{x}}_l) \exp(-\beta \mathcal{H}(\vec{\mathbf{x}}_l))/P(\vec{\mathbf{x}}_l)}{\sum_{l=1}^{M} \exp(-\beta \mathcal{H}(\vec{\mathbf{x}}_l))/P(\vec{\mathbf{x}}_l)} \tag{3.4}$$

In general it is possible to choose any form for $P(\vec{\mathbf{x}}_l)$; however, it is useful to choose one which simplifies the partition function. The obvious choice is simply the canonical probability distribution

$$P(\vec{\mathbf{x}}_l) \propto \exp(-\mathcal{H}(\vec{\mathbf{x}}_l)\beta) \tag{3.5}$$

With this choice, the thermal average in Eqn. (3.4), simply reduces to an arithmetic average of M values of $\mathcal{A}(\vec{\mathbf{x}}_l)$ evaluated at each state $\vec{\mathbf{x}}_l$

$$\langle \mathcal{A} \rangle_T = \frac{1}{M} \sum_{l=1}^{M} \mathcal{A}(\vec{\mathbf{x}}_l) \tag{3.6}$$

To realize the result in Eqn. (3.6) it is necessary to construct a Markov process where each successive state $\vec{\mathbf{x}}_{l'}$ is constructed from the previous state $\vec{\mathbf{x}}_l$ via a suitable transition probability [6]. The reader is referred to references [106, 108] for a discussion of Markov processes. This Markov process should be such that in the limit $M \to \infty$ the distribution function $P(\vec{\mathbf{x}}_l)$ tends to the equilibrium canonical distribution

$$P_{eq}(\vec{\mathbf{x}}_l) = \frac{1}{\mathcal{Z}} \exp(-\mathcal{H}(\vec{\mathbf{x}}_l)\beta) \tag{3.7}$$

A necessary and sufficient condition to obtain the result in Eqn. (3.7) is to impose the condition of detailed balance

$$P_{eq}(\vec{\mathbf{x}}_l) W(\vec{\mathbf{x}}_l \to \vec{\mathbf{x}}_{l'}) = P_{eq}(\vec{\mathbf{x}}_{l'}) W(\vec{\mathbf{x}}_{l'} \to \vec{\mathbf{x}}_l) \tag{3.8}$$

The reader is referred to Binder and Reichl [6, 106] for a derivation of the detailed balance relationship and a discussion of its relevant properties. Using Eqn. (3.8) the ratio of the transition probabilities is

$$\frac{W(\vec{\mathbf{x}}_l \to \vec{\mathbf{x}}_{l'})}{W(\vec{\mathbf{x}}_{l'} \to \vec{\mathbf{x}}_l)} = \frac{P_{eq}(\vec{\mathbf{x}}_l)}{P_{eq}(\vec{\mathbf{x}}_{l'})} = \exp(-\beta(\mathcal{H}(\vec{\mathbf{x}}_{l'}) - \mathcal{H}(\vec{\mathbf{x}}_l))) \tag{3.9}$$

This ratio depends on the energy change associated with going from state $\vec{\mathbf{x}}_l$ to state $\vec{\mathbf{x}}_{l'}$. As noted by Binder [6], the transition probability $W(\vec{\mathbf{x}}_{l'} \to \vec{\mathbf{x}}_l)$ in Eqn. (3.9) is not unique.

The Metropolis form is

$$W(\vec{\mathbf{x}}_l \rightarrow \vec{\mathbf{x}}_{l'}) = \begin{cases} \frac{1}{\tau_s}\exp(-\delta\mathcal{H}\beta) & \text{if } \delta\mathcal{H} > 0, \\ \frac{1}{\tau_s} & \text{otherwise.} \end{cases} \tag{3.10}$$

The factor τ_s in Eqn. (3.10) is an arbitrary factor and is chosen as unity, i.e., $\tau_s = 1$ [6]. Eqn. (3.10) provides a rule by which to sample consecutive states of a system.

To implement the Monte Carlo method it is necessary to have a practical working algorithm. This algorithm will consist of sampling different states based on the prescribed transition probability in Eqn. (3.10). The general Metropolis Monte Carlo algorithm is as follows

1. Begin with an initial state of the system $\vec{\mathbf{x}}_l$.
2. Change the state of the system, $\vec{\mathbf{x}}_l \rightarrow \vec{\mathbf{x}}_{l'}$.
3. Calculate the change in energy $\mathcal{H}(\vec{\mathbf{x}}_l) - \mathcal{H}(\vec{\mathbf{x}}_{l'}) = \delta\mathcal{H}$.
4. Calculate the transition probability $W(\vec{\mathbf{x}}_l \rightarrow \vec{\mathbf{x}}_{l'})$.
5. Draw a random number $\zeta \in [0, 1)$.
6. If the transition probability is such that $\zeta < W(\vec{\mathbf{x}}_l \rightarrow \vec{\mathbf{x}}_{l'})$ accept the new state, otherwise reject it and repeat the process, keeping track of observables for averaging.

The practical application of the above algorithm is discussed in Section 3.7 as applied to the self–assembly of amphiphiles. Eqn. (3.10) states that if a transition is such that the change in energy of the system is negative the transition is automatically accepted. If the transition is such that the change in energy is positive the transition is accepted or rejected by comparing a randomly chosen number to the Boltzmann factor $\exp(-\beta\delta\mathcal{H})$.

Using the transition probability in Eqn. (3.10), the thermal average $\langle\mathcal{A}\rangle_T$ will tend to the canonical ensemble average after a sufficient number of steps [5, 6]. The number of

Monte Carlo steps, i.e., the number of attempted transitions $\vec{x}_l \rightarrow \vec{x}_{l'}$ required to obtain equilibrium thermal averages, is related to the number of steps required for the system to reach equilibrium. The next section focuses on a discussion of autocorrelation times and equilibrium. These autocorrelation times are a useful tool in characterizing equilibrium in the Monte Carlo model.

3.3 Autocorrelation Times and Equilibrium

In the previous section it was illustrated that importance sampling Monte Carlo can lead to thermodynamic averages in the canonical ensemble. The remaining question is, How many states M must be sampled in order to calculate these averages? Another important question when using Monte Carlo is, How long does it take a system to reach equilibrium, in terms of the number of attempted transitions?

In order to discuss equilibrium, it is necessary to identify the time scales relevant to the behaviour of observables. For example, in a gas of hard spheres, one time scale of interest (in real time) would be the average time for a gas particle to traverse a certain characteristic length, such as the average distance between neighbouring spheres.

In order to discuss time scales in the Monte Carlo model it is necessary to describe the system as it evolves in "time" (in the Monte Carlo model the "time" will be defined in terms of the number of Monte Carlo steps, i.e., the number of sampled states). It will be useful to associate these "time" scales with the behaviour of observables defined in terms of the number states which are sampled. It is first necessary to define Monte Carlo time: unit Monte Carlo time will be defined as 1 MCS (Monte Carlo Step) per species in a system. The definition of a species will depend on the system under consideration[2]. For

[2]It is worthy to note, that it is difficult to relate Monte Carlo "time" to real time [6]. A dynamical interpretation does not in any way imply a direct correspondence with the real dynamics of a system or the real time scales in a physical system. Monte Carlo time is often referred to as stochastic time.

the amphiphile systems, a species will be an individual monomer of a molecule.

It is usual to associate the probability $P(\vec{\mathbf{x}}_l)$ with the "time" (Monte Carlo time) dependent probability $P(\vec{\mathbf{x}}, t)$ such that $P(\vec{\mathbf{x}}_l) = P(\vec{\mathbf{x}}, t)$, where $P(\vec{\mathbf{x}}_l)$ is the probability of an associated state $\vec{\mathbf{x}}_l$. This is equivalent to discussing the behaviour of $P(\vec{\mathbf{x}}_l)$ as a function of l the number of states being sampled. After a sufficient length of Monte Carlo time the probability distribution tends to the time independent equilibrium distribution, i.e.,

$$\lim_{t\to\infty} P(\vec{\mathbf{x}}, t) = P_{eq}(\vec{\mathbf{x}}_l) \tag{3.11}$$

As noted by Binder [6] a dynamic interpretation of the Monte Carlo method is important in order to discuss correlations in the Monte Carlo model. For a thorough discussion and justification of the dynamical interpretation of the Monte Carlo method, the reader is referred to Binder [5, 6].

With this understanding of the meaning of "time" in the simulations, a method of calculating each time scale associated with various observables is required. This is done by calculating autocorrelation functions and associated autocorrelation times. This allows a quantification of the time necessary for a system to reach equilibrium and the time necessary to calculate equilibrium averages [5, 6].

To discuss equilibrium in terms of fluctuations in an observable quantity $\langle \mathcal{A} \rangle$, it is convenient to consider how the mean squared fluctuations of this value $\langle (\delta \mathcal{A})^2 \rangle$ varier with time, in this case Monte Carlo time. The mean squared error in a measurement of $\langle \mathcal{A} \rangle$ is defined as

$$\begin{aligned} \langle (\delta \mathcal{A})^2 \rangle &= \left\langle \left[\frac{1}{M} \sum_{i=1}^{M} (\mathcal{A}_i - \langle \mathcal{A} \rangle) \right]^2 \right\rangle \\ &= \frac{1}{M^2} \sum_{i=1}^{M} \langle (\mathcal{A}_i - \langle \mathcal{A} \rangle)^2 \rangle + \frac{2}{M^2} \sum_{i=1}^{M} \sum_{i_1=i+1}^{M} (\langle \mathcal{A}_i \mathcal{A}_{i_1} \rangle - \langle \mathcal{A} \rangle^2) \end{aligned} \tag{3.12}$$

It is possible to carry out the summation over i_1 in Eqn. (3.12), so that

$$\langle(\delta\mathcal{A})^2\rangle = \frac{1}{M}\left[\langle\mathcal{A}^2\rangle - \langle\mathcal{A}\rangle^2 + 2\sum_{i=1}^{M}\left(1-\frac{i}{M}\right)\left(\langle\mathcal{A}_0\mathcal{A}_i\rangle - \langle\mathcal{A}\rangle^2\right)\right] \tag{3.13}$$

The total Monte Carlo time will be defined as $t_i = (1/N)i = (\delta t)i$, where M is the total number of states sampled and N is the total number of particles. Using this definition for the total Monte Carlo time, it is possible rewrite Eqn. (3.13) as an integral over time t, the continuous analog of t_i

$$\langle(\delta\mathcal{A})^2\rangle = \frac{1}{M}(\langle\mathcal{A}^2\rangle - \langle\mathcal{A}\rangle^2)\left[1+\frac{2}{\delta t}\int_0^{t_M} dt\left(1-\frac{t}{t_M}\right)\frac{(\langle\mathcal{A}(0)\mathcal{A}(t)\rangle - \langle\mathcal{A}\rangle^2)}{\langle\mathcal{A}^2\rangle - \langle\mathcal{A}\rangle^2}\right] \tag{3.14}$$

The time dependent normalized autocorrelation function $\phi_{\mathcal{A}}(t)$ (sometimes called a normalized relaxation function) of an observable $\langle\mathcal{A}\rangle$ is defined as

$$\phi_{\mathcal{A}}(t) = \frac{(\langle\mathcal{A}(0)\mathcal{A}(t)\rangle - \langle\mathcal{A}\rangle^2)}{\langle\mathcal{A}^2\rangle - \langle\mathcal{A}\rangle^2} \tag{3.15}$$

It is important to note that $\lim_{t\to\infty}\phi_{\mathcal{A}}(t) = 0$ and $\phi_{\mathcal{A}}(0) = 1$ for most physical observables of interest[3]. The associated autocorrelation time $\tau_{\mathcal{A}}$ of a given observable $\langle\mathcal{A}\rangle$ is defined as

$$\tau_{\mathcal{A}} = \int_0^{\infty}\phi_{\mathcal{A}}(t)dt = \int_0^{\infty}\frac{(\langle\mathcal{A}(0)\mathcal{A}(t)\rangle - \langle\mathcal{A}\rangle^2)}{\langle\mathcal{A}^2\rangle - \langle\mathcal{A}\rangle^2}dt \tag{3.16}$$

It is assumed that $t \ll t_M$ is the only regime for which the autocorrelation times have a non zero value, consequently in Eqn. (3.14) the term t/t_M can be neglected and it is possible to write the mean squared fluctuation $\langle(\delta\mathcal{A})^2\rangle$ as

$$\langle(\delta\mathcal{A})^2\rangle = \frac{1}{M}(\langle\mathcal{A}^2\rangle - \langle\mathcal{A}\rangle^2)\left[1+\frac{2}{\delta t}\int_0^{t_M}\frac{(\langle\mathcal{A}(0)\mathcal{A}(t)\rangle - \langle\mathcal{A}\rangle^2)}{\langle\mathcal{A}^2\rangle - \langle\mathcal{A}\rangle^2}dt\right] \tag{3.17}$$

[3]For periodic $\mathcal{A}$, the autocorrelation function will also be periodic and will not converge in the limit as $t \to \infty$.

Furthermore using the definition for the relaxation time in Eqn. (3.17) it is possible to write the mean squared fluctuation $\langle(\delta\mathcal{A})^2\rangle$ as

$$\begin{aligned}\langle(\delta\mathcal{A})^2\rangle &= \frac{1}{M}(\langle\mathcal{A}^2\rangle - \langle\mathcal{A}\rangle^2)\left[1+\frac{2\tau_{\mathcal{A}}}{\delta t}\right] \\ &= (\langle\mathcal{A}^2\rangle - \langle\mathcal{A}\rangle^2)\left[\frac{1}{M}+\frac{2\tau_{\mathcal{A}}}{\tau_M}\right] \qquad (3.18)\end{aligned}$$

where $\tau_M = M\delta t$.

The statistical fluctuations are proportional to the ratio $\frac{2\tau_{\mathcal{A}}}{\tau_M}$, that is to say, the fluctuations depend on the number of Monte Carlo steps relative to the autocorrelation time of a given quantity. This provides a convenient way of determining appropriate time scales for a system. In order to obtain averages which are representative of equilibrium averages, it is necessary to know how long it takes given quantities in a system to relax to their equilibrium values, i.e., their autocorrelation times.

In the application of Monte Carlo to self–assembly, there are several characteristic time scales of interest. Autocorrelation times are calculated for each of these. The largest of these times will be referred to as the relaxation time of the system and will determine the criterion for equilibrium. In the self–assembly of amphiphiles, it is often necessary to wait between 100 to 200 relaxation times before collecting averages and a further 100 to 200 relaxation times for the purposes of collecting averages.

3.4 Simulating Self–Assembly: The Monte Carlo Way

In recent years, Monte Carlo has become a method of choice for examining a diverse variety of physical phenomena in a wide range of disciplines including: classical mechanics, quantum mechanics, statistical mechanics and gravitational theories. The application of the Monte Carlo method to the study of self–assembly was first presented in a series of papers by Larson [59, 60, 62, 63] and Pratt *et al.* [103, 104]. The use of Monte Carlo to study self–

assembly has gained popularity, and numerous papers have been published on the subject [5, 9, 10, 15, 19, 20, 24, 27, 38, 41, 45, 50, 51, 53, 54, 70, 71, 76, 77, 97, 99, 115, 118, 121, 126, 127, 140, 145]; however, to date, few systematic studies of self–assembly using Monte Carlo have been attempted.

The first application of the Monte Carlo method to the study of a physical system was discussed in a 1953 article by Metropolis *et al.* [86] entitled "Equation of State Calculations by Fast Computing Machines." In this paper, importance sampling Monte Carlo was applied to a two dimensional gas of hard disks. The results were in good agreement with the equation of state and a four term virial coefficient expansion. The work by Metropolis *et al.* [86] opened a new venue for the investigation of physical phenomena via computer based simulations.

The remainder of this chapter provides a detailed description of the Monte Carlo method applied to study of self–assembly of amphiphiles. The first part of the discussion focuses on the model for the structure of the molecules and the space in which they exist. This is followed by a discussion of Monte Carlo moves and the calculation of model autocorrelation functions. The chapter ends with a schematic depiction of the algorithm that is used in the simulations.

3.4.1 Amphiphiles: The Coarse–Grained Description

There are numerous methods used to model molecules and their properties. These methods typically vary in their level of detail, which depends on the behaviour to be observed. The time scales which are accessible in a model are often restricted; for example, in molecular dynamics an accessible time scale is on the order of hundreds of pico–seconds and is commensurate with fast molecular reorientations and short range motions [26, 53, 57]. In molecular dynamics, aggregates are typically assigned a predefined 'shape', the molecules

are initially assigned a known crystal structure, and it is assumed that the prepared aggregate is stable. However, the time scales associated with the spontaneous formation of an aggregate are on the order of micro to milli–seconds, so molecular dynamics typically falls short of being able to simulate spontaneous self assembly [26].

Practitioners of Monte Carlo typically use a coarse grained model for molecules. These coarse grained models allow longer accessible 'time' scales which are commensurate with self–assembly [26, 132]. Using Monte Carlo, it is possible to simulate self–assembly; furthermore, accessible 'time scales' are such that spontaneous formation and dissolution of aggregates can occur.

In order to model the behaviour of molecules, it is first necessary to model their structure. This will depend on the molecules which are being modeled. For a single chain molecule one of the simplest models is to represent it as a chain of monomers where a monomer can represent a single atom or a generalized group of atoms such as a methyl group CH_3. The molecules under consideration in this thesis are modeled as chains with different monomers for the head– and tail–groups.

The linear chain molecules are composed of Z_s monomers with Z_{st} and Z_{sh} monomers comprising the tail– and head–groups respectively, such that

$$Z_s = Z_{st} + Z_{sh} \tag{3.19}$$

A typical model molecule is shown in Figure 3.1.

The linear chain model is an example of a coarse grained model. A thorough discussion and justification of the use of coarse grained models is contained in the article by Sokal [5]. It should be noted that although the coarse grained model may seem like a "ridiculous caricature" [5] of a real molecule, it can lead to exact results for certain universal properties such as the radius of gyration. It is non trivial to make direct comparisons between to the model molecules and specific molecules. However, Mattice *et al.* [76] using mapping

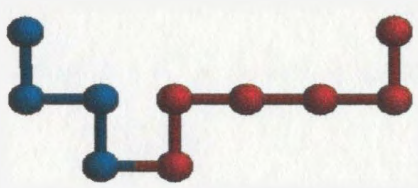

Figure 3.1: Illustration of a typical model coarse grained molecule used in this thesis, with $Z_s = 10, Z_{sh} = 4$ and $Z_{st} = 6$, the head– and tail–groups are blue and red respectively.

and reverse mapping, have shown that it is possible to map a coarse grained model onto a detailed molecular model. In doing so, it is possible to make direct comparisons with specific molecules. The linear coarse–grained model is a good approximation for single chain amphiphiles, such as single chain surfactants and polymers [5, 10].

3.4.2 The Lattice Model

In this thesis, a simple cubic lattice is used to represent the space in which the amphiphiles and solvent exist. The lattice is composed of L^3 lattice sites, i.e., an $L \times L \times L$ lattice. The simulations also use periodic boundary conditions to minimize the effects imposed by the finite lattice size [5]. The periodic boundary conditions are such that

$$x_i + nL \rightarrow x_i, \quad y_i + nL \rightarrow y_i, \quad z_i + nL \rightarrow z_i, \quad \forall\, n \in Z \tag{3.20}$$

where x_i, y_i and z_i refer to arbitrary lattice sites. The unit of length in the lattice model is such that the bond length is equal to the lattice constant.

Each monomer occupies a single lattice site, with no two monomers occupying the same site. The model is referred to as mutually and self–avoiding, i.e., double occupancy of lattice sites is not allowed, this is sometimes referred to as the excluded volume interaction. There are N_s amphiphiles in the system. Of the L^3 lattice sites, N_s groups of Z_s contiguous lattice sites are occupied by amphiphile and the remaining $L^3 - N_s Z_s$ lattice sites are

occupied by the solvent.

The volume fraction of amphiphile ϕ_s in the lattice is

$$\phi_s = \frac{V_s}{V_{tot}} = \frac{Z_s N_s}{L^3} = \frac{Z_s N_s}{Z_s N_s + N_w} \tag{3.21}$$

where V_s and V_{tot} refer to the total volume of the amphiphile and the lattice respectively, N_w and $Z_s N_s$ denote the total number of lattice sites occupied by solvent and amphiphile. Typical volume fractions used in the simulations are $\phi_s \leq 5\%$.

3.4.3 Modeling the Interactions

The interactions among the various components in the system must reflect the nature of interactions in a physical system. The model molecules must also be able to emulate the known behaviour of the 'real' molecules in solution.

The model for the interactions used in this thesis is similar to the classic Flory [22] lattice model for polymer molecules. Only the interactions between unlike first nearest neighbour pairs on the lattice are used. The coordination number z of a lattice is defined as the number of first nearest neighbours to each lattice site. The simple cubic lattice has a coordination number of $z = 6$. The inclusion of other than first nearest neighbour interactions would greatly increase the computational complexity of the simulations.

There are three distinct interacting pairs in the model systems. The interaction between the head–group and the solvent is modeled by an attractive interaction between each head–group monomer and the solvent. The interaction between the head– and tail–group monomers is repulsive, and these groups tend to avoid one another. There is also an interaction between the tail–group and solvent which is modeled by a repulsive interaction. These interactions are chosen to reflect the ambivalent behaviour of the model molecules towards a host solvent.

The model is not well suited to describe the long range polar interactions of ionic molecules; nonetheless, people compare the model molecules to ionic surfactants such as n–alkyl sulphates. The model molecules are more representative of nonionic surfactants such alkyl ethoxylates [10].

The quantities which actually enter the Monte Carlo simulations are E_{ij}/k_BT. It is convenient to introduce these as reduced interaction parameters[4]

$$\varepsilon_{ij} = \frac{E_{ij}}{k_BT} \tag{3.22}$$

where $i, j = h, t, s$ and refer to the head–, tail–group and solvent respectively, and E_{ij} represents interactions between unlike nearest neighbours of type ij. These reduced interaction parameters incorporate an intrinsic temperature dependence. An increase in ε_{ij} corresponds to a strengthening of interactions and/or a lowering of T. The three reduced interaction parameters used in this thesis are

- ε_{ts}, the tail–group solvent interaction, $\varepsilon_{ts} > 0$,
- ε_{th}, the tail–group head–group interaction, $\varepsilon_{th} > 0$,
- ε_{hs}, the head–group solvent interaction, $\varepsilon_{hs} < 0$.

The reduced interaction parameters $\varepsilon_{ts}, \varepsilon_{hs}$ and ε_{th} as defined, make this model directly comparable to the classic Flory [22] model for linear chain polymer molecules.

The interactions in the system are only between nearest neighbours so the Hamiltonian (divided by k_BT) is

$$\begin{aligned} \frac{\mathcal{H}}{k_BT} &= \frac{1}{2} \sum_{LatticeSites} \sum_{n.n} \frac{E_{ij}}{k_BT} \\ &= n_{ts}\varepsilon_{ts} + n_{hs}\varepsilon_{hs} + n_{th}\varepsilon_{th}. \end{aligned} \tag{3.23}$$

[4]Introduction of reduced interaction parameters is a common procedure in physics.

where the terms n_{ts}, n_{hs} and n_{ht} represent the total number of tail–, head–solvent and head–tail contacts, respectively, in the entire system. The subscript $n.n$ on the second summation refers to a sum over nearest neighbours. A typical set of interaction parameters used in the simulations in this thesis and in the literature [10, 105] are such that $\varepsilon_{hs} = -2\varepsilon_{ts} = -2\varepsilon_{th} = \varepsilon$. The total energy in the system can be written as

$$\begin{aligned} \frac{\mathcal{H}}{k_B T} &= n_{ts}\varepsilon_{ts} + n_{hs}\varepsilon_{hs} + n_{th}\varepsilon_{th} \\ &= -2\varepsilon(n_{hs} - \frac{1}{2}(n_{ts} + n_{th})). \end{aligned} \tag{3.24}$$

As the reduced interaction parameters $\varepsilon_{ts}, \varepsilon_{hs}$ are decreased to zero, i.e., $\varepsilon_{ts}, \varepsilon_{hs} \rightarrow 0$, the solvent becomes athermal.

It is also necessary to calculate the energy change in going from one state to another. With the reduced interaction parameters as defined and the Hamiltonian as in Eqn. (3.24), the change in energy $\delta\mathcal{H}$ is

$$\frac{\delta\mathcal{H}}{k_B T} = -2\varepsilon(n_{hs}^A - \frac{1}{2}(n_{ts}^A + n_{th}^A)) + 2\varepsilon(n_{hs}^B - \frac{1}{2}(n_{ts}^B + n_{th}^B)) \tag{3.25}$$

where the superscripts B and A refer to before and after the state has changed respectively. In the Metropolis algorithm, the probability of a transition occurring is

$$\exp\left(\frac{-\delta\mathcal{H}}{k_B T}\right) = \exp\left(-2\varepsilon(n_{hs}^A - \frac{1}{2}(n_{ts}^A + n_{th}^A)) + 2\varepsilon(n_{hs}^B - \frac{1}{2}(n_{ts}^B + n_{th}^B))\right) \tag{3.26}$$

Clearly the change in energy depends only the number of contacts of each type n_{ts} n_{hs}, n_{ht} and the value of ε. This provides a very convenient way of calculating the change in energy and the associated probability of successive configurations in the Monte Carlo model. This has facilitated a method in which energy calculations are carried out not as direct lattice sums but rather as sums of local positions of molecules and the tabulation of numbers of nearest neighbours. This is discussed in references [50, 51, 99].

3.5 Monte Carlo Moves

The previous two sections provided a description of the model amphiphiles and their interactions. The depiction of the model systems, so far, has been static and limited to molecules 'existing' and 'interacting' on the lattice; however, aggregation is intrinsically a dynamic process. At equilibrium, there is a continual exchange of molecules between aggregates and solution, and between other aggregates; the conformations of the molecules are also continually changing [26, 99, 132]. A practical method of generating new conformations and positions of the molecules is required. This method involves using Monte Carlo moves; successive configurations are then generated using importance sampling Monte Carlo.

The Monte Carlo moves used in this thesis fall under the general classification of local, bi–local and nonlocal N–conserving Monte Carlo moves as defined in the article by Sokal [5]. Local moves refer to moves in which a few consecutive sites of the lattice are affected by the move. Bi–local moves are defined as moves which alter two small disjoint groups of consecutive lattice sites. For a general discussion of Monte Carlo moves and their properties the reader is referred to Sokal [5]. There are four types of N–conserving Monte Carlo moves used in this thesis: reptation, kink–flip, crank–shaft and Brownian motion (a nonlocal move). A thorough description of these four moves is provided in the following discussion.

3.5.1 Reptation

The reptation move is known informally as the slithering snake move, as it essentially allows a molecule to "slither" around the lattice. A monomer at either end of the molecule is allowed to move to any of the available unoccupied lattice sites adjacent to it, and the remainder of the monomers of that molecule move one lattice site along the chain (hence the name slithering snake).

The reptation move is effective as it allows molecules to both diffuse around the lattice and adopt new chain configurations [5]. Reptation is the most commonly used of the Monte Carlo moves for systems of chain–like molecules and many practitioners implement only reptation[10, 58, 59, 121]. Figure 3.2 shows an example of the reptation move in two dimensions

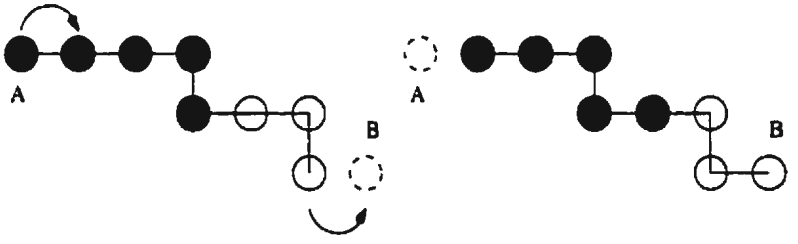

Figure 3.2: Illustration of reptation motion.

In two dimensions the reptation move can 'trap' a molecule in a local conformation; however, in three dimensions, entrapment of molecules in local conformations is not possible [6].

3.5.2 Kink–Filp

The kink–flip Monte Carlo move involves rotating a 'kink' in the molecule by either $\pm 90°$ or $\pm 180°$ depending on the position of the monomer along the chain. This move can flip either an end of a molecule or a part of the molecule interior to the ends. One type of kink–flip motion is depicted in the following diagram,

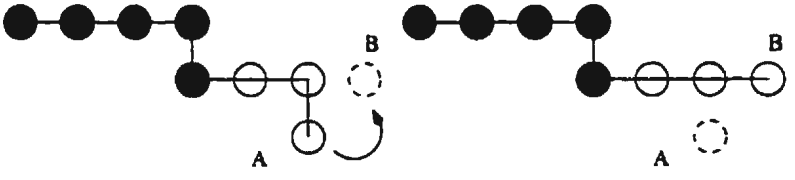

Figure 3.3: Illustration of kink–flip motion.

The kink–flip move plays an important role in the relaxing of the local chain conformations in aggregates [99]. Using only reptation, local chain conformations relax much more slowly than when kink–flip moves are also used.

3.5.3 Crank–Shaft

The crank–shaft move also plays an important role in the relaxation of chain conformations in an aggregate. This move allows a crank–shaped bend in the molecule to rotate by $\pm 90°$. A schematic picture of the crank–shaft motion is shown in Figure 3.4.

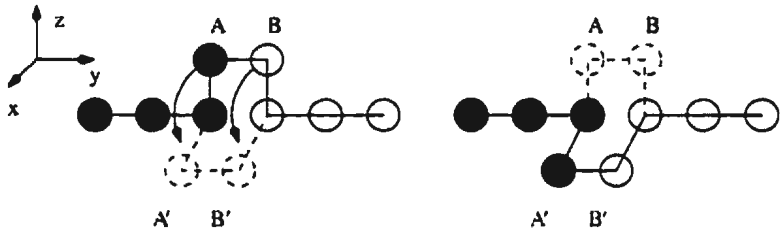

Figure 3.4: Illustration of crank–shaft motion.

3.5.4 Brownian Motion

Brownian motion involves moving a molecule a specified number lattice sites, n_b, while retaining the relative positions of the monomers with respect to one another. Typically n_b is such that $n_b < L/2$, where L is the dimension of the lattice. Figure 3.5 shows a schematic representation of a Brownian motion move of $n_b = 7$ lattice sites. Brownian motion is important in allowing the molecules to diffuse around the lattice as the molecules are allowed to move many lattice sites with a single move, unlike the other previously mentioned moves.

It is important to note that a single Monte Carlo move corresponds to a change in the state of the system, i.e., a single move corresponds to a transition from state l to $l + 1$,

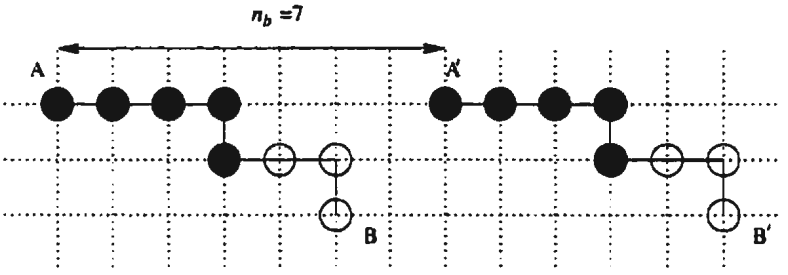

Figure 3.5: Illustration of Brownian motion.

$\vec{x}_l \rightarrow \vec{x}_{l+1}$. Since the Monte Carlo moves only affect lattice sites local to the old and new positions of the molecules, the change in energy of a system need only be calculated with respect to the positions of the lattice sites before and after a move has been carried out. This has allowed a method of energy calculation which does not involve direct sums over all lattice sites. The energy calculations are carried out over the subset of lattice sites which are affected by a single move.

In the simulations, moves are chosen randomly within an overall weighting of each kind of move. The typical weighting scheme used in the simulations is: reptation 50%, kink–flip 40%, crank–shaft 8% and Brownian motion 2%. Work by Pépin [99] has shown that equilibrium results are independent of the relative weighting of the moves provided they are approximately in this range. The above weighting scheme has been effective, but is not necessarily the most efficient combination of moves.

3.6 Model Autocorrelation Functions and Times

As stated in Section 3.3 the autocorrelation times serve as guides to how long it is necessary to run the simulations. The autocorrelation times also allow a classification of the time scales associated with the observable behaviours. The discussion of autocorrelation functions in Section 3.3 was very general, this general discussion is now cast in a more

practical setting.

In this thesis there are four time scales associated with the characteristic behaviour of observables, these are:

1. **Chain Extraction**; a time scale associated with the extraction of a molecule from an aggregate.

2. **Chain Exchange**; a time scale associated with the exchange of molecules between aggregates.

3. **Diffusion**; a time scale associated with the diffusion of a molecule over a distance which is equal to the average distance between molecules.

4. **End–to–end vector**; a time scale associated with the correlation of the end–to–end vector of a molecule from its original orientation.

As noted by Wennerström and Lindman [132], there are other processes which have time scales associated with them. They include:

- Formation and dissociation of an aggregate.

- Change in the shape and size, both dimensionally (i.e., the radius of the aggregate) and through changes in the aggregation number of an aggregate.

The exchange and extraction of molecules play significant roles in the growth of aggregates [21]. Eisenberg [21] has suggested that there are two possible mechanisms associated with micellar growth and morphological transitions, such as the transition from spherical aggregates to rod–like aggregates. The suggested mechanisms involve chain extraction and chain insertion and the combining of aggregates to form larger aggregates. Figure 3.6 illustrates the two suggested mechanisms of micelle growth. Smaller unstable aggregates can

also dissociate and the molecules can be incorporated into larger aggregates. If the chain exchange and extraction mechanisms play an important role in micelle growth, then the autocorrelation times for these mechanisms provide a guide to ensure that aggregates have had sufficient time to equilibrate.

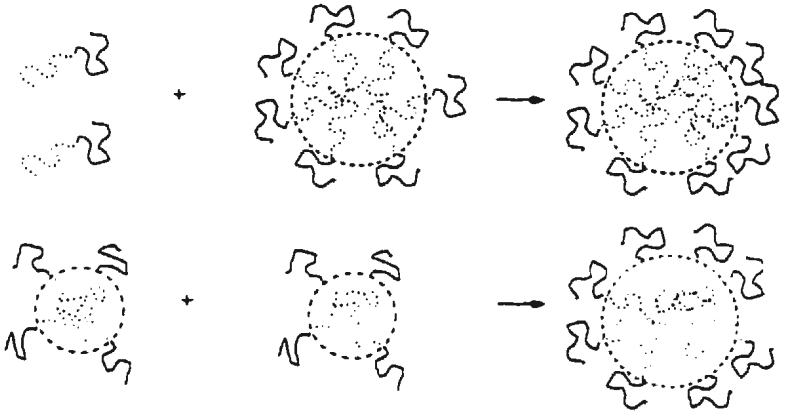

Figure 3.6: Two possible mechanisms for micelle growth.

The characteristic time scales can depend markedly on the value of the reduced interaction parameters ϵ_{ij}. The autocorrelation times are roughly constant below a characteristic interaction parameter and, above this parameter, increase by orders of magnitude with small changes in the interaction parameter. It will be seen that the characteristic interaction parameters at which the autocorrelation times begin to increase correspond to the onset of micellization in the system.

The autocorrelation times are defined in terms of N–bead cycles, where one N–bead cycle is $N_s Z_s$ attempted Monte Carlo moves. The increase in the autocorrelation times with the onset of micellization implicitly implies that the number of Monte Carlo steps required to reach equilibrium increases. The actual computational time necessary to carry out the simulations increases markedly beyond the characteristic interaction parameter at which micellization begins. The increase of the autocorrelation times as a function of the interaction parameter ultimately limits its maximum value that can be obtained in the

simulations.

The chain exchange autocorrelation times are the largest of the four autocorrelation times. The maximum of the autocorrelation times will be referred to as the relaxation time of the system, in the simulations the relaxation time will always correspond to the chain exchange correlation time. The relaxation time will provide a method of determining the minimum number of N–bead cycles that are required for the system to reach equilibrium. The next four sections define the model autocorrelation functions.

3.6.1 Chain Extraction

There are two chain extraction autocorrelation functions that are calculated, the weighted and the unweighted. The weighted autocorrelation function is weighted relative to the number of molecules in an aggregate. They both can be defined by

$$\phi_{ext}(t) = \frac{\langle \theta(t)\theta(0) \rangle}{\langle \theta^2(0) \rangle} \tag{3.27}$$

where $\theta(t)$ is defined as

1. **Unweighted Chain Extraction;** $\theta(t) = 1$ if the amphiphile was in an aggregate at time $t = 0$ and remains at time t; otherwise $\theta(t) = 0$.

2. **Weighted Chain Extraction;** $\theta(t) = N_i$ if the amphiphile was in an aggregate of size N_i at time $t = 0$ and remains at time t; otherwise $\theta(t) = 0$.

It is then possible to calculate the weighted and unweighted autocorrelation times as

$$\tau_{ext} = \frac{\int_0^{t_i} \phi_{ext}(t)dt}{1 - \phi_{ext}(t_i)} \tag{3.28}$$

where $\phi_{ext}(t_i) = 1/e$, which implicitly defines t_i. Typically the weighted autocorrelation times are larger than the unweighted times; however, both are calculated and the larger of the two is used to determine the relevant time scale associated with chain extraction.

3.6.2 Chain Exchange

The chain exchange mechanism involves the transfer of molecules between aggregates There are also two types of chain exchange autocorrelation times, the weighted and unweighted. They can be defined as

$$\phi_{ex}(t) = \frac{\langle \theta(t)\theta(0) \rangle}{\langle \theta^2(0) \rangle} \tag{3.29}$$

In Eqn. (3.29) the function $\theta(t)$ is defined as:

1. **Unweighted Chain Exchange;** $\theta(t) = 1$ if the amphiphile was in an aggregate at time $t = 0$ and has not migrated to another aggregate at time t; otherwise, $\theta(t) = 0$.

2. **Weighted Chain Exchange;** $\theta(t) = N_i$ if the amphiphile was in an aggregate of size N_i at time $t = 0$ and has not migrated to another aggregate at time t; otherwise, $\theta(t) = 0$.

The associated chain exchange autocorrelation times are

$$\tau_{ex} = \frac{\int_0^{t_i} \phi_{ex}(t)dt}{1 - \phi_{ex}(t_i)} \tag{3.30}$$

3.6.3 End–to–End

The end–to–end vector autocorrelation is defined as

$$\phi_{\vec{\mathbf{x}}}(t) = \frac{\langle \vec{\mathbf{x}}(t) \cdot \vec{\mathbf{x}}(0) \rangle - \langle \vec{\mathbf{x}}(t) \rangle \cdot \langle \vec{\mathbf{x}}(0) \rangle}{\langle \vec{\mathbf{x}}(0)^2 \rangle - \langle \vec{\mathbf{x}}(0) \rangle^2} \tag{3.31}$$

where $\vec{\mathbf{x}}$ corresponds to one of the following

- End–to–end vector of an amphiphile $\vec{R}_s$.

- End–to–end vector of either block of the amphiphile, the head group $\vec{R}_h$ or the tail group $\vec{R}_t$.

The corresponding end–to–end vector autocorrelation time is then calculated from

$$\tau_{\vec{\mathbf{x}}} = \frac{\int_0^{t_i} \phi_{\vec{\mathbf{x}}}(t)dt}{1 - \phi_{\vec{\mathbf{x}}}(t_i)}. \tag{3.32}$$

3.6.4 Diffusion

It is also necessary to allow time for the amphiphiles to move throughout the system. The diffusion time characterizes the relevant time scale associated with the diffusion of molecule through the system. The diffusion constants D are calculated as

$$D = \lim_{t\to\infty} \frac{\langle \vec{d}^2(t) \rangle}{6t} \tag{3.33}$$

where $\vec{d}(t) = \vec{r}(t) - \vec{r}(0)$ is the displacement of a molecule from its initial position at time t relative to its position at time $t = 0$. A relevant time scale associated with this is the time necessary for a polymer to travel the average distance between molecules

$$\tau_D = \frac{\bar{x}^2}{6D} \tag{3.34}$$

where $\bar{x} = (6V/\pi N_s)^{1/3}$ [99], N_s denotes the total number of amphiphiles in the system and V is the total volume of the system.

There are other autocorrelation functions that can be calculated. Nelson *et al.* [95] have used the weight average aggregation number autocorrelation function which is defined as

$$\phi_N(t) = \frac{\langle N(t)N(t'+t) \rangle - \langle N \rangle^2}{\langle N^2 \rangle - \langle N \rangle^2} \tag{3.35}$$

where $N(t)$ is the weight average aggregation number at time t [95] and the averages are over all molecules and all times t'. The associated aggregation number autocorrelation time τ_N is calculated as

$$\tau_N = \frac{\int_0^{t_i} \phi_N(t)dt}{1 - \phi_N(t_i)} \tag{3.36}$$

Nelson *et al.* also claim that it is possible to estimate a time scale τ_{size} necessary to achieve a smooth aggregate size distribution as

$$\tau_{size} = \frac{\langle N(0)\rangle\langle N^2(0)\rangle}{N_s}\tau_N \tag{3.37}$$

where N_s is the total number of molecules in the simulation. A worthwhile future endeavour would be to include this autocorrelation time and compare the time scale with those being calculated in this thesis.

It is noteworthy that the calculated autocorrelation times from the simulations appear to be strictly monotonically decreasing functions of the number of Monte Carlo steps used. They are exponential or stretched exponential functions and may be composed of contributions from several different time scales in the systems [99]. For example, the end–to–end autocorrelation time may have contributions arising from free molecules, aggregates of two molecules, and so forth [100].

3.7 Monte Carlo Simulations: A Practical Algorithm

This chapter has provided a description of the model used to study the self–assembly of amphiphilic molecules in terms of: model interactions, structures of the model molecules and model autocorrelation functions. It is useful to construct a general picture of the Monte Carlo simulations and how they are carried out in terms a practical working algorithm. This algorithm is the basis of the simulation code for the Monte Carlo simulations.

The simulation code has been written predominantly in **Fortran 77** with some **C**. The code itself is platform independent and is a serial code, in the sense that it runs on a single processor. The simulations have been carried out on a multitude of different computing platforms at various high performance computing sites across Canada made available through the nationwide computing initiative **C3.ca** Inc. A full copy of the current code is

also included in the CD-ROM accompanying this thesis.

Algorithm 1 The Monte Carlo Algorithm: Applied to Self–Assembly

Require: Read appropriate input data files: These files specify the details of the simulation, including: the length of the molecules Z_s, Z_{st}, Z_{sh}, number of molecules N_s, the dimensions of the lattice L^3, τ_{max} and all other variables.

if New Simulation **then**

Perform all necessary initializations, including input parameters.

Place molecules randomly on lattice.

else if Simulation is to be restarted or continued. **then**

Perform all necessary initializations.

Read previous data.

Do necessary analysis on the previously recorded data and record results.

end if

if Warmup stage is needed **then**

Set $\varepsilon_{ts}, \varepsilon_{th}, \varepsilon_{hs} = 0$ and iterate system for N_{warm} N–bead cycles. This is done to randomize the system before a simulation is carried out. A warm up stage is usually required.

end if

Increment interaction parameters by $\delta\varepsilon_{ij}$

Algorithm 2 The Monte Carlo Algorithm: Applied to Self–Assembly (cont.)

while $\varepsilon < \varepsilon_{max}$ **do**

Implement Metropolis algorithm, choosing moves and molecules at random.

Monitor autocorrelation times and calculate the relaxation time.

Iterate system for specified number of relaxation times.

Collect averages over specified number of relaxation times.

Record results and positions of molecules.

Increment interaction parameters ε_{ij} by $\delta\varepsilon_{ij}$.

end while

STOP

Chapter 4

A Systematic Study of Self–Assembly

"Discovery consists of seeing what everybody has seen

and thinking what nobody has thought."

Albert von Szent–Gyorgyi.

4.1 Introduction to Model Systems of Interest

The focus of this chapter is to implement the Monte Carlo model as described in Chapter 3 to examine systems of amphiphiles and solvent, and to make qualitative comparisons with the theories of Chapter 2. A systematic examination of the aggregation of amphiphilic molecules based on the variation of the length of the molecules Z_s and the reduced interaction parameters ε_{ij} is carried out. The crux of the work is based on the variation of Z_s and its effects on various observables in the system including: aggregate composition, the aggregate size distribution, the critical micelle concentration and aggregate morphology. A better understanding of systems of self–assembling amphiphiles can provide predictive capabilities for their properties and behaviour.

4.1.1 Model Systems: An Overview

Monte Carlo simulations were first used to study systems of self–assembling amphiphiles by Larson [59, 60, 62, 63] and Pratt *et al.* [103, 104]. These studies focussed on short chain lengths, typically with $Z_s \leq 4$, in two dimensions, with relatively large amphiphile concentrations, $\phi_s > 40\%$. A number of subsequent studies have appeared in recent years, most notably those contained in references [4, 10, 27, 51, 59, 76, 99, 105, 121, 140]. Other simulation techniques have been employed to study aggregation including Molecular Dynamics [5, 9, 24, 25, 38, 48, 56, 97, 126, 143] and vector field models [13]. Monte Carlo, nevertheless, has remained a popular method.

The range of Z_s used in the simulations in this thesis is $5 \leq Z_s \leq 22$, with the molecules ranging from symmetric, $Z_{st} = Z_{sh}$, to highly asymmetric $Z_{st} \gg Z_{sh}$. Typical interaction parameters used in the simulations are such that

$$0 \leq \varepsilon_{ts} \leq 1.5 \tag{4.1}$$

The accessible range of interaction parameters, in the model, is severely restricted by the length of the molecules Z_s and other criteria including the total concentration. This will be illustrated in the section on relaxation times.

A simple schematic phase diagram for a dilute solution of amphiphiles is shown in Figure 4.1. Region I corresponds to a solution of free amphiphiles and small aggregates of typically less than 10 molecules. Region II is a single phase region consisting of a dilute solution of micelles in dynamic equilibrium with free molecules. Region III corresponds to free molecules in equilibrium with precipitated crystals. Region IV is a two phase region with both a solute and solvent rich phase [17].

The typical phase behaviour for a dilute solution of amphiphiles in a solvent is: micelles

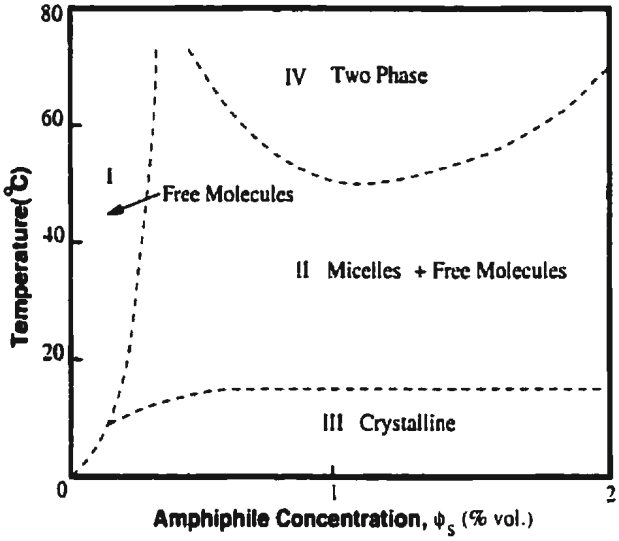

Figure 4.1: Schematic phase diagram for a dilute solution of amphiphiles and solvent. (Reproduced from DeGiorgio [17]).

form above a temperature T_o and a amphiphile concentration ϕ_{cmc} [17] [1]. In Region II the average micelle aggregation number increases with decreasing temperature and increasing concentration [17]. Degiorgio [17] notes that the effects of temperature and concentration (for low concentrations) are rather small. As an example, consider sodium dodecyl sulphate (SDS) in water. At 25°C and at the CMC, this system has an average aggregation number of approximately 95. At a concentration of 100 times the CMC the average aggregation number is approximately 112 [17]. For the same system at the CMC and at 40°C, the average aggregation number is roughly 85 [17]. For more discussion of the phase behaviour of dilute systems, the reader is referred to references [17, 42, 91, 132].

The transition to the micellar phase is not a true phase separation process [17] since there is no well defined critical concentration at which the transition occurs; rather, there exists a very narrow concentration range below which no micelles exist and above which

[1] ϕ_{cmc} is referred to as the critical micelle concentration; however, the transition to the micellar phase is not a true phase transition, and ϕ_{cmc} does not indicate a critical point.

essentially all added amphiphile enters the micellar phase [17]. For this reason ϕ_{cmc} is usually defined in terms of the fraction of molecules in aggregates. The Monte Carlo simulations in this thesis operate at a fixed concentration and vary the reduced interaction parameters (corresponding to varying the temperature). Each simulation explores a small section of the phase diagram for a given concentration, the concentration range used in the simulations in this thesis is roughly $2.5\% \leq \phi_s \leq 9\%$. The results from the simulations represent vertical tracts on the phase diagram in Figure 4.1 going from Region I to Region II, i.e., they examine the transition from a region of free molecules to a region of micelles in dynamic equilibrium with free molecules.

4.1.2 Relaxation Times and Equilibrium

The relaxation times as outlined in Chapter 3 are used to determine the appropriate time scales over which to collect averages. In this section, the autocorrelation and diffusion time(s) from several simulations are presented.

It is useful to (re)introduce some of the notation that will be used throughout the following discussion:

- Z_s, Z_{st}, Z_{sh}: The total length of the amphiphile, tail– and head–group respectively in monomer units.
- ϕ_s, X_{tot}: The total volume and mole fraction of amphiphile, respectfully.
- N_s: The total number of amphiphiles in the system.
- τ_{max}: The number of relaxation times used for equilibrating and collecting averages.
- h_i: i denotes the ratio of the tail to head–solvent interaction parameters, i.e., $i = |\frac{\varepsilon_{hs}}{\varepsilon_{ts}}|$.

Consider a system composed of $N_s = 2000$ symmetric molecules of length $Z_s = 14$, $Z_{st} = Z_{sh} = 7$, a total volume fraction of $\phi_s = 2.5\%$ and a total mole fraction of $X_{tot} = 0.1857\%$. A plot of the logarithm of the various correlation and the diffusion time(s) as a function of the interaction parameter is shown in Figure 4.2. The range of the interaction parameters for this system is $0 \leq \varepsilon_{ts} \leq 0.75$. This system is a h_2 system, i.e., $|\frac{\varepsilon_{hs}}{\varepsilon_{ts}}| = 2$.

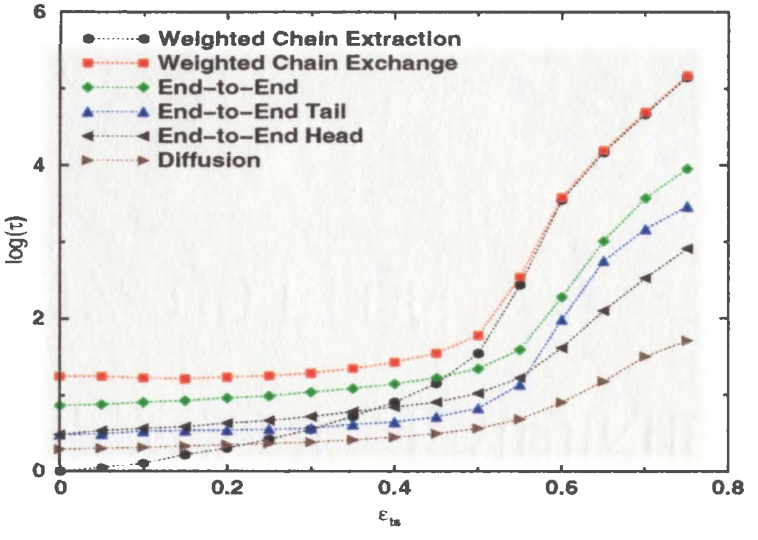

Figure 4.2: Logarithm of the diffusion and autocorrelation time(s) for a h_2 system of $N_s = 2000$ symmetric molecules with $Z_s = 14$, $Z_{sh} = Z_{st} = 7$ and a volume fraction of $\phi_s = 2.50\%$.

The diffusion and correlation time(s) are roughly constant up to an interaction parameter of $\varepsilon_{ts} = 0.5$. Upon further increase in ε_{ts}, several of the times increase by an order of magnitude with small increments in the interaction parameter. The relaxation time for the system corresponds to the weighted chain exchange correlation time for all values of the interaction parameter. The increase in the relaxation time limits the accessible range of interaction parameters since an order of magnitude increase in the relaxation time (in some instances) increases the computational time necessary to carry out the simulations, from days to weeks (depending on the value of the interaction parameter). As will be illustrated

later in this chapter this increase in the relaxation time, above an interaction parameter of $\varepsilon_{ts} = 0.5$, corresponds to the onset of micellization in the system. The value of ε_{ts} at which this occurs is system specific and depends on the value of Z_s, the concentration in the system, and other parameters.

Next, consider a system composed of 2000 asymmetric molecules of length $Z_s = 5$ with $Z_{st} = 2$, $Z_{sh} = 3$ and a total volume fraction of $\phi_s = 5.14\%$. Figure 4.3 shows the diffusion and autocorrelation time(s) for this system as a function of the interaction parameter ε_{ts}.

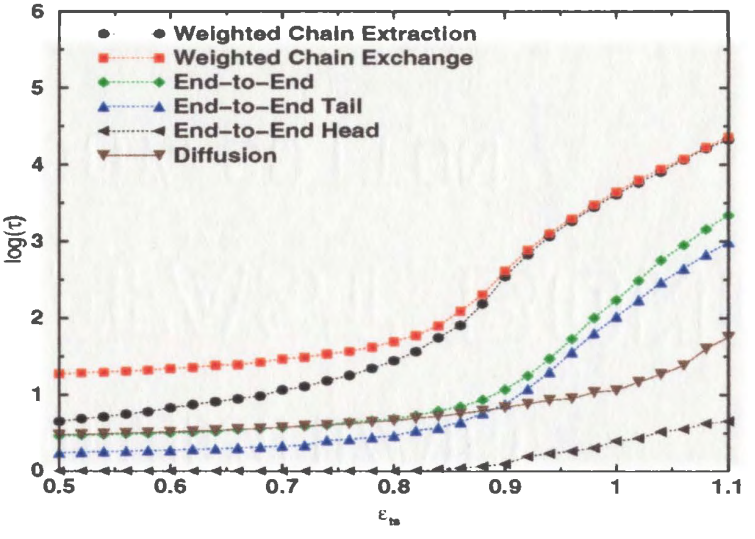

Figure 4.3: Logarithm of the diffusion and autocorrelation time(s) for a h_2 system of $N_s = 2000$ asymmetric molecules of length $Z_s = 5$, $Z_{st} = 3$ and a total volume fraction of $\phi_s = 5.14\%$.

In this system the times are roughly constant up to an interaction parameter of $\varepsilon_{ts} = 0.8$, then rapidly increase up to an interaction parameter of $\varepsilon_{ts} = 1.10$. The relaxation time for the system, corresponding to the weighted chain exchange correlation time increases by nearly four order of magnitude from $\varepsilon_{ts} = 0.8$ to $\varepsilon_{ts} = 1.1$.

From a physical perspective, it is possible to understand why the chain exchange cor-

relation time corresponds to the relaxation time of the system in the following manner. For small ε_{ts}, the formation of aggregates is essentially a random process, and there are very few of these aggregates at any time. Once an amphiphile leaves one of these random aggregates it takes a long time to encounter another one. For large ε_{ts}, most chains are in aggregates, and the rate determining step is the escape of a molecule from an aggregate. This takes a relatively long time, because of the large energetic penalty associated with the extraction of a molecule from an aggregate to solution. Once a molecule has escaped from a micelle, it then takes some additional time for it to be reabsorbed (to join) another aggregate. The result is that the extraction and exchange times are nearly equal, but the latter is always somewhat larger since it takes more time for a molecule to be extracted and further reabsorbed into an aggregate. In all cases in this thesis, the weighted chain exchange correlation time corresponds to the relaxation time of the system.

The value of ε_{ts} at which the diffusion and correlation time(s) begin to increase depends on the length of the molecules Z_s. As Z_s increases, this value decreases. This, compounded with the consequent increase in computational time, limits the range of interaction parameters which are accessible as a function of Z_s. This, in turn, affects the examination of properties of the systems as a function of Z_s at constant value of the interaction parameter.

Chain extraction and chain exchange are key to the formation, growth and dissolution of aggregates [21]. In general, it is seen that the chain exchange correlation time corresponds to the relaxation time of a system. Pépin [99, 100] has shown that it is sufficient to iterate the system for 100 to 200 multiples of the relaxation time for the purposes of equilibrating the system and collecting averages. Pépin [99, 100] has also investigated relaxation times and hysteresis. It has been shown that cooling and heating lead to no hysteresis in the correlation times, provided at least 100 times the relaxation time are used [99, 100].

Previous investigations in the literature typically have not used this method of relaxation times for determining when the system is at equilibrium [10, 58, 105]. The published results

in the literature typically iterate the systems for a specified number of iterations and assume that equilibrium results are obtained. The relaxation times suggest that the characteristic time scale varies by orders of magnitude with small increments in the interaction parameter and so choosing a fixed number of iterations with which to run the simulations at different values of the interaction parameter will not ensure equilibrium. Many of the results in the literature exhibit nonequilibrium effects, especially in terms of the size distribution [10, 58, 105].

For most systems in which a distinct micellar phase exists, the autocorrelation and diffusion time(s) behave in a similar manner; however, the actual value of the interaction parameter at which the times begin to increase depends on the properties of the system such as Z_s and ϕ_s. Typical simulations (in real time) often take a few days to reach the critical interaction parameter at which micellization onsets. The stopping criterion for the simulations is simply to gauge whether data can be generated in a feasible amount of time.

4.2 Micelle Composition

In many theoretical treatments such as those discussed in Chapter 2 of this thesis, the aggregates are assumed to be spherical clusters with the tail–groups lying exclusively interior to the core and the head–groups protruding into the solvent surrounding it, as depicted in Figure 2.2 [2]. It is also often implicitly assumed that each core is of uniform density up to some radius R_c after which it is zero as discussed in Chapter 2. It is assumed in the calculation of the free energy that there is an interfacial region of negligible thickness for the purposes of calculating the entropic and surface contributions to the free energy. In this

[2]The reader should note that this composition corresponds to an average micelle composition not an instantaneous composition. In general it is possible to observe instantaneous aggregates which have no well defined shape since in the Monte Carlo model an aggregate is defined as any group of molecules which are connected to one another by at least one nearest neighbour contact.

section the interior composition of the micelles will be examined using the results from the Monte Carlo simulations.

It is advantageous to visualize the results from the simulations. The computer code has been written so as to allow the visualization of these systems in three dimensions either as individual pictures or as time lapse movies. The visualization of these systems allows a unique insight into how the aggregates behave and, using them, it is possible visualize the formation, growth and dissolution of aggregates. Several movies are included on the CD–ROM accompanying this thesis, along with several **.pdb** files, an electronic copy of this thesis, and a copy of the simulation code.

Figure 4.4 is a snapshot from the simulation with 2000 asymmetric molecules of length $Z_s = 18$, $Z_{st} = 14$, $Z_{sh} = 4$ and a total volume fraction of 4.9%. This Figure shows that there is a broad range of aggregate sizes and shapes present. It should be clear that the interface between the core and the corona is not well defined. It will be seen in the following discussion that this interfacial region has a finite width and, in some instances, is very broad. This is in contrast to the assumptions of the free energy model where it was assumed that the interfacial region was of negligible width. This picture was generated using **Rasmol v2.7**.

In the simulations the directionally averaged density profiles for the micelles are calculated. This allows an examination of the interior micelle composition in greater detail. The five calculated distribution functions are the head–, tail–group volume fraction, and the head–, tail–end and joint distribution functions. The head–, tail–end and joint distributions correspond to the end monomer of the head/tail and the joint between the head/tail respectively.

Figure 4.5 shows these distributions as a function of the distance from the center of mass

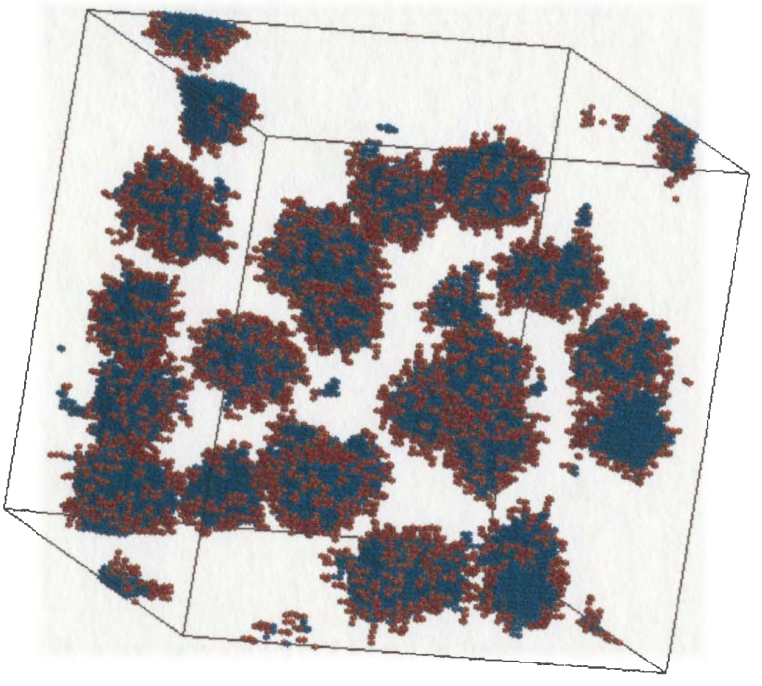

Figure 4.4: Snapshot from simulation for a system with $N_s = 2000$, $Z_s = 18$, $Z_{sh} = 4$, $Z_{st} = 14$ and $\phi_s = 4.9\%$. The unit of length is equal to a bond length.

of the micelles resulting from the same simulation as Figure 4.4[3]. This figure illustrates that the density of the core block is not uniform. The density is nearly equal to one near the center of mass; however, there is nonzero solvent penetration into the core. The core block density is approximately $\phi = 0.98$ up to 4 units from the center of mass after which it decreases to zero at about 8 units. The density profile illustrates that the aggregates have a relatively wide interfacial region which is occupied by both the core and the corona. This interfacial region is located in the range of about 4 to 8 units from the center of mass and includes most of the corona forming block.

The tail, head and joint distribution functions in Figure 4.5 contain other important in-

[3]It should be noted that the distributions are calculated as averages over ranges of aggregate sizes. The range used in Figure 4.5 is 69 to 83 molecules per aggregate. This range includes about 10% of the aggregates and coincides with the peak in this distribution.

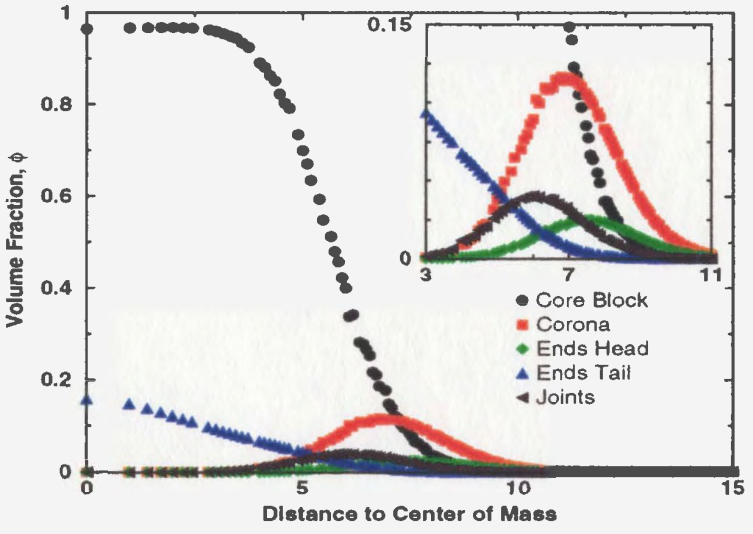

Figure 4.5: Directionally averaged density profiles and related distributions for a h_1 system with $N_s = 2000$, $Z_s = 18$, $Z_{sh} = 4$, $Z_{st} = 14$ and $\phi_s = 4.9\%$ for aggregates in the range of 69 to 83 molecules per aggregate and for $\varepsilon_{ts} = 0.45$. This is the same system as in Figure 4.4. The unit of length is equal to a bond length.

formation about the composition of the core and corona. The tail–end distribution function suggests that it is most probable to locate the tail–end of the molecule near the center of mass; however, there is a non zero probability of finding the tail–ends anywhere inside the core region. Similar results have been observed using molecular dynamics by Karaborni *et al.* [26, 48]. Marangoni [72] has also observed similar behaviour in experiments on systems of sodium dodecyl sulphate using NMR, finding that the ends of the molecules can be found throughout the core.

The joint distribution function illustrates that the joints between the head– and tail–groups are predominantly located at the center of the interfacial region (approximately 6 units from the center of mass). The head–end distribution function also illustrates that there is a greater probability of finding the head–ends farther from the center of mass than the joints, i.e., the head–groups protrude into the solvent. The peak in the head–end distribution

is located at 8 units from the center of mass. There is a non zero probability of finding the head–ends anywhere inside the coronal region and in the outer edge of the core.

The next system illustrated is composed of 1000 symmetric molecules with $Z_{st} = Z_{sh} = \frac{1}{2}Z_s = 7$ and a total volume fraction of $\phi_s = 2.5\%$. The density profile for this system is shown in Figure 4.6. These density profiles are for aggregates in the range of 35 to 40 molecules per aggregate and an interaction parameter $\varepsilon_{ts} = 0.75$.

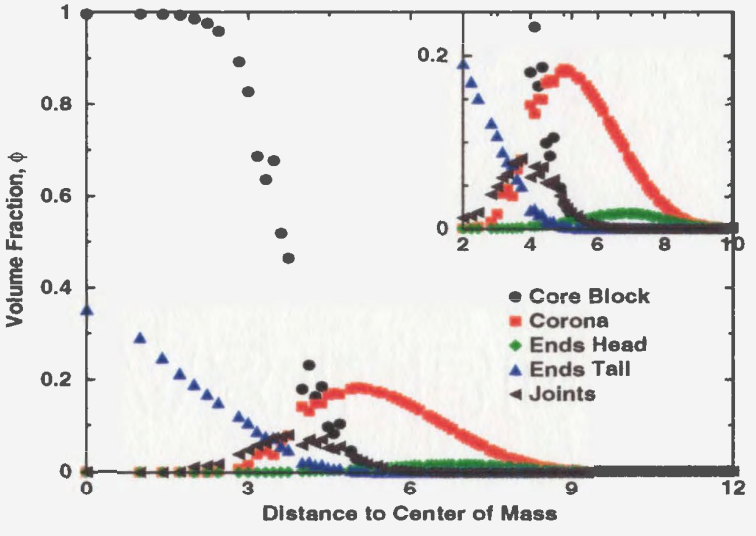

Figure 4.6: Directionally averaged density profiles and related distributions for a h_2 system with $N_s = 1000$, $Z_s = 14$, $Z_{st} = Z_{sh} = 7$ and $\phi_s = 2.5\%$ for aggregates in the range of 35 to 40 molecules per aggregate and for $\varepsilon_{ts} = 0.75$. The unit of length is equal to a bond length.

The density of the core block is very nearly $\phi = 1$ up to 3 units from the center of mass. It has a more narrow interfacial region located in the range of 3 to 5 units from the center of mass. In this system, the head–end monomers are predominantly located outside the core region. In fact, more of the head–group lies outside the core and interfacial region than was the case in Figure 4.5. In this example there is a more well defined interface and separation of the core and corona regions.

The center of the joint distribution is located at 4.0 units from the center of mass, near the outer region of the core distribution. The tail–end distribution function suggests that, although it is most likely to locate the tail–ends of the molecules near the center of mass, there is a non zero probability of locating them anywhere in the core block as in the case of the asymmetric molecules. The two previous examples are indicative of other results in terms of the density profiles.

A discussion of the aggregate morphology is provided in the second last section of this chapter. Density profiles will also be further discussed in the last section of this chapter where the relationships between the size, shape and scaling of the dimensions of the aggregates are examined.

These results illustrate that the assumed micelle composition as described in Chapter 2 can significantly differ from that obtained using the simulations. The main differences are the degree of penetration of the corona into the core block and the definition and relative width of the interfacial region. These differences manifest themselves in the comparison of the size distributions and the free energy with the results from the Monte Carlo simulations. The effects of these differences will examined in the next section.

4.3 Size Distributions

In this section an examination of the aggregate size distributions based on a systematic variation of the molecular weight Z_s and the reduced interaction parameters ε_{ij} will be presented. This examination will include a qualitative comparison between the predicted aggregate size distribution, the free energy and the results from the Monte Carlo simulations. The results show good qualitative agreement with the form of the aggregate size distribution and the free energy as discussed in Chapter 2, for a wide variety of systems. The limitations of this model will also be discussed.

4.3.1 General Discussion

One interesting aspect of the amphiphilic systems is that the aggregates which form do not have a static identity. Their size, shape and aggregation number fluctuate. These systems are in dynamic equilibrium, with a continual exchange of molecules between aggregates and solution, and among aggregates. The aggregates are polydisperse with a distribution of sizes.

The distribution of aggregate sizes is a sensitive function of system parameters including total concentration, amphiphile composition and temperature (i.e., reduced interaction parameters). Significant information about the system, such as the free energy and the CMC (critical micelle concentration) can be obtained from it. In this section a general discussion of the aggregate size distribution and its properties will be given.

Figure 4.7 illustrates the typical behaviour of the aggregate size distribution superimposed with plot of the free energy per molecule, as functions of n for two sets of interaction parameters. For low interaction parameters (high T) the bulk of the molecules are either free in solution or are in very small aggregates of fewer than 10 molecules. For high interaction parameters (low T) the system is no longer composed of mainly free molecules. Rather, the distribution develops a distinct second peak centered at a finite aggregation number, in this case at roughly $n = 25$.

The behaviour of this size distribution depends on the free energy per molecule, δ_n, and the free molecule concentration X_1. Figure 4.7 also shows a plot of the corresponding free energies. For $\varepsilon_{ts} = 1.10$, there is a shallow minimum in the free energy which corresponds roughly to the second peak in the distribution. The location of this minimum is an increasing function of ε_{ts}, i.e., it is energetically favourable to form larger aggregates with increasing ε_{ts}.

For both values of ε_{ts}, the free energy has the same general shape; however, the mini-

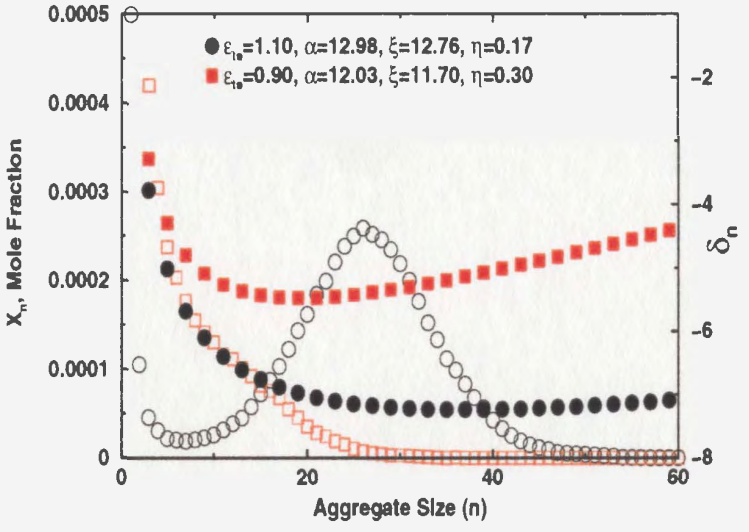

Figure 4.7: Size distribution, X_n, and free energy, δ_n, for a h_2 system with $N_s = 2000$ molecules with $Z_s = 5, Z_{st} = 3$ and a total volume fraction of $\phi_s = 5.14\%$. The size distributions correspond to the unfilled symbols and the free energy corresponds to the filled symbols.

mum in δ_n shifts to larger n with increasing ε_{ts} and becomes quite shallow. For $\varepsilon_{ts} = 0.90$ there are small aggregates but there is no well defined second peak in the distribution even though there is a well defined minimum in the free energy. For $\varepsilon_{ts} = 1.10$ there is a well defined peak at $n = 25$ and the free energy has a shallow minimum near the same value of n.

4.3.2 Calculated Size Distributions

In this section the results from the Monte Carlo simulations for the aggregate size distributions will be presented. Comparisons of results from the simulations with the expression for the size distribution and free energy of Chapter 2 are also presented. There are a number of simulations which are summarized in this section. For convenience, Table 4.1 lists them. A complete listing of the simulations is contained in Appendix A.

Figure	N_s	Z_s	Z_{sh}	Z_{st}	h_i	ϕ_s	Max ε_{ts}
4.8	2000	5	2	3	h_2	5.14%	1.10
4.12	1000	6	2	4	h_2	2.51%	0.90
4.13	1000	6	2	4	h_1	9.37%	0.95
4.14	1000	6	3	3	h_2	2.52%	0.90
4.16	500	7	2	5	h_2	5.46%	0.80
4.17	1000	8	4	4	h_1	4.55%	1.05
4.18	1000	10	2	8	h_1	8.00%	0.60
4.19	1000	15	5	10	h_1	4.73%	0.55
4.20	1000	16	4	12	h_2	3.79%	0.45
4.21	1000	20	5	15	h_2	2.56%	0.40

Table 4.1: Table of simulations contained in this section along with the Figure number in which the size distributions are shown.

The first system to be considered has 2000 molecules with $Z_s = 5, Z_{st} = 3$ and a total volume fraction of $\phi_s = 5.14\%$. Although it is convenient to plot the aggregate size distributions in two dimensions simply as functions of the aggregation number n, it is more illustrative to use a surface plot. This plot allows a convenient and unique way to visualize the distributions as functions of both ε_{ts} and the aggregation number n. The size and surface aggregate distributions for this system are plotted in Figure 4.8 and Figure 4.9, respectively, as a function of n and for $0.90 \leq \varepsilon_{ts} \leq 1.10$.

The aggregate size distributions for low values of ε_{ts} are rapidly decreasing functions of n, and the system is mainly composed of free molecules with few aggregates of greater than 20 molecules. The distribution develops a distinct second maximum (at roughly $\varepsilon_{ts} = 0.94$) which is an increasing function of ε_{ts}. For $\varepsilon_{ts} = 1.10$, the distribution has essentially

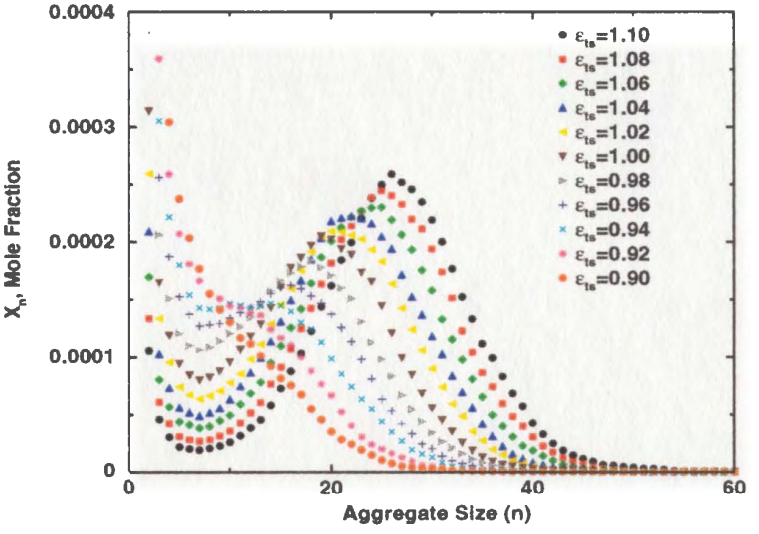

Figure 4.8: Aggregate size distributions for a h_2 system with $N_s = 2000$, $Z_s = 5$, $Z_{st} = 3$, $Z_{sh} = 2$ and a total volume fraction of $\phi_s = 5.14\%$.

separated into a distinct Gaussian peaked at $n = 27$ and a rapidly decreasing function in the range of 1 to 10 molecules per aggregate. The surface aggregate size distribution illustrates very clearly the behaviour of the aggregate size distributions over the entire accessible range of aggregation numbers and interaction parameters.

To make quantitative comparisons between the predicted form of the aggregate size distribution and the Monte Carlo simulations, nonlinear least squares fits of Eqn. (2.53) to the distributions were performed using *Xmgr* (version 4.1.2). Matlab was also used to perform curve fitting for comparison with the results from *Xmgr* and the results were in excellent agreement with each other. The results shown for the fitted curves throughout this thesis were obtained using *Xmgr*.

Figure 4.10 shows the results from the Monte Carlo simulations superimposed with the fitted curves using Eqn. (2.53). The fitting parameters are shown in the legend. The general behaviour of the distributions is emulated quite well by the fitted curves. The quality of the fit increases as ε_{ts} increases. This is, in part, due to the extreme sensitivity

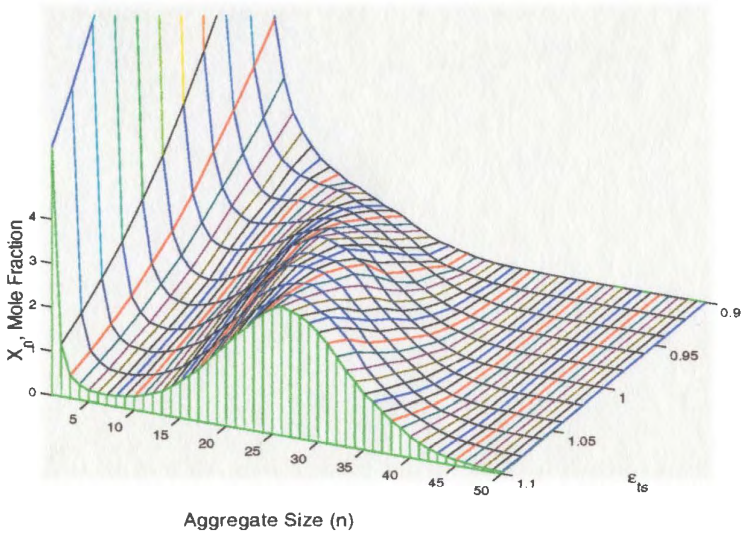

Figure 4.9: Surface aggregate size distribution for a system with $N_s = 2000$, $Z_s = 5$, $Z_{st} = 3$, $Z_{sh} = 2$ and a total volume fraction of $\phi_s = 5.14\%$.

of the distribution function to the free molecule concentration X_1, which is not a fitted parameter but is obtained directly from the simulations. The only fitted parameters are the three parameters from the free energy expression α, ξ and η.

For low interaction parameters, the systems have a large free molecule concentration X_1 which is often an order of magnitude larger than all the other X_n. It is by far the controlling factor in the expression for the distribution function, for low ε_{ts}. A small change in X_1 can significantly alter the quality of the fit. With increasing ε_{ts} the fitted curves capture the behaviour of the distributions progressively better over the whole range of aggregate sizes, which suggests that the aggregates conform somewhat better to the model used in the free energy calculations at larger ε_{ts}. The quality of fits at lower interaction parameters suggests some possible inconsistencies with the free energy expression and the model systems as detailed in Chapter 2. One of these points has already been identified, namely, the differences between the assumed micelle structure and that obtained from the Monte Carlo simulations. It will become apparent that the expression for the distribution typically leads

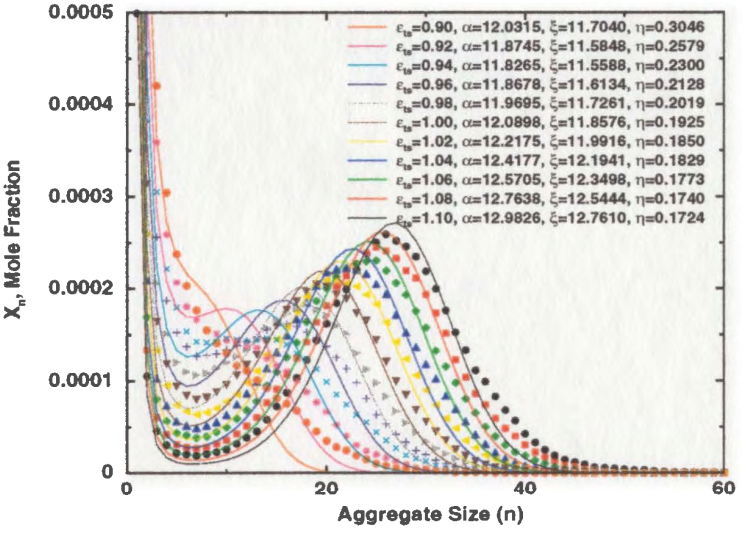

Figure 4.10: Fitted curves for a h_2 system with $N_s = 2000$ molecules with $Z_s = 5$, $Z_{sl} = 3$ and a total volume fraction of $\phi_s = 5.14\%$

to a better fit for symmetric molecules than for the asymmetric molecules.

Previous attempts in the literature to fit the distributions with similar functional forms have yielded fits which do not capture the behaviour of the distributions very well [10, 105]. Other attempts to fit them have used various functional forms [3]. These fits often describe the distribution over the whole range of aggregate sizes very well; however, there is no physical basis for describing the distributions by these arbitrarily introduced functions [3].

Figure 4.11 shows a plot of the fitted parameters as a function of ε_{ts}. These fitted parameters will be used to calculate the CMC as a function of ε_{ts}. The bulk and surface terms, α and ξ respectfully, exhibit similar behaviour; they decrease with increasing ε_{ts} up to an interaction parameter of $\varepsilon_{ts} = 0.94$ and then they both increase. The value at which they are both minimum corresponds roughly to the interaction parameter at which the total concentration is equal to the critical micelle concentration and the second peak appears in the distribution. The increase in the bulk term, α, reflects the fact that it becomes less favourable for molecules to remain in solution as ε_{ts} is increased.

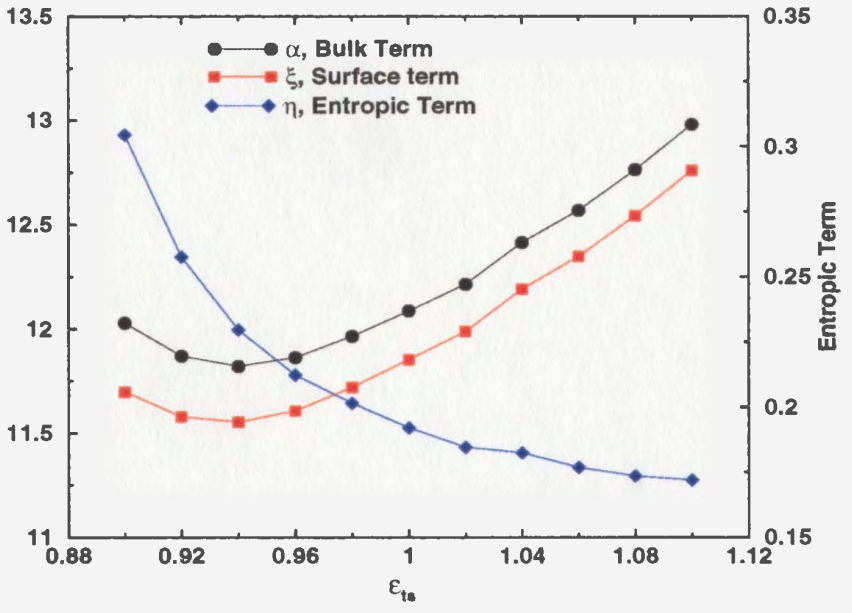

Figure 4.11: Variation of fitting parameters α, ξ and η with the interaction parameter ε_{ts}. This corresponds to the same system as in Figure 4.10.

Another useful piece of information is contained in the monotonic decrease of η with ε_{ts}. It might be expected that η would increase as a function of ε_{ts} reflecting the stretching (i.e., an increase in the average end–to–end distance) of the chains in micelles, compared with that of a free molecule. In the calculation of the entropic contribution to the free energy of Chapter 2, it is assumed that the root mean squared end–to–end distance of the tail–groups, l_{tail} is proportional to the radius of the core block of the aggregates, i.e., $l_{tail} \propto R_c$. It is also assumed that $R_c \propto n^{\frac{1}{3}}$ since it is assumed that the aggregates are tightly packed which implies that $l_{tail} \propto n^{\frac{1}{3}}$.

From the simulation results, in fact, it is found that l_{tail} is an increasing function of ε_{ts} corresponding to the elongation of the chains in micelle, as expected, but that R_c is a decreasing function of ε_{ts}. This will be discussed in more detail in the section on aggregate shape. Hence, the model calculation of the entropy incorporates a decrease in l_{tail} with ε_{ts}, when in fact it increases. The result of this difference is that the parameter η is a decreasing

function of ε_{ts}. A possible way around this (although we do not explore this) is to assume that l_{tail} in micelles is instead proportional to n^{Σ} where $0 < \Sigma < 1/3$. The scaling of the size of the aggregate as a function of n will be discussed in a later section.

The next system examined is a h_2 system with 1000 molecules of length $Z_s = 6, Z_{st} = 4$ and a total volume fraction of $\phi_s = 2.51\%$. Compared with the last system described, Z_s is increased from 2 to 3 and ϕ_s is roughly doubled. The size distributions and fitted curves for this system are shown in Figure 4.12. For interaction parameters below $\varepsilon_{ts} = 0.75$, the system is composed mainly of free amphiphiles with few aggregates of greater than 20 molecules. At an interaction parameter of $\varepsilon_{ts} = 0.80$, the distribution develops a second peak at $n = 22$, whereas for the previous system the second peak appeared at roughly $\varepsilon_{ts} \simeq 0.92$ and $n = 15$. As ε_{ts} is increased, this peak shifts towards larger aggregation numbers. At $\varepsilon_{ts} = 0.90$ the distribution is Gaussian–like, and centered at 37 molecules per aggregate; however, there is a distinct tail in the distribution extending to 70 molecules per aggregate.

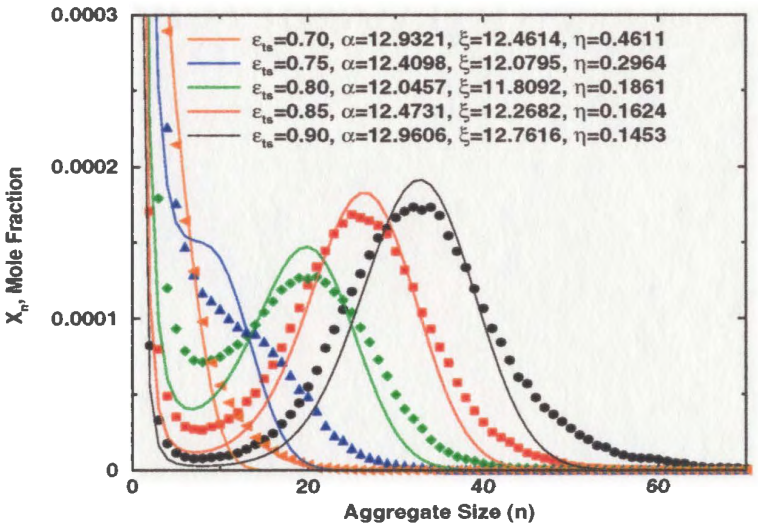

Figure 4.12: Aggregate size distribution and fitted curves for a h_2 system with $N_s = 1000$ molecules with $Z_s = 6, Z_{st} = 4, \tau_{max} = 150$ and $\phi_s = 2.51\%$.

It will be seen in a later section that the long tail in the distribution in the range from 50 to 70 molecules per aggregate corresponds to (highly) nonspherical micelles. These nonspherical aggregates are not explicitly accounted for in the expression for the free energy that was derived in Chapter 2, since the aggregates were assumed to be spherical. The tail is seen in many of the simulations and will be discussed in detail in a later section. Aside from it, the fits are relatively good, although they underestimate the width of the distribution. It is interesting to note that there appears to be a distinct knee in the distribution at roughly twice the aggregation number of the peak in the distribution for an interaction parameter of $\varepsilon_{ts} = 0.90$. This knee most likely corresponds to two aggregates coming in contact with one another.

The next system to be considered is a h_1 system of 1000 molecules with $Z_s = 6, Z_{st} = 4$ and a total volume fraction of $\phi_s = 9.37\%$. This system has a concentration of about 3 times that of the previous simulation and weaker head–group/solvent interactions. Figure 4.13 shows the aggregate size distributions for this system along with a fit to the distribution for one value of ε_{ts}. This system was examined for only two values of ε_{ts} and was not simulated from $\varepsilon_{ts} = 0$; rather, it was quenched, i.e., it was started at an interaction parameter of $\varepsilon_{ts} = 0.90$. Nonetheless, the usual process of calculating and examining the relaxation times is used, and it indicates that the system is in equilibrium and the distributions are representative of equilibrium distributions [99, 100]. System quenching was examined by Pépin [99, 100], who showed that equilibrium is achieved provided that upwards of 100 relaxation times are used for iterations.

At $\varepsilon_{ts} = 0.90$ the distribution is a relatively narrow Gaussian centered about an aggregation number of $n = 40$, plus a distinct tail which begins at an aggregation number of about $n = 50$. For $\varepsilon_{ts} = 0.95$ the shape of the distribution is significantly altered and no longer is Gaussian like. An attempt to fit the distribution for a value $\varepsilon_{ts} = 0.95$ was carried out; however, the function does not fit over the range of aggregate sizes. In order to fit

this distribution, it is necessary to modify the free energy expression to explicitly include the change in the shape of the aggregate as a function of the aggregation number. It will be seen that the long tail in the distribution extending to roughly $n = 120$ corresponds to nonspherical aggregates.

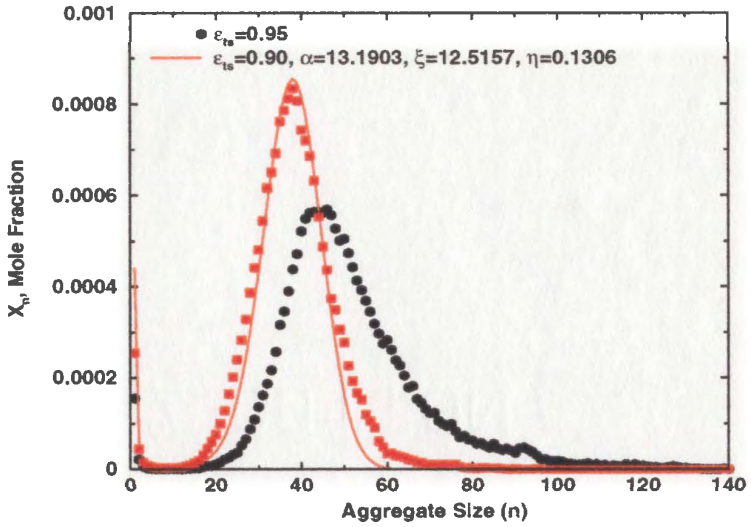

Figure 4.13: Aggregate size distributions and fitted curves for a h_1 system of 1000 molecules with $Z_s = 6$, $Z_{st} = 4$ and $\phi_s = 9.37\%$.

These distributions are markedly different than the previous example with molecules of the same length. This is in part attributed to the weaker head–group solvent interactions. Qualitatively this can be understood from the smaller energetic penalty for a head–group monomer to enter the core in a h_1 system. The energy change associated with removing a single head–group solvent contact and replacing it with a head tail contact for a h_1 system is $\varepsilon_{th} + \varepsilon_{ts}$ and for a h_2 system is $\varepsilon_{th} + 2\varepsilon_{ts}$.

Similar results have been observed by Nelson *et al.* [95] for a h_1 system with $Z_s = 4$, $Z_{st} = Z_{sh} = 2$, a volume fraction of $\phi_s = 20\%$, and at an interaction parameter of $\varepsilon_{ts} = 1.5$. A replica of this simulation was carried out in order to make comparisons, the two were in excellent agreement.

So far, the systems considered have been for moderately asymmetric molecules. Consider now a system of 1000 symmetric molecules with $Z_{st} = \frac{1}{2}Z_s = 3$, and a volume fraction of $\phi_s = 2.52\%$. This is a similar system as the first one considered in this section in Figure 4.8, except that Z_{sh} is increased from 2 to 3 and the concentration is halved. Figure 4.14 shows the aggregate size distributions and the fitted curves for this system. The distributions in Figure 4.8 and Figure 4.13 are similar. At $\varepsilon_{ts} = 1.10$ the peak in the distribution is located at $n = 20$, compared with $n = 25$ for the first system at the same interaction parameter.

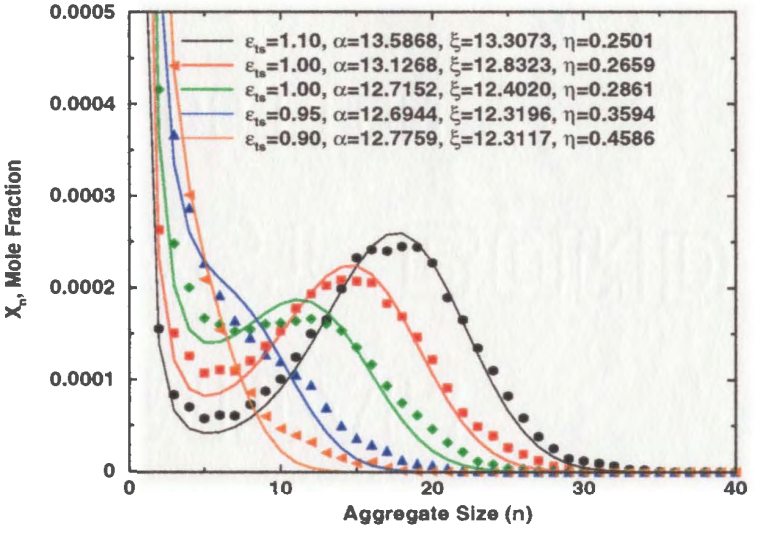

Figure 4.14: Aggregate size distributions and fitted curves for a h_2 system of $N_s = 1000$ molecules with $Z_s = 6, Z_{st} = 3$ and $\phi_s = 2.52\%$.

Figure 4.15 shows a snapshot of this system for an interaction parameter of $\varepsilon_{ts} = 1.10$. There are significantly more free molecules and smaller aggregates than in the case of the $Z_s = 5, Z_{st} = 3$ system. Even from a single snapshot it is clear that there is a broad range of aggregate sizes.

The distributions for this system have some key differences as compared with the systems in Figure 4.8. On average, the aggregates are smaller and the distributions are more

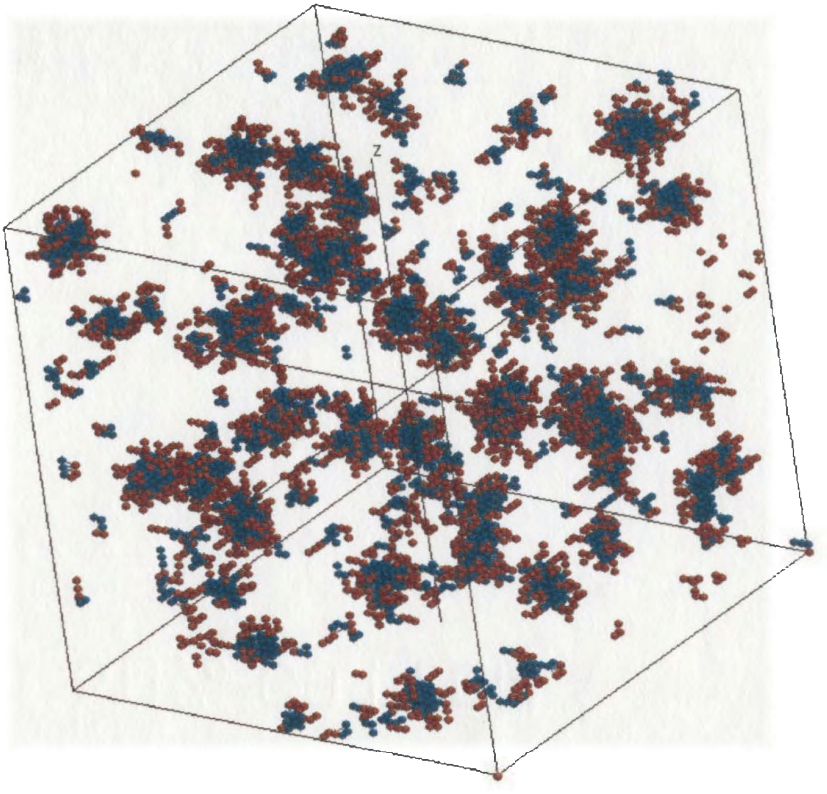

Figure 4.15: Snapshot of simulation for system with 1000 molecules with $Z_s = 6, Z_{st} = 3$, at $\varepsilon_{ts} = 1.10$ and a total volume fraction of $\phi_s = 2.52\%$.

narrow. At $\varepsilon_{ts} = 1.10$ there are few aggregates of greater than 30 molecules, whereas for the system in Figure 4.8 there are an appreciable number. These differences are attributed in part to the smaller concentration in this system and the fact that Z_{sh} is different.

In the simulations there is a minimum number of molecules required to obtain good statistics in terms of the aggregate size distributions. For most of the simulations $N_s = 1000$ has been used. The necessary minimum number of molecules compounded with the inherent increase in the relaxation times as a function of Z_{st} makes it increasingly difficult to simulate molecules as Z_{st} is increased.

The next system to be examined is a system of 500 molecules with $Z_s = 7, Z_{sh} = 2, Z_{st} = 5$, and a total volume fraction of $\phi_s = 5.46\%$. Figure 4.16 shows the fitted distri-

butions for this system superimposed with results from the simulations. The distributions are not as smooth as those in the previous system. The fitted curves still capture quite well the behaviour of the distributions over the whole range of ε_{ts} and n.

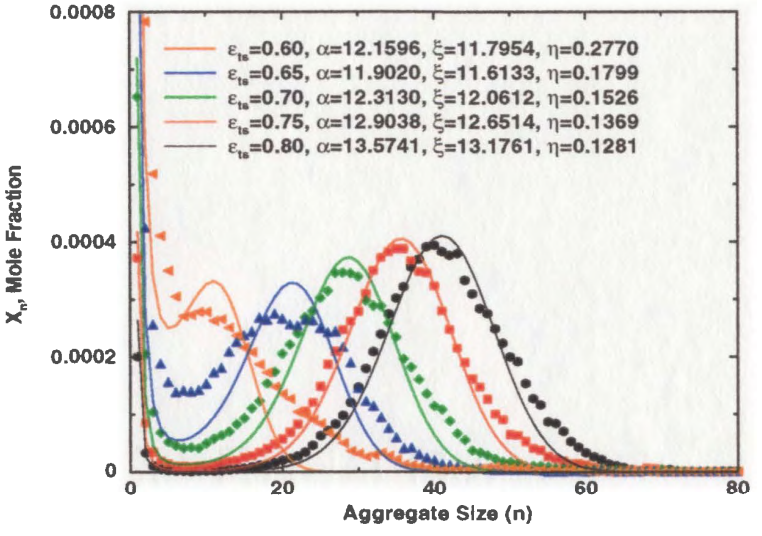

Figure 4.16: Aggregate size distributions and fitted curves for a h_2 system of 500 molecules with $Z_s = 7$, $Z_{st} = 5$ and $\phi_s = 5.46\%$.

The same system was examined with $\tau_{max} = 200$, and the results exhibit somewhat smoother size distributions. However, the shape of the distributions is the same and fits to the distributions yield the same values for the fitting parameters. A similar system with twice the number of molecules at the same volume fraction was also examined. It exhibits similar distributions as the one shown and the distributions were somewhat smoother, but with no significant improvements.

The next system to be considered is a h_1 system of 1000 symmetric molecules with $Z_s = 8$, $Z_{st} = 4$ and a total volume fraction of $\phi_s = 5.46\%$. The size distributions for this system are shown in Figure 4.17. This system differs from the previous system in that Z_{sh} has been doubled from 2 to 4 and Z_{st} has been decreased from 5 to 4.

The fitted curves capture the behaviour of the distributions very well over the whole

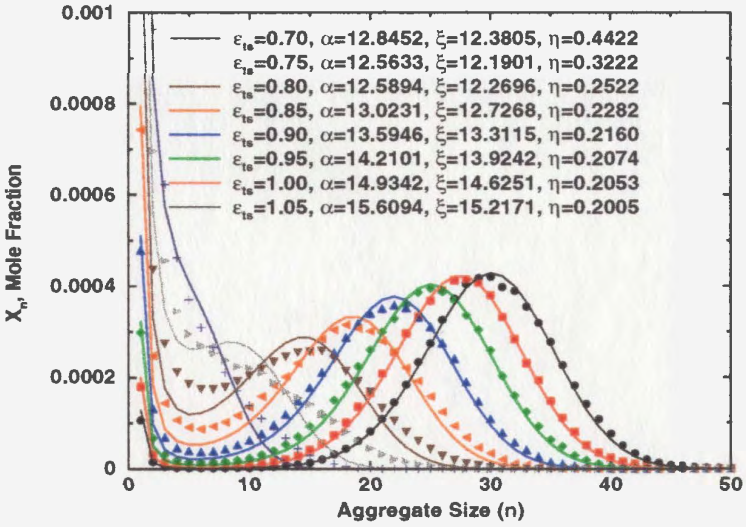

Figure 4.17: Aggregate size distribution and fitted curves for a h_1 system with $N_s = 1000$ molecules with $Z_s = 8$, $Z_{st} = 4$ and $\phi_s = 4.56\%$.

range of aggregate sizes and ε_{ts}. There is no long extended tail in the distribution as seen in some of the previous simulations. It is interesting to note that the fitted curves describe the data better as the interaction parameter increases. This is in part due to the decrease in free molecule concentration X_1.

At an interaction parameter of $\varepsilon_{ts} = 0.80$ this system has a second peak in the distribution (which is not well separated from the initial distribution) at roughly 15 molecules per aggregate, for the previous system at the same ε_{ts} the distribution had separated into a distinct Gaussian centered at approximately 40 molecules per aggregate. The dominant effect is due to the decrease in the length of the tail–group Z_{st}, since the energetic penalty for a molecule to remain in solution is roughly a linearly increasing function of Z_{st}.

Not all of the systems examined actually exhibit a well defined micellar phase. The existence of a micellar phase depends on a delicate balance between: the interactions in the system, the relative lengths of the head– and tail–groups, and the total concentration.. Some systems exhibited a non–micellar phase, with the molecules aggregating into a macrophase.

The next system illustrates this behaviour. It is a h_1 system of 1000 asymmetric molecules with $Z_s = 10$, $Z_{st} = 2$ and a total volume fraction of $\phi_s = 8.00\%$, and is shown in Figure 4.18.

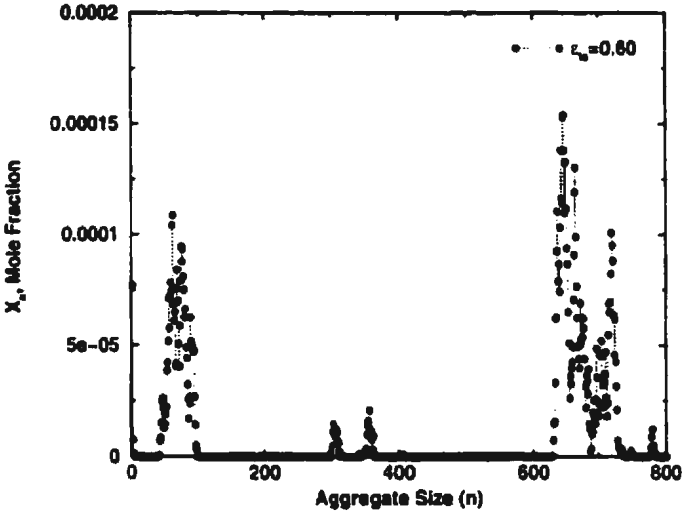

Figure 4.18: Non–micellar aggregate size distribution for a h_1 system of 1000 molecules with $Z_s = 10$, $Z_{st} = 2$ and $\phi_s = 8.00\%$.

This system is clearly macrophase separating, as indicated by the appearance of a peak in the distribution located at approximately $n = 700$. This single aggregate would contain about 70% of all of the molecules in the system. As the number of iterations increases this peak grows and becomes better defined. However, this system has not yet reached equilibrium. The reader will recall that the relevant autocorrelation times are the weighted extraction and exchange times. In this case, for such a large aggregate, these weighted times become extremely large, and in fact too large for equilibrium to be reached in a reasonable amount of computational time.

There are several reasons why this system does not exhibit distributions similar to the other systems: the molecules are highly asymmetric, it is a h_1 system and it has a relatively large concentration of $\phi_s = 8.0\%$. Similar h_2 and h_3 systems with the same chain lengths

were examined and exhibit characteristic micellar behaviour in terms of the distributions.

The next three systems are composed of asymmetric molecules with chain lengths of $Z_s = 15$, $Z_s = 16$ and $Z_s = 20$ respectively. The first of these is a h_1 system of 1000 molecules with $Z_s = 15, Z_{st} = 10$ at a total volume fraction of $\phi_s = 4.73\%$. This system, as with previous examples, exhibits a distinct second peak in the distribution above a certain interaction parameter, in this instance above $\varepsilon_{ts} = 0.40$. The distributions and the fitted curves for this system are shown in Figure 4.19.

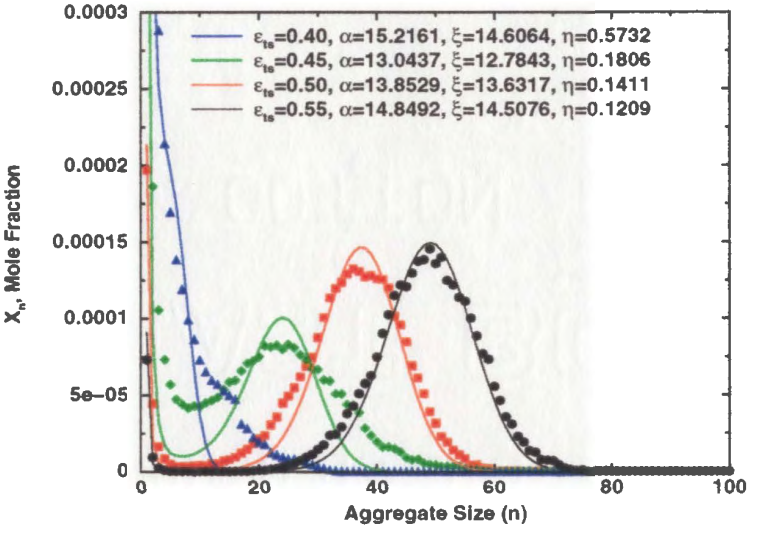

Figure 4.19: Aggregate size distributions and fitted curves for a h_1 system of 1000 molecules with $Z_s = 15, Z_{st} = 10, \tau_{max} = 60$ and $\phi_s = 4.73\%$.

For low values of ε_{ts} the fitted curves do not correctly reproduce the peak height and width. These discrepancies are attributed, in part, to the possible inconsistencies in the expression for the free energy which were discussed earlier in this section. These include the differences between the assumed micelle composition in the free energy model and that obtained from the Monte Carlo simulations. For $\varepsilon_{ts} = 0.55$, the curves fit very well over the whole range of aggregate sizes and the distribution has separated into a distinct Gaussian like distribution centered at about 50 molecules per aggregate and an initial distribution

which describes very small aggregates and free molecules.

The next system is composed of 1000 molecules with $Z_s = 16$, $Z_{st} = 12$ and a total volume fraction of $\phi_s = 3.79\%$. The differences between the simulation data and the fitted distributions shown in Figure 4.20 are similar to those in the previous case; however, it is worthwhile to bear in mind that the free molecule concentration for the system at $\varepsilon_{ts} = 0.40$ is almost an order of magnitude larger than the value of the peak in the distribution. For a value of ε_{ts} the value of X_1 is twice that of the peak in the distribution. This single point dominates the fit and affects the quality of the rest of the fit to the distribution.

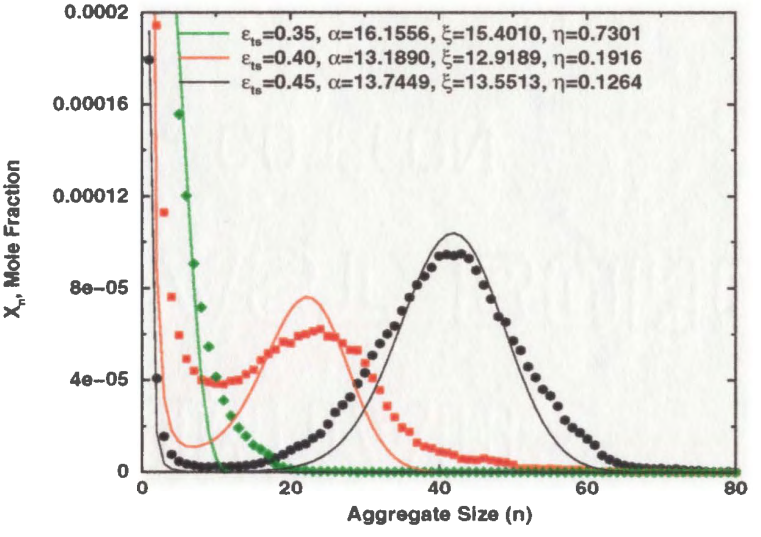

Figure 4.20: Aggregate size distributions and fitted curves for a h_2 system of 1000 molecules with $Z_s = 16$, $Z_{st} = 12$ and $\phi_s = 3.79\%$.

The final simulation of this section is shown in Figure 4.21. It corresponds to a system with 1000 molecules of length $Z_s = 20$, $Z_{st} = 15$ at a total volume fraction of $\phi_s = 2.56\%$. The behaviour of the size distribution is similar to the previous two cases. The change in the shape of the distributions may appear to be abrupt, this is an artifact of the large increment in ε_{ts}. A smaller increment would yield distributions which vary in a more incremental manner.

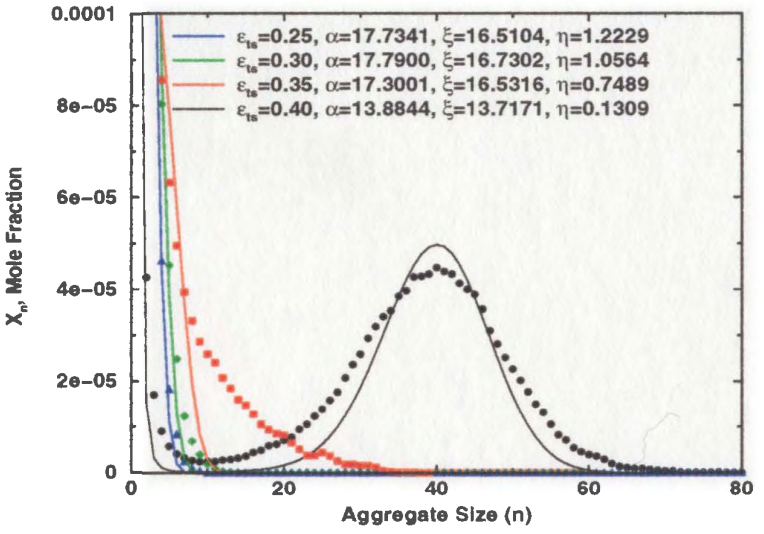

Figure 4.21: Aggregate size distributions and fitted curves for a h_2 system of $N_s = 1000$ molecules with $Z_s = 20, Z_{st} = 15$ and $\phi_s = 2.56\%$.

The fitted distributions capture the overall behaviour of the distributions obtained from the simulations; however, even for the largest value of ε_{ts}, they underestimate the width of the distribution. Again as with previous examples, the distribution exhibits distinct Gaussian behaviour, in this case at an interaction parameter of $\varepsilon_{ts} = 0.45$.

The size distributions examined in this section illustrate the behaviour of the distribution for a wide range of Z_s and ε_{ts}. The majority of the distributions behave in a very similar manner for low ε_{ts} they are rapidly decreasing functions of n. With increasing ε_{ts} the distributions develop a distinct second peak, corresponding to the onset of micellization. The value of ε_{ts} at which this occurs depends on the characteristics of the system. The distribution usually tends to a Gaussian peaked at a particular aggregation number with increasing ε_{ts}. This Gaussian distribution will be seen to correspond to roughly spherical micelles. If the interaction parameter is further increased, the distribution develops a tail extending to large aggregation numbers and the distribution is no longer Gaussian. The appearance of the tail in the distribution will be seen to correspond to the morphological

transition of aggregates with increasing n. In some cases, macrophase separation occurred, as for the system in Figure 4.18.

Using the form for the aggregate size distribution and the free energy of Chapter 2, it was also possible to fit the distributions and examine the variation of the fitting parameters as a functions of ε_{ts}. This qualitative comparison yielded good agreement. The fitting parameters will be utilized in the next section to examine the variation of the critical micelle concentration.

4.4 The Critical Micelle Concentration (CMC)

The onset of micellization in a system is typically characterized by a relatively sharp transition in observable properties as a function of concentration, with micellization occurring in a very narrow concentration range [91, 92, 93, 94, 122]. The approximate concentration at which it begins is referred to as the critical micelle concentration and denoted by X_{cmc} (in mole fractions). The phrase 'micellization begins' is somewhat misleading since the CMC is usually defined as the concentration at which there is a certain fraction of molecules in aggregates. The concept of the CMC will be refined in the following discussion.

The following discussion will focus on an examination of the CMC and its relation to the size distribution and the free energy. There are many discussions of the CMC in the literature, the interested reader is referred to references [26, 42, 91, 92, 101, 102, 122, 141].

Physically, X_{cmc}, is the total concentration in the system at which the concentration of free molecules begins to saturate. Any further amphiphile that is added to the system goes into an aggregate while the free molecule concentration remains roughly constant [12, 26, 42, 91, 105]. The interaction parameter at which the second maximum in the distribution appears corresponds roughly to the point at which the total concentration is equal to the critical micelle concentration.

Using a method suggested by Nagarajan and Ruckstein [91], it is possible to obtain an expression for X_{cmc} from the size distribution X_n defined as

$$X_n = X_1^n \exp\left(-\frac{n\delta_n}{k_BT}\right) = X_1^n \exp\left(-\frac{\Delta_n}{k_BT}\right) \tag{4.2}$$

where $\Delta_n = n\delta_n$ and where δ_n is defined as

$$\frac{\delta_n}{k_BT} = \left(-\alpha + \xi n^{-1/3} + \eta n^{2/3}\right) \tag{4.3}$$

The minimum in δ_n occurs at a specific aggregation number which can be obtained from

$$\frac{d}{dn}\left(\frac{\delta_n}{k_BT}\right)_{n=n_{cmc}} = 0 \tag{4.4}$$

The value of n at which the free energy is a minimum is denoted by n_{cmc} where

$$n_{cmc} = \frac{\xi}{2\eta} \tag{4.5}$$

It is now possible to estimate the critical micelle concentration X_{cmc}. Nagarajan and Ruckstein [91, 92] use the approximation that

$$X_{n_{cmc}} \simeq X_{n_{cmc}-1} \tag{4.6}$$

where $X_{n_{cmc}}$ is Eqn. (2.53) evaluated at n_{cmc}. Equating these two terms it is possible to write

$$X_1^{n_{cmc}} \exp\left(\frac{-n_{cmc}\delta_{n_{cmc}}}{k_BT}\right) = X_1^{n_{cmc}-1} \exp\left(\frac{-(n_{cmc}-1)\delta_{n_{cmc}-1}}{k_BT}\right) \tag{4.7}$$

It is also assumed that $\delta_{n_{cmc}} \approx \delta_{n_{cmc}-1}$, so the above expression becomes

$$X_1^{n_{cmc}} = X_1^{n_{cmc}-1} \exp\left(\frac{\delta_{n_{cmc}}}{k_BT}\right) \tag{4.8}$$

It is possible to solve the above equation for $\ln(X_1)_{cmc}$ (the logarithm of the free molecule concentration at the CMC) which is

$$\ln(X_1)_{cmc} = \frac{\delta_{n_{cmc}}}{k_BT} \tag{4.9}$$

The definition used for the CMC is the total concentration at which $X_{cmc} = 2(X_1)_{cmc}$, i.e., when half of the molecules are in aggregates [91, 105]. The critical micelle concentration in terms of the free energy evaluated at n_{cmc} is then

$$X_{cmc} = 2\exp\left(\frac{\delta_{n_{cmc}}}{k_B T}\right) \tag{4.10}$$

This is a conventional definition for the CMC; however, it is possible to define the CMC as the concentration at which an arbitrary fraction of the molecules are in aggregate [26, 91, 105]. The free energy evaluated in terms of α, ξ and η at n_{cmc} is

$$\frac{\delta_{n_{cmc}}}{k_B T} = \frac{3}{4^{1/3}}(\xi^2\eta)^{1/3} - \alpha \tag{4.11}$$

X_{cmc} can then be written as

$$X_{cmc} = 2\exp\left(\frac{3}{4^{1/3}}(\xi^2\eta)^{1/3} - \alpha\right) \tag{4.12}$$

From the simulations it is possible to calculate X_{cmc} for each value of the interaction parameter ε_{ts}. The calculated CMC values can also be examined as a function of Z_s to a limited degree, for reasons which will become apparent.

4.4.1 CMC versus Interaction Parameter ε_{ts}

In this section, the results for X_{cmc} as a function of ε_{ts} are discussed [4]. As the temperature decreases (increasing ε_{ts}) it becomes less energetically favourable for molecules to remain in solution. It is also expected that a decrease in temperature (increasing interaction parameter) would decrease the CMC. This behaviour is examined for a variety of chain lengths and X_{cmc} is calculated from the fitting parameters α, ξ and η over a whole range of interaction parameters and values of Z_s as prescribed in the previous discussion.

[4] All systems use a value of $\tau_{max} = 100$ unless otherwise specified.

The first group of molecules to be considered are those with $5 \leq Z_s \leq 9$ and various values of Z_{st} and Z_{sh}. A plot of $\ln(X_{cmc})$ as a function of ε_{ts} is shown in Figure 4.22. It is clear that $\ln(X_{cmc})$ varies approximately linearly with ε_{ts}, i.e., X_{cmc} decreases exponentially as a function of ε_{ts}.

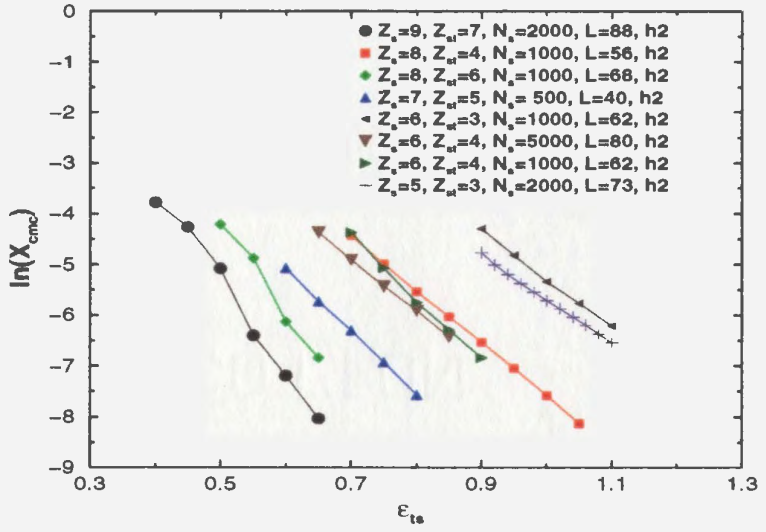

Figure 4.22: Logarithm of X_{cmc} as a function of ε_{ts} for molecules with $5 \leq Z_s \leq 9$ and various values of Z_{st} and Z_{sh}. The lines are shown as a guide to the eye.

There is little deviation from linearity of $\ln(X_{cmc})$ versus ε_{ts} even though X_{cmc} varies over several orders of magnitude. Similar behaviour is seen in systems of n–alkyl sulphates examined in analytical calculations by Nagarajan *et al.* [91, 92, 93, 94]. It is interesting to note that the systems in which the molecules are highly asymmetric are the ones in which the values for the CMC exhibit the greatest deviation from linearity.

The next set of results is for molecules with constant total length $Z_s = 10$ and various values of Z_{st}. Figure 4.23 shows a plot of $\ln(X_{cmc})$ versus ε_{ts} for these systems. For $Z_{st} = 8$, the data are localized to a small region of the graph. In fact several of the data sets nearly over lap each other, these correspond to similar systems iterated for different multiples of the relaxation time and for different values of h_i. The values of $\ln(X_{cmc})$ for

the h_3 and h_2 systems with $Z_{st} = 8$ vary only slightly by a constant amount over the range of interaction parameters $0.45 \leq \varepsilon_{ts} \leq 0.6$.

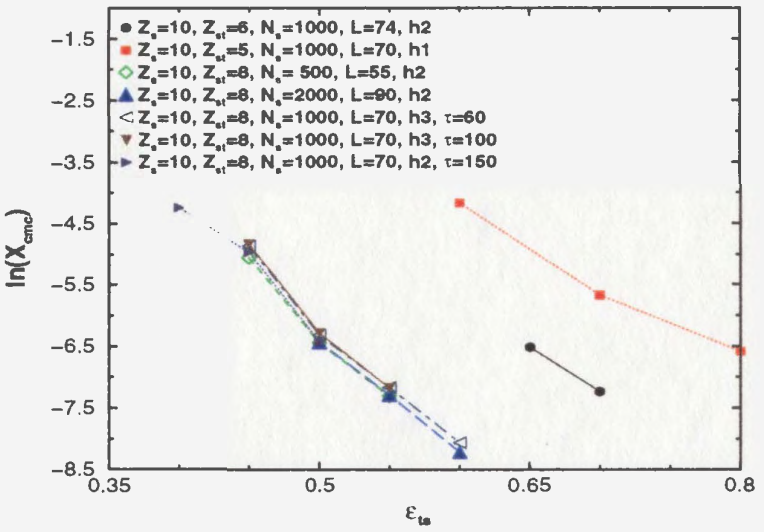

Figure 4.23: Logarithm of X_{cmc} as a function of ε_{ts} for molecules with lengths $Z_s = 10$ and various values of Z_{st}.

Figure 4.24 shows the variation of X_{cmc} with ε_{ts} for molecules with total lengths in the range $11 \leq Z_s \leq 22$. As with the previous two figures, the key thing to note is the variation of the CMC with Z_{st}. Again as in the previous examples, $\ln(X_{cmc})$ varies approximately linearly with the interaction parameter especially for the shorter chain length molecules. The highly asymmetric molecules exhibit the largest deviation from linearity; whereas, the symmetric molecules are consistently more linear.

4.4.2 X_{cmc} versus Chain Length Z_{st}

In this section the variation of the CMC as a function of the chain length of the molecules for a fixed ε_{ts} is examined. As Z_{st} increases it becomes less energetically favourable for molecules to remain free in solution since $(z-2)\varepsilon_{ts}Z_{st}$ (z is the coordination number of the lattice) is roughly the energy penalty for a molecule to remain in solution. It is also

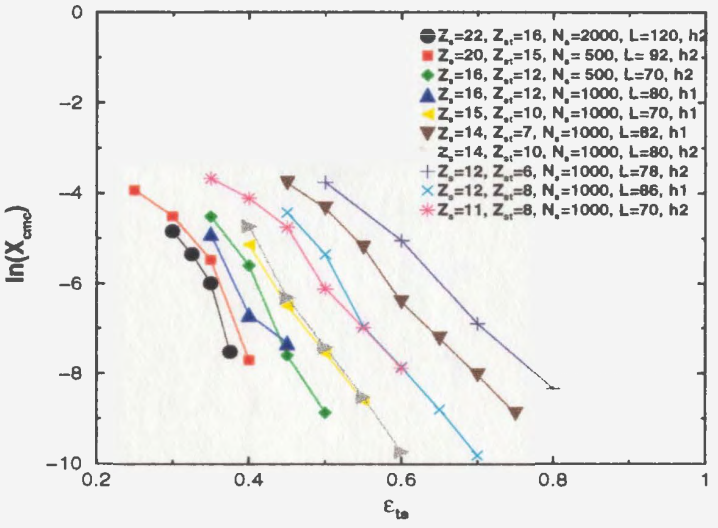

Figure 4.24: Logarithm of the CMC as a function of ε_{ts} for molecules in the range $11 \leq Z_s \leq 22$ with various values of Z_{st}.

expected that, as the chain length is increased, (at constant interaction parameter) X_{cmc} should also decrease [91, 92].

Figure 4.25 shows a plot of the logarithm of the CMC as a function of Z_{st} for two different head–group lengths. It is quite clear that $\ln(X_{cmc})$ varies linearly with Z_{st}. Even though there are few points, the data show very little deviation from linearity. The lines of best fit are given in the legend of the graph. Tanford [122] illustrates that the CMC is a linearly varying function of the carbon chain length for a variety of nonionic surfactants, including alkyl hexaoxyethylene glycol monoethers. These systems also exhibit the same linear behaviour of $\ln(X_{cmc})$ as a function of the number of carbon atoms.

The onset of micellization occurs at lower values of ε_{ts} for longer chain lengths than for shorter ones. It is difficult to bring systems with different chain lengths Z_{st} to the same interaction parameter ε_{ts} because of the increasing time scales in the simulation as a function of the interaction parameter. The relaxation time for the system begins to increase at a lower value of ε_{ts} for longer chain lengths Z_{st}.

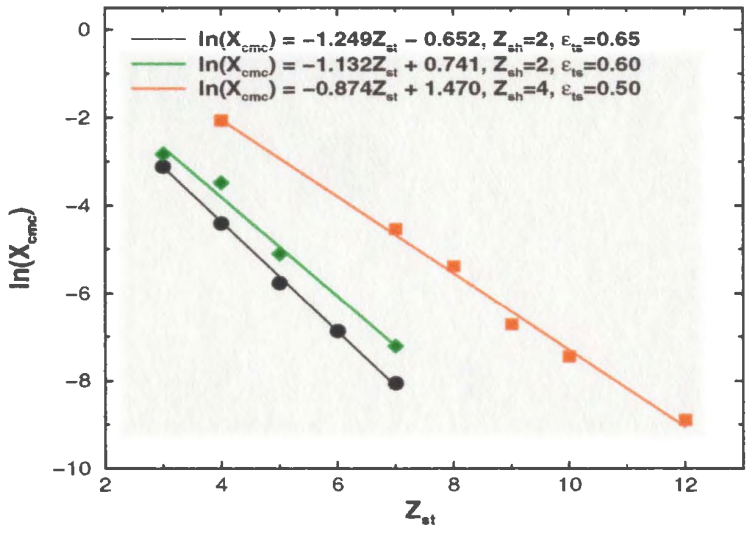

Figure 4.25: Plot of the logarithm of X_{cmc} versus Z_{st}.

4.5 Aggregate Shape and the Size Distribution

In this section a discussion of the shape of the aggregates is presented. Also included is a further discussion of the density profile and its relationship to the aggregation number. The picture which emerges from this discussion coincides with the generally accepted view of roughly spherical aggregates for low aggregation numbers and the transition of the shape of the aggregates as a function of the aggregation number [17, 26, 43].

One of the useful aspects of the Monte Carlo simulations in this thesis is that it is possible to examine, in detail, the composition, shape and structure of the aggregates over the whole range of aggregate sizes n. Most simulation techniques such as molecular dynamics typically simulate a single preconfigured aggregate [48]. As such molecular dynamics usually falls short of being able to simulate the entire aggregate size distribution [48, 53].

The shape of the size distribution will be seen to correlate with the morphology of the aggregates. For spherical aggregates, the distribution is essentially a Gaussian. It will also be seen that the appearance of highly nonspherical aggregates corresponds to the appearance of the tail in the distributions.

4.5.1 Aggregate Shape/Morphology

So far the shape of the aggregate has not been examined except in the free energy model of Chapter 2 where the aggregates were assumed *a priori* to be spherical[5]. The validity of this assumption is examined here. The morphology of the aggregates will be seen to vary markedly as a function of n.

Experimentally, measuring the shape of aggregates is a notoriously difficult problem [17, 42] and there is still some debate about the shape of aggregates in solution [17, 26, 43]. The results from the Monte Carlo simulations suggest that the average shape of an aggregate is not that of a perfect sphere (even for low aggregation numbers) rather the aggregates are prolate spheroids with increasing eccentricity as a function of n.

In order to discuss the shape of the aggregates, it is useful to quantify their shape. This is done by calculating the three ordered instantaneous principal radii of gyration and the so called asphericity parameter α_s. It is necessary to calculate the squared radius of gyration tensor of each aggregate defined as

$$\mathbf{R}^2 = \begin{pmatrix} R^2_{x_1x_1} & R^2_{x_1x_2} & R^2_{x_1x_3} \\ R^2_{x_2x_1} & R^2_{x_2x_2} & R^2_{x_2x_3} \\ R^2_{x_3x_1} & R^2_{x_3x_2} & R^2_{x_3x_3} \end{pmatrix} \tag{4.13}$$

The matrix elements $R^2_{x_ix_j}$ are defined as

$$R^2_{x_ix_j} = \frac{1}{Z_s n} \sum_{k=1}^{Z_s n} (x_{i,k} - x_{i,cm})(x_{j,k} - x_{j,cm}) \tag{4.14}$$

where $Z_s n$ is the total number of monomers in an aggregate of size n, x_i, x_j represent the three principal directions in the lattice for $1 \leq i \leq 3$, $1 \leq j \leq 3$ and $x_{i,k}$ and $x_{j,k}$ are the i^{th} and j^{th} components of the positions of the k^{th} monomer. The coordinates of the center

[5]The astute reader will note that this assumption does not apply to the aggregates in the simulations where there are no pre–assumed constraints on the aggregate shape.

of mass $x_{i,cm}$ of this aggregate are

$$x_{i,cm} = \frac{1}{Z_s n} \sum_{k=1}^{Z_s n} x_{i,k} \tag{4.15}$$

The square root of the eigenvalues of the matrix in Eqn. (4.13) are the three instantaneous principal radii of gyration of the aggregate and are denoted by $(R_x^2)^{\frac{1}{2}}$, $(R_y^2)^{\frac{1}{2}}$ and $(R_z^2)^{\frac{1}{2}}$ respectively. In the calculations these eigenvalues are ordered such that $(R_x^2)^{\frac{1}{2}} \leq (R_y^2)^{\frac{1}{2}} \leq (R_z^2)^{\frac{1}{2}}$ are calculated as averages over all aggregates of size n The average values of these ordered eigenvalues are calculated in the simulations and will be referred to as the average principal radii of gyration (or simply the principal radii of gyration for brevity) and will be denoted by $\langle R_x^2 \rangle^{\frac{1}{2}}$, $\langle R_y^2 \rangle^{\frac{1}{2}}$ and $\langle R_z^2 \rangle^{\frac{1}{2}}$ herein.

For a perfect sphere the three principal radii of gyration are equal, i.e.,

$$\langle R_x^2 \rangle^{\frac{1}{2}} = \langle R_y^2 \rangle^{\frac{1}{2}} = \langle R_z^2 \rangle^{\frac{1}{2}} \tag{4.16}$$

For an infinite cylinder two of the principal radii of gyration are equal while the third is infinite , i.e., $\langle R_x^2 \rangle^{\frac{1}{2}} = \langle R_y^2 \rangle^{\frac{1}{2}} < \infty$ and $\langle R_z^2 \rangle^{\frac{1}{2}} \to \infty$. A more thorough analysis of the aggregates (in the Monte Carlo model) would include calculations of the radii of gyration of both the core block and of the entire aggregate and the mean squared fluctuations of these values.

Another useful quantification of the shape of the aggregates is the asphericity parameter α_s [95, 105] defined by

$$\alpha_s = \frac{\sum_{i>j=1}^{3} \left(\langle R_i^2 \rangle^{\frac{1}{2}} - \langle R_j^2 \rangle^{\frac{1}{2}} \right)^2}{2 \left(\sum_{i=1}^{3} (\langle R_i^2 \rangle^{\frac{1}{2}})^2 \right)} \tag{4.17}$$

The asphericity parameter of an aggregate has a value of $\alpha_s = 0$ and $\alpha_s = 1$ for a perfect sphere and an infinite cylinder, respectfully. Conventionally, an aggregate is considered

spherical [95, 105] if

$$0 \leq \alpha_s \leq 0.1 \tag{4.18}$$

The results of Section 4.3.2 show that the distribution functions often exhibit distinct Gaussian like behaviour with an extended tail. In a complementary way to the principal radii of gyration, the Gaussian like nature of the distributions and the appearance of the extended tail will be used to examine the change in the shape of the aggregates.

It is possible to fit the distributions (excluding the tail) with a Gaussian. Furthermore, it is possible to introduce an expression which explicitly accounts for the tail in the distribution. This expression cannot be derived from a physical context, rather it is introduced on a mathematical basis. Nonetheless, combining these two approaches and using the principal radii it will be possible to examine the change in aggregate shape as a function of n and interpret this growth in terms of a change in the shape of the aggregate distribution function as a function of ε_{ts}.

Israelachvilli [43] notes that it is possible to express the aggregate size distribution in terms of a Gaussian like distribution of the following form

$$X_n = n\left\{\left(\frac{X_M}{M}\right)\exp\left[M\beta(\mu_M^\circ - \mu_n^\circ)\right]\right\}^{\frac{n}{M}} \tag{4.19}$$

where M corresponds to the position of the peak in the Gaussian, X_M the mole fraction at this peak position, and where μ_n° are the standard chemical potentials as discussed in Chapter 2. This is a trivial extension of the formalism discussed in Chapter 2. The existence of a Gaussian distribution will be seen to correspond to a system composed of roughly spherical micelles.

To fit the distributions from the simulations a Gaussian of the following form is used

$$X_n^{sphere} = C_M \exp\left[\frac{-(n-M)^2}{2\sigma^2}\right] \tag{4.20}$$

where C_M is the mole fraction at M and σ is the standard deviation of the distribution. It should be noted that the only parameters for fitting the curves are M, σ and C_M[6].

Nelson *et al.* [95] note that it is possible to fit the distributions including the tail by superimposing the Gaussian in Eqn. (4.20) with a so called matching function of the form

$$X_n^{tail} = \zeta \exp(-\psi n)(1 - X_n^{sphere}/C_M) \quad n \geq M \tag{4.21}$$

where ζ and ψ are constants. Combining Eqn. (4.20) and Eqn. (4.21) it is possible to fit (continuously) the distributions including the tail with a function of the following form[7]

$$X_n = \begin{cases} C_M \exp\left[\frac{-(n-M)^2}{2\sigma^2}\right] & n \leq M, \\ C_M \exp\left[\frac{-(n-M)^2}{2\sigma^2}\right] + \zeta \exp(-\psi n)\left(1 - \exp\left[\frac{-(n-M)^2}{2\sigma^2}\right]\right) & n \geq M \end{cases} \tag{4.22}$$

Although this procedure accounts for the tail in the distribution on a purely mathematical basis, it will allow an interpretation of the transition from spherical to nonspherical micelles. It will be seen that a nonzero contribution of the matching function can be correlated with the appearance of an appreciable number of highly nonspherical micelles (cylinders) in the system.

In this description it is presumed implicitly that the highly nonspherical micelles do not exist for aggregation numbers below $n = M$ corresponding to the peak in the distribution. Above this aggregation number there may exist a region of coexistence between spherical and nonspherical micelles. Physically it is expected that the absolute cutoff aggregation number for spherical micelles, n_{crit} corresponds roughly to $n_{crit} = Z_{st}{}^2 \frac{4\pi}{3}$.

This corresponds to the aggregation number at which the micelles are tightly packed into spheres (under the assumption of perfectly spherical micelles) with a radius equal to the fully stretched chain length of the molecules. Since the aggregates are not close packed, this value of n_{crit} is just used as a guide to understand the growth of the aggregates.

[6]Typically $C_M \approx X_M$ but since C_M is a fitted parameter a different notation is used.

[7]In actually fitting the distributions the range of n is typically restricted to be such that $n > 10$.

To illustrate the previous discussion, several sets of simulation results will be presented. The first system to be considered is composed of 2000 molecules with $Z_s = 5, Z_{sh} = 3$, a total volume fraction of $\phi_s = 5.14\%$ and an interaction parameter of $\varepsilon_{ts} = 1.10$. This is the same system as considered previously and is shown in Figure 4.8. Figure 4.26(a) and Figure 4.26(b) show the size distribution superimposed with the principal radii of gyration, a Gaussian fit to the distribution (for $\varepsilon_{ts} = 1.10$) and the asphericity parameter.

It is clear from Figure 4.26(a) that the three principal radii of gyration are not equal over the whole range of aggregate sizes. In fact, the two smallest principal radius of gyration increase slightly up to an aggregation number of approximately $n = 30$ after which they both remain roughly constant. The third principal radius of gyration also increases slowly up to $n \simeq 30$ after which it increases rapidly. It is not surprising that the radii of gyration increase since the size of the aggregate increases with increasing n. However, the interesting thing to note is that the two smaller dimensions of the aggregate tend to an approximate value of 1.5 and the third increases dramatically with increasing n.

According to the convention that aggregates with $\alpha_s < 0.1$ are considered spherical, it would appear that aggregates with less than roughly 30 molecules are nearly spherical. By inspection of the principal radii it would seem that the inflection point in the largest radius of gyration is located near 30 molecules per aggregate. This corresponds to the transition from spherical to prolate spherical micelles with increasing aggregation number.

There are very few aggregates of greater than 30 molecules. In an entirely complementary way, this is reflected in the fits to the distribution functions using the prescribed Gaussians and so–called matching functions. The fitted distributions and the simulation results are shown in Figure 4.27. The fits were performed for aggregates with greater than 10 molecules per aggregate. It is clear that the matching function makes a contribution to the fit which is almost negligible even for an interaction parameter of $\varepsilon_{ts} = 1.10$. This corresponds to the very small number of aggregates that are highly nonspherical, i.e., with

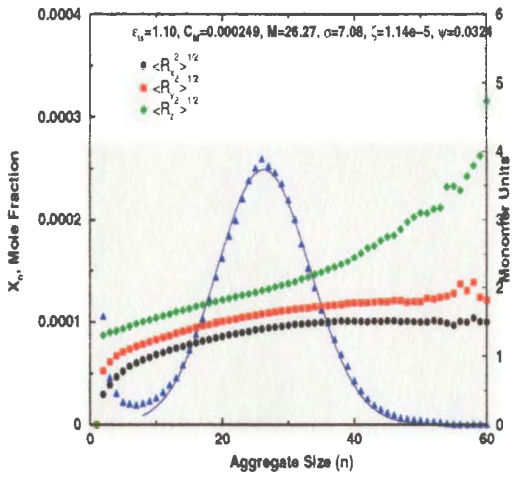

(a) Principal radii of gyration versus aggregation number and Gaussian fit to distribution.

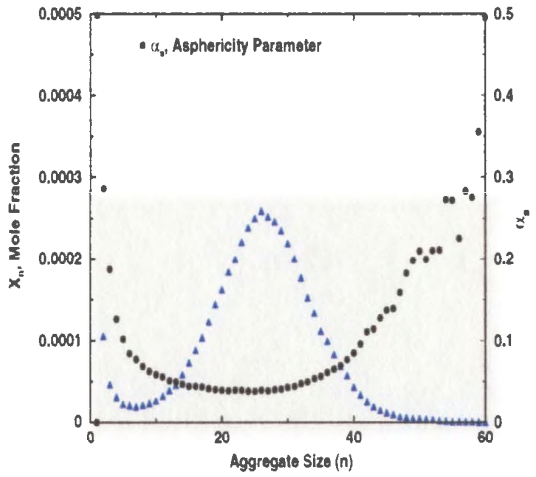

(b) Asphericity parameter α_s versus aggregation number.

Figure 4.26: The shape distribution and asphericity parameter for a h_2 system with 2000 molecules of length $Z_s = 5, Z_{st} = 3$ and $\phi_s = 5.14\%$.

an asphericity greater than 0.1.

The Gaussian + matching function description of the aggregate size distribution implicitly implies a region of coexistence of nonspherical micelles and roughly spherical micelles. This description is not particularly transparent in this example since there is not an appreciable number of large nonspherical aggregates.

Using this description of the system it is also possible to examine the variation of the position of the peak in the distribution function as a function of ε_{ts}. This is shown in Figure 4.28 along with a linear fit to the data. It is clear that the position of the peak in the distribution varies linearly as a function of the interaction parameter ε_{ts}. Similar results have been seen in analytical calculations by Nagarajan *et al.* [91, 92].

The next simulation will illustrate the effect of significant numbers of highly nonspher-

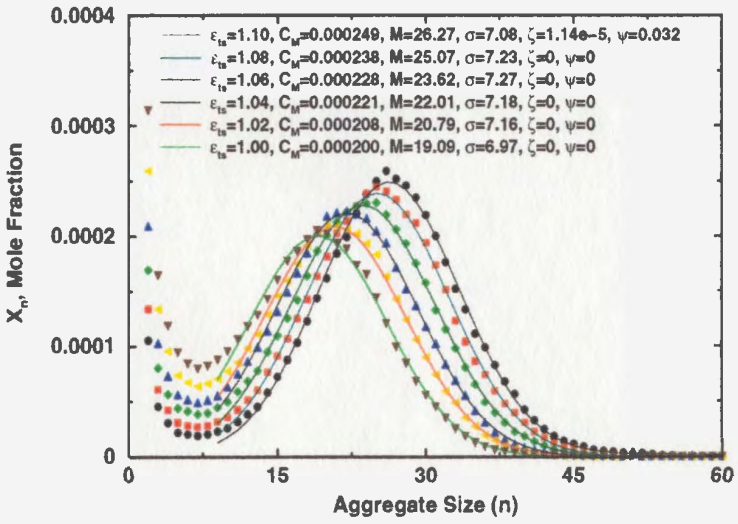

Figure 4.27: Gaussian + matching function fits using Eqn. (4.21) for a h_2 system with 2000 molecules of length $Z_s = 5$, $Z_{st} = 3$ and $\phi_s = 5.14\%$.

ical micelles and the use of the Gaussian + matching function description to interpret the transition in the shape of the aggregates and the region of coexistence. This system is composed of 1000 molecules with $Z_s = 6$, $Z_{st} = 4$ and a volume fraction of $\phi_s = 9.37\%$. The principal radii of gyration (for an interaction parameter of $\varepsilon_{ts} = 0.95$) and the fits to the aggregate size distribution are shown in Figure 4.29 and Figure 4.30 respectively. This system is different from the previous system in that the length of the tail–group has been increased from $Z_{st} = 3$ to $Z_{st} = 4$ and the concentration is about 4% higher.

It is clear that $\langle R_z^2 \rangle^{\frac{1}{2}}$ increases rapidly past roughly $n \simeq 45$. The two smaller principal radii of gyration, $\langle R_x^2 \rangle^{\frac{1}{2}}$ and $\langle R_y^2 \rangle^{\frac{1}{2}}$, tend towards a roughly constant value of $\langle R_x^2 \rangle^{\frac{1}{2}} = \langle R_y^2 \rangle^{\frac{1}{2}} \approx 2.0$ monomer units. The increase in $\langle R_z^2 \rangle^{\frac{1}{2}}$ corresponds to the aggregates growing as highly nonspherical aggregates. A small increment in ε_{ts} from $\varepsilon_{ts} = 0.90$ to $\varepsilon_{ts} = 0.95$ significantly alters the shape of the distribution.

With a change from $\varepsilon_{ts} = 0.90$ to $\varepsilon_{ts} = 0.95$, the peak in the distribution shifts from a value of 37 to 43 molecules per aggregate and the height at the peak significantly decreases.

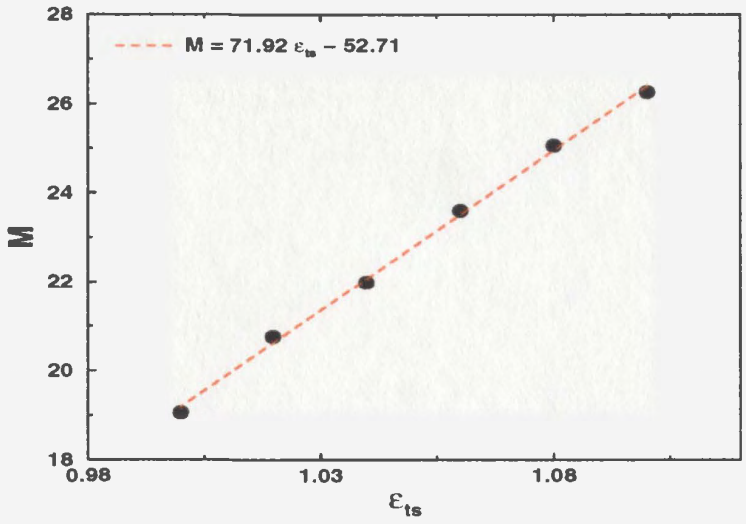

Figure 4.28: Variation of the peak in the aggregate size distribution as a function of the interaction parameter ε_{ts}. This is the same system as depicted in Figure 4.27.

The distribution also exhibits a long tail in the range of 60 to 120 molecules per aggregate corresponding to the appearance of an appreciable number of large nonspherical micelles.

Figure 4.30 shows the aggregate size distributions and fitted curves, using the Gaussian + matching function description. For an interaction parameter of $\varepsilon_{ts} = 0.90$, the distribution is essentially Gaussian with a short tail corresponding to a very small number of nonspherical aggregates. For an interaction parameter of $\varepsilon_{ts} = 0.95$ the situation is significantly altered. The distribution is no longer strictly Gaussian; however, using the Gaussian + matching function it is possible to approximately separate the contributions from the roughly spherical aggregates and the highly nonspherical aggregates. The distribution of 'spheres', corresponding to the Gaussian has a peak at 43 molecules per aggregate for an interaction parameter of $\varepsilon_{ts} = 0.95$. The distribution corresponding to the nonspherical micelles has a peak at an aggregation number of approximately 56 molecules per aggregate.

For $\varepsilon_{ts} = 0.90$ the range of coexistence of sphere–like and nonspherical aggregates is 43 to 70 molecules per aggregate. From this description the system is still mainly com-

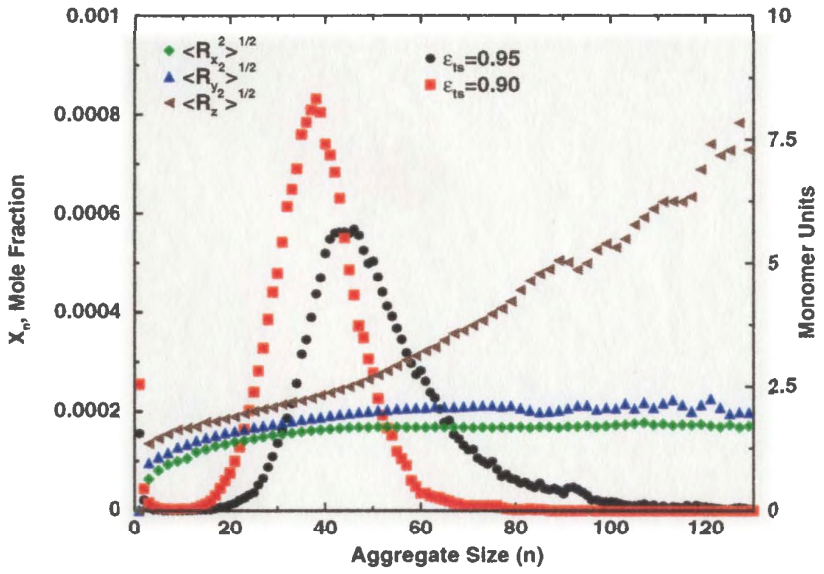

Figure 4.29: Principal radii of gyration (for $\varepsilon_{ts} = 0.95$) and the aggregate size distributions for a h_1 system with $N_s = 1000$ molecules with $Z_s = 6$, $Z_{st} = 4$ and $\phi_s = 9.37\%$

posed of roughly spherical aggregates. It is not possible to directly determine from the simulations the relative populations of nonspherical and spherical aggregates separately. However, using the Gaussian and matching function description it is, since the area under each respective curve will yield the mole fraction of either spheres or nonspheres.

A possible future calculation could include the mean squared fluctuations in the principal radii of gyration. This would indicate the relative spread in aggregate sizes and would provide some credence to the interpretation of the coexistence of the spherical and nonspherical aggregates.

The next system considered is a system composed of 1000 molecules with $Z_s = 10$, $Z_{st} = 6$ and a total volume fraction of $\phi_s = 2.46\%$. This system will be seen to be composed of mainly spherical micelles even at the maximum interaction parameter of $\varepsilon_{ts} = 0.70$. A plot of the principal radii and the asphericity parameter superimposed with the aggregate size distribution are shown in Figure 4.31(a) and Figure 4.31(b). The three

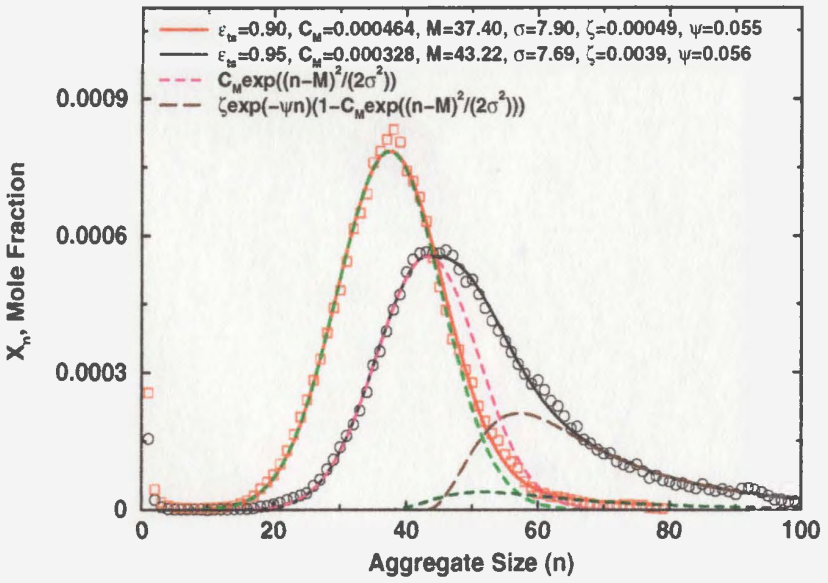

Figure 4.30: Gaussian + matching function fit to the distributions for a h_1 system of $N_s = 1000$ molecules with $Z_s = 6$, $Z_{st} = 4$ and a volume fraction of $\phi_s = 9.37\%$

principal radii are seen to increase with increasing aggregation number. There is evidence of an inflection point in the largest radius of gyration; however, the effect is less pronounced in this system since there are very few large aggregates and in fact the asphericity parameter is $\alpha_s < 0.1$ for (nearly all) aggregates in the range from 10 to 60 molecules per aggregate.

Figure 4.32 shows a plot of the Gaussian + matching function fitted curves and the simulation data. The coefficients of the matching function are zero and the distribution for an interaction parameter of $\varepsilon_{ts} = 0.70$ is very nearly a perfect Gaussian, with a peak position of 30 and a half width $\sigma = 6.98$. This description coincides with that of the previous discussion, since the aggregates appear to be essentially spherical over the range of aggregate sizes and the asphericity parameter for the aggregates in the range of 10 to 60 molecules per aggregate is less than 0.1.

The next system considered will again illustrate the appearance of the long tail in the distribution and its correlation with the appearance of an appreciable number of large non-

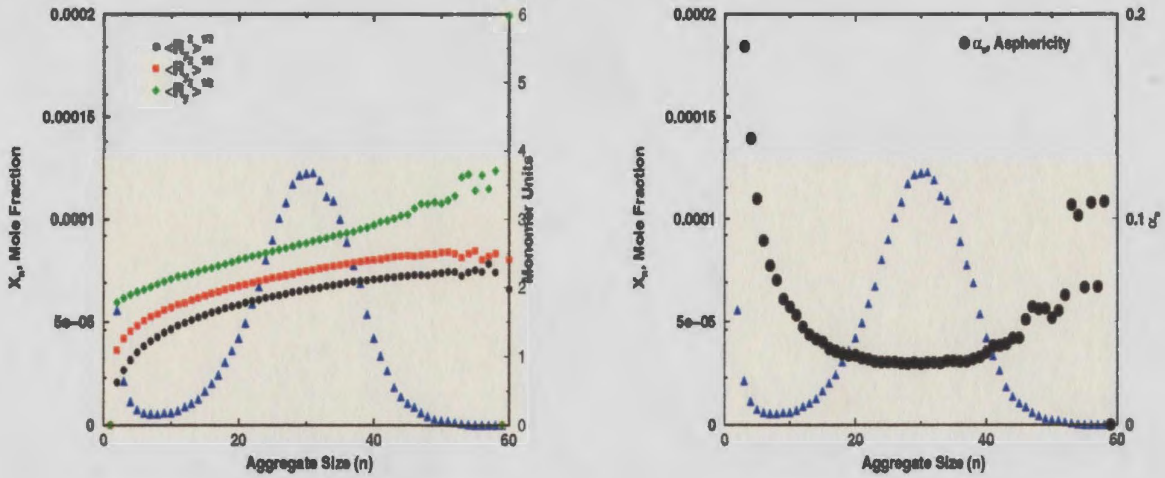

(a) Principal radii of gyration versus aggregation number

(b) Asphericity parameter α_s versus aggregation number

Figure 4.31: The principal radii, asphericity parameter and aggregate size distribution for a h_1 system of 1000 molecules with $Z_s = 10$, $Z_{st} = 6$, $\varepsilon_{ts} = 0.70$ and $\phi_s = 2.46\%$.

spherical aggregates. This system is a h_2 system composed of 1000 (highly asymmetric) molecules with $Z_s = 10$, $Z_{st} = 8$ and a total volume fraction of $\phi_s = 2.70\%$. These distributions are shown in Figure 4.33(a) and Figure 4.33(b) respectively.

Similar behaviour is observed for this system as for the previous systems in terms of the size distributions. For a value of $\varepsilon_{ts} = 0.50$ the distribution is roughly Gaussian with a peak located at $M = 32$. This distribution is not well separated from the initial distribution describing small aggregates and free molecules. However, at an interaction parameter of $\varepsilon_{ts} = 0.55$ the distribution has separated into a well defined Gaussian and a small tail. With further increase in the interaction parameter to a value of $\varepsilon_{ts} = 0.60$, the peak position shifts to $M = 57$ and the distribution develops a relatively long tail extending to roughly $n = 120$.

The three principal radii of gyration (corresponding to an interaction parameter of $\varepsilon_{ts} =$

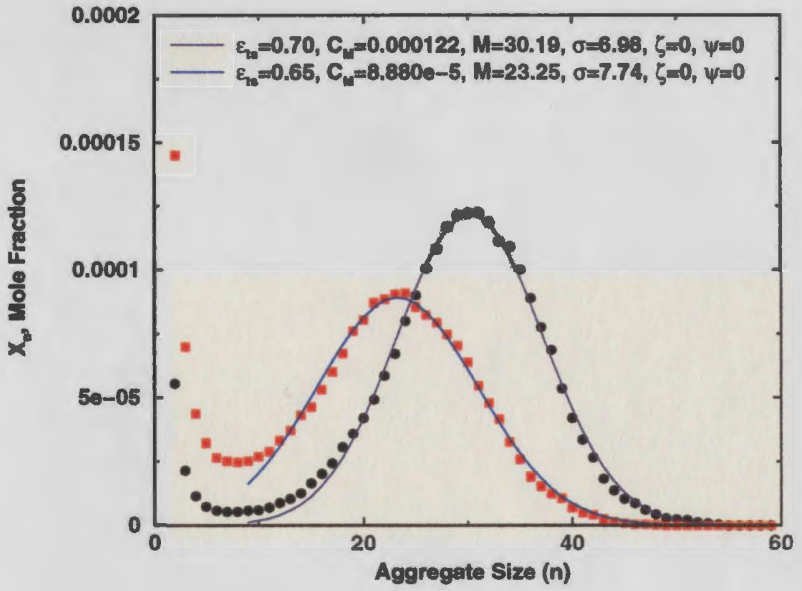

Figure 4.32: Gaussian + matching function fit to the distributions for a system of $N_s = 1000$ molecules with with $Z_s = 10$, $Z_{st} = 6$ and a volume fraction of $\phi_s = 2.46\%$

0.60) increase up to an aggregation number of roughly $n = 75$. The two smaller radii remain constant up to an aggregation number of 120 after which $\langle R_y^2 \rangle^{\frac{1}{2}}$ begins to increase with n. The increase in $\langle R_y^2 \rangle^{\frac{1}{2}}$ (and to some degree $\langle R_x^2 \rangle^{\frac{1}{2}}$ past $n = 120$) might be attributed to the growth of the aggregate in two dimensions. The aggregates grow roughly as spheres up to an aggregation number of $n = 75$ after which they start to grow as prolate spheres or cylinders. When the aggregation number reaches roughly $n = 120$ the aggregates start to grow in two dimensions.

Using the Gaussian and matching function description of these systems, it is possible to examine the variation of the peak position in the distribution as a function of the interaction parameter. Figure 4.34 shows the peak positions of the Gaussian distribution as a function of the interaction parameter for a wide variety of systems. It is clear that the peak position is a linearly varying function of the interaction parameter ε_{ts}.

In summary, using the principal radii of gyration and the complementary discussion

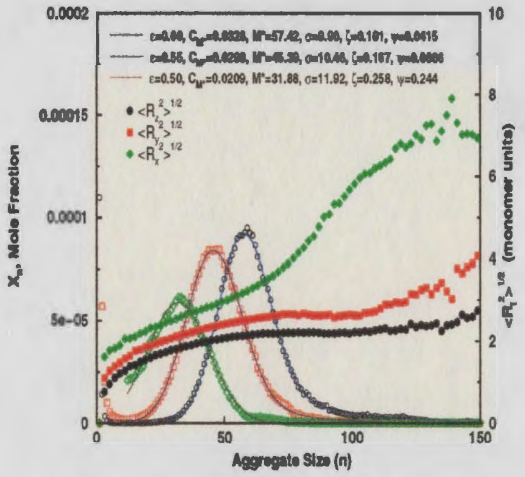

(a) Principal radii for $\varepsilon_{ts} = 0.60$ and Gaussian + matching function fits to the distributions as functions of n.

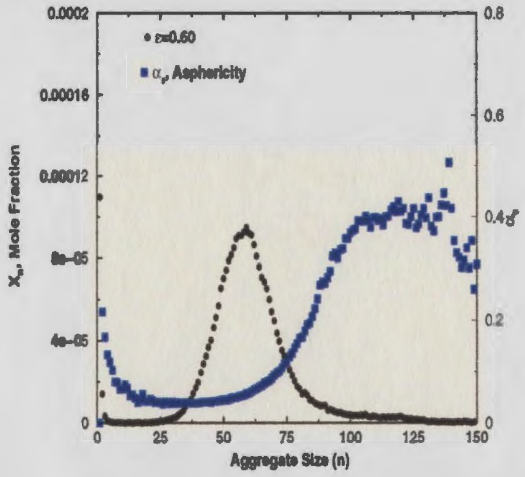

(b) Asphericity parameter versus aggregation number for $\varepsilon_{ts} = 0.60$.

Figure 4.33: The principal radii, asphericity and distributions for a h_2 system of $N_s = 2000$ molecules with $Z_s = 10$, $Z_{st} = 8$ and $\phi_s = 2.74$.

of the Gaussian + matching function, it has been possible to examine the shape of the aggregates over a broad range of aggregate sizes and ε_{ts}. The resulting picture which emerges is the following:

- Below an aggregation number, say n_{sphere}, the aggregates are roughly spherical with an asphericity parameter that is below $\alpha_s = 0.1$. The value of n_{sphere} depends on the characteristics of the system including the length of the chains and the value of the interaction parameter ε_{ts}. The distribution function which describes these 'spherical' micelles is in most cases a very well defined Gaussian.

- When the aggregation number exceeds the value of n_{sphere} the aggregates begin to grow in one dimension and the other two dimensions of the aggregate remain approx-

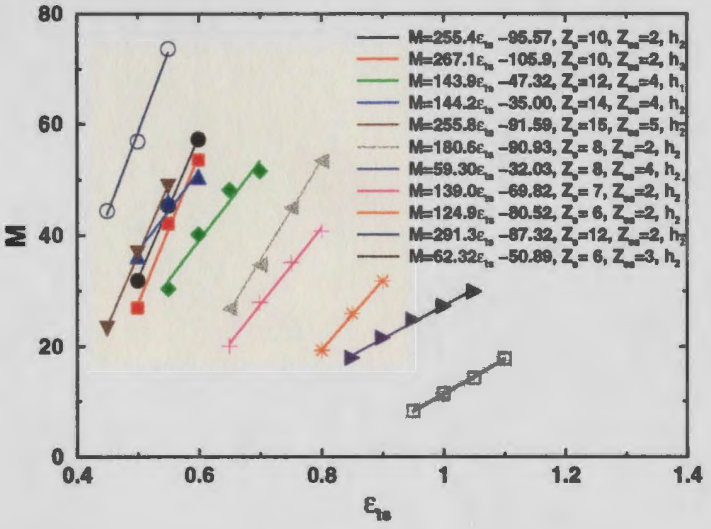

Figure 4.34: Variation of the Gaussian peak in the distribution as a function of the interaction parameter ε_{ts} for a wide range of Z_s.

imately constant. This corresponds to the aggregates growing as prolate spheres or small hemispherically capped cylinders with a length that is an increasing function of the aggregation number. The values of n_{sphere} often corresponds approximately to the location of the peak in the Gaussians, although this is not always the case.

- The use of the Gaussian + matching function implies a small region of coexistence of roughly spherical and nonspherical micelles.

Physically, the reason that the large aggregates extend in one dimension is that, once the radius of the core block is on the order of the fully stretched chain length, Z_{st}, it is highly energetically unfavourable for the aggregates to remain as spheres. The reason for this is that the remaining volume in the core would then have to be filled with solvent, i.e., it will result in an increase in the number of unfavourable solvent tail–group contacts. As well, there is a large entropic penalty due to the elongation of the chains. The net result is that the large aggregates are prolate or hemispherically capped cylinders. This argument is related to the discussion of Chapter 1 where the maximum sizes of the aggregates were

discussed.

4.5.2 Aggregate Scaling and Density Profiles

In Section 4.2 the interior composition of the aggregates was discussed using the simulation results for the density profiles and distributions. This helped provide a physical picture of the aggregate composition. These profiles were averaged over both direction and a range of aggregate sizes, this range corresponds to the peak in the distribution. In this section, an examination of the density profiles as a function of n will be examined using the principal radii of gyration discussed in the previous section.

In order to facilitate this discussion the mean squared radius of gyration R^2_{mean} [94, 105] is introduced and defined as

$$R^2_{mean} = \left(\langle R^2_x\rangle\langle R^2_y\rangle\langle R^2_z\rangle\right)^{\frac{1}{3}} \tag{4.23}$$

It is expected that R^2_{mean} will vary markedly with n since $\langle R^2_x\rangle$, $\langle R^2_y\rangle$, and $\langle R^2_z\rangle$ are functions of n, as illustrated in the previous section. It will be seen that the variation of R^2_{mean} with n will provide information about the behaviour of the density profile as a function of n.

To motivate this discussion, log–log plots of R^2_{mean} versus n for several systems are shown. The first of these corresponds to a system composed of 2000 molecules with $Z_s = 5$, $Z_{st} = 3$ and a total volume fraction of $\phi_s = 5.14\%$ is shown in Figure 4.35. This is the same system as considered in previous sections.

It is quite clear that $\ln(R^2_{mean})$ varies linearly with $\ln(n)$, except for large values of n where the aggregates are no longer roughly spherical. The line of best fit is shown in the

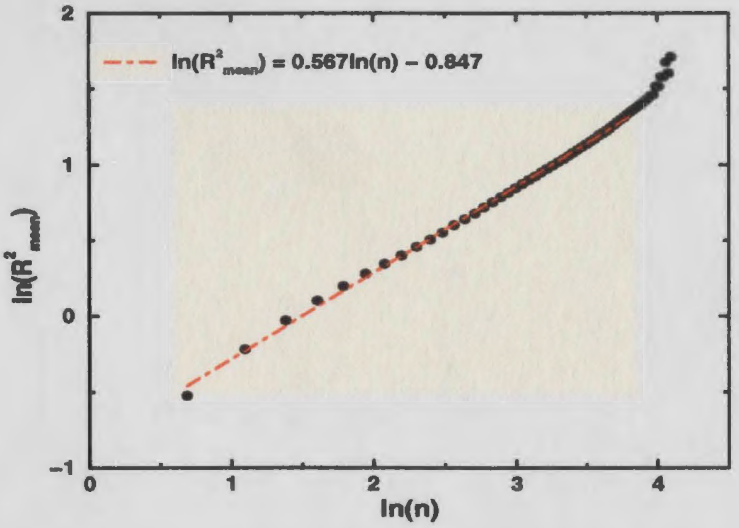

Figure 4.35: Log–log plot of R^2_{mean} as a function of n for a h_2 system of 2000 molecules with $Z_s = 5$, $Z_{st} = 3$ at a total volume fraction of $\phi_s = 5.14\%$. The unit of length is equal to the lattice constant.

legend of the graph[8]. The linear form of this relationship implies

$$R^2_{mean} \propto n^d \tag{4.24}$$

where $d \simeq 0.57$.

The next two systems illustrate the same behaviour for different chain lengths. The first of these systems is composed of 1000 symmetric molecules with $Z_s = 6$, $Z_{st} = 3$ and a volume fraction of $\phi_s = 2.52\%$. Figure 4.36 shows a log–log plot of R^2_{mean} as a function of n, the line of best fit has a slope of $d = 0.537$.

The final system is composed of 1000 asymmetric molecules with $Z_s = 14$, $Z_{st} = 10$ and a volume fraction of $\phi_s = 2.73\%$. Figure 4.37 shows a log–log plot of R^2_{mean} as a function of n. The slope of the best fit line is $d = 0.541$. Again it will be seen as with the other two examples that this behaviour is correlated to the behaviour of the density profiles

[8]The fitted line does not include the last 20 points on the graph (since these correspond to aggregates which are not spherical).

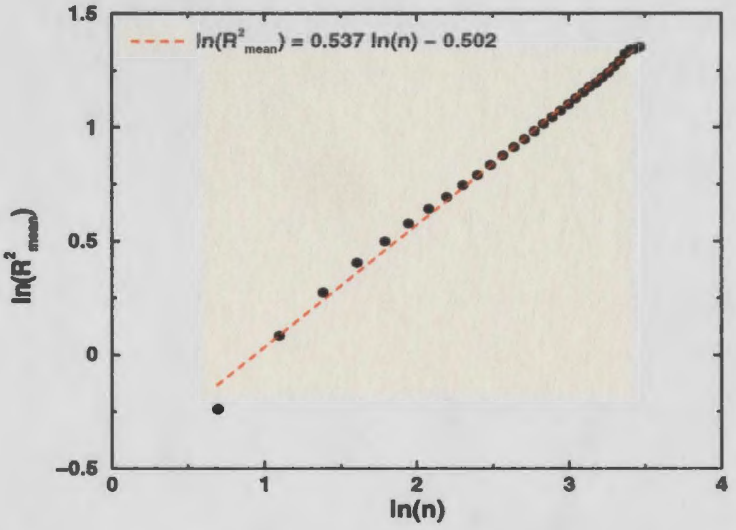

Figure 4.36: Log–log plot of R^2_{mean} versus n for a h_2 system of 1000 molecules with $Z_s = 6$, $Z_{st} = 3$ and a volume fraction of $\phi_s = 2.52\%$. The unit of length is equal to the lattice constant.

as a function of n.

To illustrate this discussion, consider a tightly packed spherical aggregate. Its volume V_n is

$$V_n = \frac{4\pi}{3} R_n^3 = Z_s n \tag{4.25}$$

The squared radius of the aggregate R_n^2 (in terms of n) is then

$$R_n^2 = \frac{3}{4\pi} (n Z_s)^{\frac{2}{3}} \tag{4.26}$$

so R_n^2 is proportional to $n^{2/3}$, i.e.,

$$R_n^2 \propto n^{\frac{2}{3}} \tag{4.27}$$

So for a tightly packed aggregate, $d = 2/3$.

This contrast to the range of $0.53 < d < 0.57$ obtained in the simulations. The reason for this difference is that the aggregates are not tightly packed (over the whole aggregate).

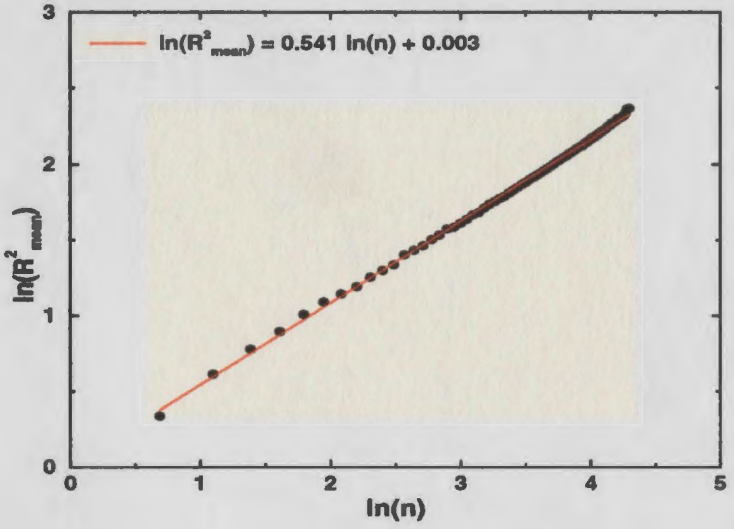

Figure 4.37: Log–log plot of R^2_{mean} versus n for a h_2 system of 1000 molecules with $Z_s = 14$, $Z_{st} = 10$ and a volume fraction of $\phi_s = 2.72\%$. The unit of length is equal to the lattice constant.

Instead there is a densely packed (nearly) uniform interior region and a finite interfacial region. The packing of chains in the aggregate has been examined in a limited capacity in Section 4.2. This scaling (of R^2_n with n) can be explained by assuming that the (densely packed) core radius increases with n while the interfacial region remains approximately of constant width.

To illustrate the underlying picture, assume for simplicity that the density profile is modeled as a Fermi–Dirac function $\rho(r)$ of the form

$$\rho(r) = \frac{1}{1 + \exp((r - a)/l)} \tag{4.28}$$

where a and l are constants which describe the radius of the uniform densely packed core and the width of the interfacial region, respectively, and where r is the distance from the center of mass of the aggregate. Figure 4.38 shows plots of this function for a few typical values of a and l. The reader should note the resemblance of these profiles to those presented in Section 4.2. In fact, a fit to the core block density profile for the systems de-

picted in Figure 4.5 and Figure 4.6 yields values of $a = 3.61, 5.67$ and $l = 0.408, 0.769$ respectively.

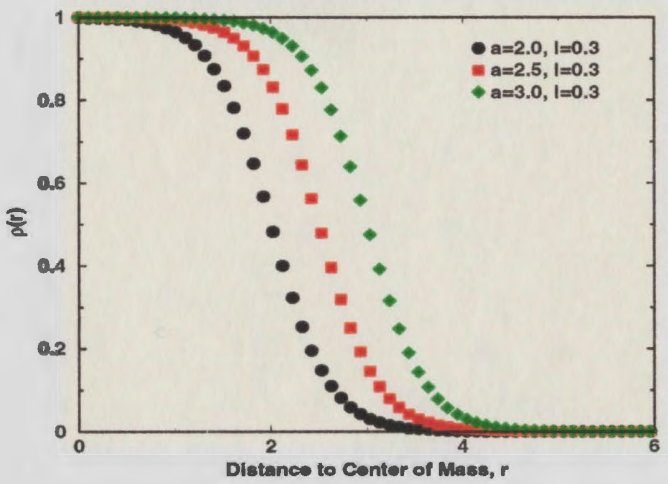

Figure 4.38: Schematic behaviour of the model density profile in Eqn. (4.28) for some typical values of a and l.

Using the function in Eqn. (4.28) the number of molecules n in an aggregate is simply

$$n = \frac{1}{Z_s}\int_0^\infty 4\pi r^2 \rho(r) dr = \frac{1}{Z_s}\int_0^\infty 4\pi r^2 \frac{1}{1+\exp((r-a)/l)} dr \qquad (4.29)$$

Furthermore the squared radius of gyration R^2 of an aggregate (of size n) is

$$R^2 = \frac{1}{nZ_s}\int_0^\infty 4\pi r^2 r^2 \rho(r) dr = \frac{1}{nZ_s}\int_0^\infty 4\pi r^4 \frac{1}{1+\exp((r-a)/l)} dr \qquad (4.30)$$

These integrals can be evaluated in terms of a and l (expressed as an infinite series). It is then possible to plot $\ln(R^2)$ versus $\ln(n)$ by evaluating these terms numerically. The values for n and R^2 as defined in Eqn. (4.29) and Eqn. (4.30) are calculated by picking a value of l and calculating these terms numerically over a range of a. Appropriate values for a and l can be estimated from the actual density profiles. Some typical values are $a = 2 \ldots 5$ and $l = 0.3 \ldots 0.5$. Figure 4.39 shows a plot of $\ln(R^2)$ versus$\ln(n)$ for a typical value of l and a range of a. The slope of the line in Figure 4.39 is approximately 0.50.

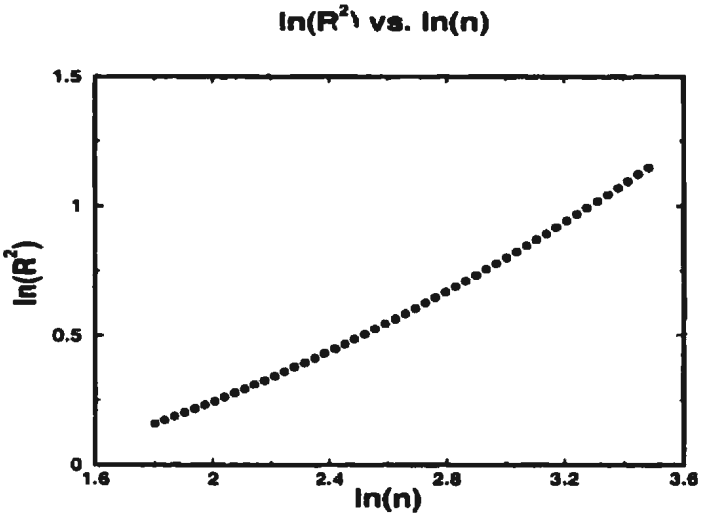

Figure 4.39: Log–log plot of the squared radius of gyration as a function of the aggregation number n for value of $a = 1..2$ with $l = 0.2$. The slope of this line is approximately 0.50.

For the system in Figure 4.6, using the values $a = 2 \ldots 5$ and $l = 0.408$ [9] the slope of the $\ln(R^2)$ versus $\ln(n)$ plot is approximately $d = 0.54$. From the principal radii calculations in the simulations, the plot of $\ln(R^2_{mean})$ versus $\ln(n)$ yields a line with slope $d = 0.56$. The two values are in excellent agreement.

It is possible to directly interpret the linearity of a log–log plot R^2 versus n in terms of the density profiles. Essentially the density profile has a fixed interfacial width l and a region of nearly uniform density (with $\phi \simeq 1$) of radius a near the center of the aggregate. The schematic behaviour of the density profile is shown in Figure 4.40. This behaviour is seen in all of the simulation results, where the value of d is in the range $0.45 \leq d \leq 0.66$.

Table (4.2) shows the scaling parameter d for a wide variety of systems including those considered in this section. The behaviour as illustrated in this section is seen in most of the simulations and the parameter d typically lies in the range $0.50 \leq d \leq 0.63$. The parameter

[9]The approximate value of l is obtained by fitting the Fermi–Dirac distribution in Eqn. (4.28) to the density profiles for the system in Figure 4.6. The values of a correspond roughly to the range of aggregate sizes.

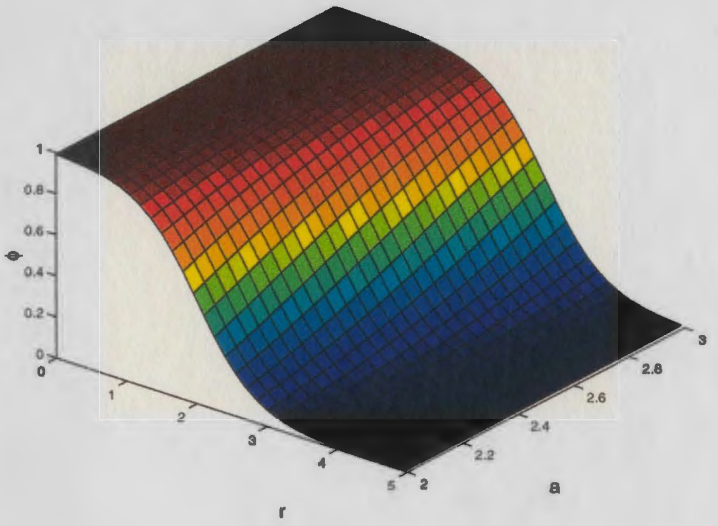

Figure 4.40: Behaviour of the density profile as a function of the parameter a with $l = 0.408$ corresponding to the system in Figure 4.6. Increasing a corresponds to increasing n.

d typically has a lower value for symmetric molecules than for asymmetric molecules, although this is not necessarily the case. It is suspected that the value of d depends not only of the relative lengths of the Z_{st} and Z_{sh} but also on the value of the interaction parameter and h_i. The main result is that the aggregates have a nearly uniform tightly packed interior and an interfacial region and that as the aggregates become larger (increasing n), the interfacial region remains of fixed width and the core radius increases.

In this chapter the results from the Monte Carlo simulations have been presented. Discussions of the relaxation times, density profiles, size distributions, comparisons of the size distribution with a phenomenological model and expression for the free energy, critical micelle concentration, aggregate shape, aggregate growth and the scaling of the radius of gyration have been presented. These discussions combined have given an overview and provided a thorough and systematic examination of aggregates of amphiphilic molecules with lengths $5 \leq Z_s \leq 20$.

N_s	Z_s	Z_{sh}	Z_{st}	h_i	ϕ_s	Max ε_{ts}	d
2000	5	2	3	h_2	5.14%	1.10	0.567
1000	6	2	4	h_1	9.37%	0.95	0.630
5000	6	2	4	h_2	5.85%	0.90	0.563
1000	6	3	3	h_2	2.52%	0.90	0.537
500	7	2	5	h_2	5.46%	0.80	0.566
1000	8	2	6	h_2	2.54%	0.65	0.581
1000	8	4	4	h_2	4.55%	1.05	0.530
1000	9	2	7	h_2	2.61%	0.65	0.571
1000	10	5	5	h_1	2.91%	0.80	0.507
1000	10	4	6	h_2	2.91%	0.70	0.534
1000	12	4	8	h_1	1.88%	0.70	0.547
1000	12	6	6	h_2	2.55%	0.80	0.504
1000	14	4	10	h_2	2.52%	0.55	0.541
1000	14	7	7	h_1	2.50%	0.75	0.493
1000	18	4	14	h_2	4.93%	0.45	0.561

Table 4.2: Table of scaling parameter d and associated parameters.

Chapter 5

Concluding Remarks

"The fruit derived from labour is the sweetest of all pleasures."

Marquis de Vauvenargues.

5.1 Review and Further Discussion of Results

This thesis has provided a systematic examination of self–assembling amphiphiles using Monte Carlo simulations. The study of self–assembling systems is a very active field of research in a broad array of disciplines. An understanding of these systems has potential benefits in many fields. As illustrated throughout this thesis, the behaviour of these systems is complex, even for the two component systems considered here.

The work has focused on an examination of the regime in which the amphiphiles self–assemble into roughly spherical or prolate spherical micelles. In Chapter 2, the statistical mechanical approach of Hill [36] was used to derive an explicit expression for the aggregate size distribution X_n. This is a general expression in terms of the free energy Δ_n, associated with the aggregation of n molecules from solution to an aggregate of size n. In order to utilize this general expression for, X_n, an existing model for the free energy, Δ_n originally

derived by Goldstein [28] for symmetric molecules was modified for both symmetric and asymmetric molecules. The end result was an expression for the aggregate size distribution of self–assembling amphiphiles in terms of Δ_n.

The Monte Carlo simulations were introduced in Chapter 4 both in a general context and as applied to the modeling of amphiphiles. One of the important discussions provided was that associated with the autocorrelation and relaxation times. The results indicate that the relaxation time for the system corresponded to the weighted chain exchange correlation time. This is true for all systems considered in this thesis.

As illustrated in Chapter 4, the relaxation times are an invaluable tool by which to gauge how long it is necessary to iterate the simulations to ensure that the results obtained are representative of equilibrium. One of the key things to note is the behaviour of the correlation times as a function of ε_{ts}. They suggest that the characteristic time scales in a system vary dramatically as a function of ε_{ts}. Using the method of relaxation times ensures (to the best of our abilities) that the results presented are representative of equilibrium averages. Other practitioners of Monte Carlo normally assume that a fixed number of Monte Carlo steps can be used to collect averages in the system, this often leads to results which are not necessarily representative of equilibrium [105].

In order to examine the interior composition of the aggregates and compare it to the composition assumed in the free energy model, the density profiles and distributions from the Monte Carlo simulations were probed. There were several key differences between the assumed composition and that observed in the Monte Carlo simulations, including the finite thickness of the interfacial region. These differences in composition most likely manifest themselves in the comparison of the free energy with the Monte Carlo results, since the assumed composition is in contrast with the results from the simulations.

In order to more accurately model the free energy of the systems it would be necessary to make additions to the free energy expression which explicitly account for the differences

in the assumed composition relative to the Monte Carlo results. A possible future endeavour would be to modify the existing free energy expression to include these contributions and make comparisons with the same Monte Carlo results.

Another very subtle difference appeared in Chapter 4 in the examination of the variation of the fitted parameters as a function of the interaction parameter ε_{ts}. The parameter η which is related to the stretching entropy of the chains, is a decreasing function of ε_{ts}. This is an artifact of the approximation used in the free energy expression which implicitly assumed that the end–to–end distance of a molecule in micelle is equal to the radius of the micelle. It turns out from the simulations that the end–to–end distance increases whereas the micelle radius decreases as a function of ε_{ts}. This results in the apparent decrease in the stretching term η.

A significant part of the discussion in Chapter 4 focused on a qualitative examination of the behaviour of the aggregate size distributions for a wide range of chain lengths Z_s. It was illustrated that the shape and behaviour of the distributions depend very distinctly on the characteristics of the model systems including: chain length, concentration, interaction parameters and the relative lengths of the head– and tail–groups.

These distributions exhibit a universal behaviour in the sense that, in all systems in which micelles form, they behave in the following manner: for low ε_{ts}, most molecules are free in solution and there are very few large aggregates. With increasing ε_{ts} (decreasing temperature) the distribution develops a distinct second maximum at some aggregation number n^* which corresponds to the appearance of micelles in the system. With a further increase in ε_{ts} this maximum shifts to larger aggregation numbers. In fact, it was seen that the position of this maximum is a linearly increasing function of ε_{ts} for most systems.

The comparison between the Monte Carlo simulations and the expected form for the size distributions yielded very good agreement in most instances. The quality of the fit to the distributions depends on the characteristics of the specific system. It is worth noting

that the fitted curves for small ε_{ts} were not as good as those for large ε_{ts}. This is in part attributable to the deviation of the aggregate composition from the assumed composition in the free energy model of Chapter 2 for low ε_{ts}, compounded with the extreme sensitivity of the distributions to the free molecule concentration X_1 in the systems. Nonetheless, the fits to distributions did emulate their behaviour quite well.

In some systems at sufficiently large ε_{ts}, the distribution separates into a distinct Gaussian peaked at some aggregation number M. With further increase in ε_{ts}, some of the systems exhibited a further change in the shape of the distribution with the appearance of the long tail corresponding to highly nonspherical micelles.

The fitting parameters ξ and η were used in the calculation of the critical micelle concentration and the examination of its variation as a function of the ε_{ts} and Z_{st}. The CMC for many of the simulations is in fact an exponentially varying function of ε_{ts} and Z_{st}. This is true for a wide variety of systems.

The examination of the shape of the aggregates of Chapter 4 led to some interesting results in the sense that the aggregates appear to undergo a morphological change as a function of the aggregation the number. Using the simulations, it was possible to examine and characterize this transition using the principal radii of gyration calculations. The results suggest that the aggregates are approximately spheres up to some aggregation number. Beyond which, it is energetically unfavourable to remain spherical and hence the aggregates grow primarily in one dimension as prolate spheres or hemispherically capped cylinders whose length is an increasing function of the aggregation number n.

It was possible to fit the distributions to Gaussians and a so called matching function as described in Chapter 4. In an entirely complementary manner to the principal radii calculations, it was possible to use this Gaussian + matching function to interpret the shapes of the aggregates. Moreover it was possible to separate out the contributions of the 'spherical' and 'nonspherical' aggregates. The 'spherical' aggregates correspond to a Gaussian

distribution and the 'nonspherical' aggregates correspond to the matching function.

Using the Gaussian plus matching function description, it was also possible to examine the variation of the peak position in the distribution as a function of the ε_{ts}. It also appears that the peak aggregate size is a linearly varying function of ε_{ts} for many systems.

In the last section of Chapter 4, the scaling of the aggregate sizes (for spherical aggregates) was examined in terms of the density profiles. Essentially, the density profile has a fixed interfacial width with a densely packed region of nearly $\phi = 1$. The dense region of the core grows as a function of the aggregation number and the interfacial region remains of fixed width. Using a simple Fermi–Dirac function to model the density profile, the behaviour of the mean principal radius of gyration as a function of n could be understood.

The results from the Monte Carlo simulations have provided valuable information about many aspects of the aggregation of amphiphilic molecules. The comparison between the predicted form for the aggregate size distribution and the phenomenological model for the free energy of Chapter 2 yielded good agreement. There are obvious flaws in the model for the free energy, which include the finite width of the interfacial region. It is suspected that inclusion of terms in the free energy attributable to these contributions would increase the quality of the fit over the entire range of aggregate sizes.

One obvious limitation of the Monte Carlo simulations is that it can be difficult to make comparison with experiment and, although we do not do so, such a comparison would be quite useful. Due to the level of detail (or lack thereof) used in the Monte Carlo simulations and the accessible range of Z_s comparisons with experimental work are quite difficult. However, it is possible to compare the general behaviour of the systems in terms of the behaviour of the CMC, the change in the shape of the aggregates and the scaling of the aggregates as a function of the aggregation number to those observed in experiment; however, that is beyond the scope of this work.

5.2 Further Studies and Modifications Using This Model

This model is versatile in many regards and in terms of the actual simulations it is very easy to make modifications and additions to carry out extra analysis. The programs are written in a modular manner which facilitates modification.

There are several possible modifications that can be made to the simulations. The first is to parallelize the code so that it can make use of multi–processor machines more efficiently. The parallelization of the simulations would allow the examination of systems with longer chain lengths and possibly the inclusion of more realistic interaction potentials. However the task of parallelizing such a large simulation is not to be taken lightly and would require major revisions to how the code is written.

Another possible future endeavour is to modify the simulations to examine multi–component systems of amphiphile, i.e., to examine systems of N_i molecules of type i and length Z_i, N_j molecules of type j and length Z_j etc. This modification was carried out in its preliminary stages and a few systems were examined. To carry out a systematic study of multi–component systems would be extremely fruitful since there is very little work in the current literature which looks at the partitioning of multi–component systems and their phase behaviour. It is expected that these systems would exhibit much more complex behaviour than the two component systems. A similar analysis could be carried out in terms of the size distributions and a free energy model developed for the multi–component systems. The simulations could also be quite easily modified to examine multi–block amphiphiles.

The current simulations have the capability of including a third component (amphiphile or solvent) which is either solvent liking or solvent disliking; however, no simulations with this component have been included in the thesis. The inclusion of this component and an examination of its effects on the formation of aggregates would also be an interesting future endeavour.

As discussed, the expression for the free energy of aggregates developed in Chapter 2 has some limitations and also is unable to explicitly account for the tail in the distribution function that appears due to aggregates which are nonspherical. It would be useful to make modifications to the free energy expression to explicitly account for the finite thickness of the interfacial region. It would also be advantageous to include an expression which describes the continuous change in the shape of aggregates from spheres to cylinders.

Monte Carlo simulations provide an excellent starting point for the investigation of self–assembly and can be used to test and improve theories. Recent advances and increased availability of high powered computational resources have broadened the field which is available for study via computational methods. The use of computers to investigate physical phenomena has opened a new venue in which researchers can simulate, explore and provide a basis for comparison of experimental and theoretical work and, in some instances, provide quite accurate predictive capabilities. The use of computational methods such as Monte Carlo have, in recent years, aided in gaining a better understanding of problems in many branches of the sciences.

Bibliography

[1] R. Balescu. *Equilibrium and non–equilibrium statistical mechanics.* John Wiley and Sons Inc., New York, 1975.

[2] R. Baranowski and M. D. Whitmore. *Theory of the structure of adsorbed block copolymers: Detailed comparison with experiment.* J. Chem. Phys., **103**, 6, 755–768, 1995.

[3] A. Bhattacharya and S. D. Mahanti. *Energy and size fluctuations of amphiphilic aggregates in a lattice model.* J. Phys. Conds. Matter, **12**, 6141–6160, 2000.

[4] A. T. Bernardes, V. B. Henriques and P. M. Bisch. *Monte Carlo simulation of a lattice model formation.* J. Chem. Phys., **101**, 1, 645–650, 1994.

[5] K. Binder. *Monte Carlo and Molecular Dynamics Simulations in Polymer Science.* Oxford University Press, Oxford, 1995.

[6] K. Binder and D. W. Heerman. *Monte Carlo Simulations in Statistical Physics.* Springer Verlag, Berlin, Germany, 1988.

[7] J. .M. Blitz and M. R. Fisch. *Aggregation numbers of micelles in semi–dilute solutions.* Langmuir, **11**, 9, 3595–3597, 1995.

[8] D. Blankschstein, G. M. Thurston and G. Benedek. *Phenomenological theory of equilibrium thermodynamic properties and phase separation of micellar solutions.* J. Chem. Phys., **85**, (1986), 12, 7268–7288, 1986.

[9] S. Boyden, N. Jan and T. Ray. *Monte Carlo simulations of microemulsions.* Nuevo Cimento D.S.I.F.D.C., **16**, 2, 1439–1445, 1994.

[10] C. M. Care. *Cluster size distribution in a Monte Carlo simulation of the micellar phase of an amphiphile and solvent mixture.* J. Chem. Soc. Faraday Trans., **83**, 9, 2905–2912, 1987.

[11] D. Chandler. *Introduction to statistical mechanics.* Oxford University Press, New York, 1987.

[12] S. R. Chen and R. Rajagopalan. *Micellar Solutions and Microemulsions: Structure, Dynamics and Statistical Thermodynamics.* Springer–Verlag, New York, 1990.

[13] P. V. Coveney, A. N. Emerton and B. Boghosian. *Simulation of self–reproducing micelles using lattice gas automaton.* J. Amer. Chem. Soc., **118**, 10719–10724, 1996.

[14] J. M. G. Cowie. *Polymers: Chemistry and Physics of Modern Materials.* International Textbook Company Limited, Great Britain, 1973.

[15] N. Dan and S. A. Safran. *Self–assembly in mixtures of diblock copolymers.* Macromolecules, **27**, 20, 5766–5772, 1994.

[16] P. Debye. Ann. N.Y. Acad. Sci., **51**, 575, 1949.

[17] V. Degiorgio and M. Corti. *Physics of Amphiphiles: Micelles, Vesicles and Microemulsions.* Proceedings of the International School of Physics North–Holland Physics Publishing. The Netherlands, 1985.

[18] M. Depner, B. Deloche and P. Sotta. *Uniaxiality induced in a strained polymer network: Theory and Monte Carlo simulations.* Macromolecules, **27**, 18, 5129–5199, 1994.

[19] J. C. Desplat and C. M. Care. *A Monte Carlo simulation of the micellar phase of an amphiphile and solvent mixture.* Molecular Physics, **87**, 2, 441–453, 1996.

[20] I. Dornic and B. Widom. *Development of periodic order in disordered surfactant–solution phases.* Molecular Physics, **86**, 4, 675–684, 1995.

[21] A. Eisenberg and L. Zhang. *Crew–cut aggregates from self–assembly of polystyrene poly(acrylic acid) block copolymers and homopolystyrene in solution.* J. Poly. Sci. Part–B. Polymer Physics, **37**, 13, 1469–1484, 1999.

[22] P. J. Flory. *Principles of Polymer Chemistry.* Cornell University Press, Ithaca New York, 1954.

[23] P. J. Flory. *Statistical Mechanics of Chain Molecules.* Nanser Publishers, New York, New York, 1989.

[24] J. Forsman, B. Jonsson and C. .E. Woodward. *Computer simulations of water between hydrophobic surfaces: the hydrophobic force.* J. Phys. Chem., **100**, 36, 15005–15010, 1996.

[25] S. Fujiwara and T. Sato. *Molecular dynamics simulation of structural formation of short polymer chains.* Physical Review Letters, **80**, 5, 991–994, 1998.

[26] W. M. Gelbart, A. Ben–Shaul and D. Roux. *Micelles, Membranes, Microemulsions and Monolayers.* Springer, New York, 1994.

[27] A. E. van Giessen and I. Szleifer. *Monte Carlo simulations of chain molecules in confined environments.* J. Chem. Phys., **102**, 22, 9069–9076, 1995.

[28] R. Goldstein. *Model for phase equilibria in micellar solutions of nonionic surfactants.* J. Chem. Phys. **84**, 6, 3367–3378, 1986.

[29] G. Gompper and M. Schick. *Self–Assembling Amphiphilic Systems.* Academic Press, London, 1994.

[30] H. Gilhoj, M. Laradji *et al. Effects of vacancies and surfactants on the dynamics of ordering processes in multi–component systems.* Math. Comp. in Simul., **40**, 319–317, 1996.

[31] D. W. R. Gruen and E. H. B. Lacey. *The packing of amphiphile chains in micelles and bilayers.* Surfactants in Solution, 279–306, 1984.

[32] E. Hackett, E. Manias and E. .P. Giannelis *Molecular dynamics simulations of organically modified layered silicates.* J. Chem. Phys., **108**, 17, 7410–7415, 1998.

[33] T. Haliloglu, R. Balaji and W. L. Mattice. *Mobility of free ends and junction points in a lamellar block copolymer.* Macromolecules, **35**, 6, 1473–1476, 1994.

[34] G. S. Hartley. *Aqueous Solutions of Paraffin Chain Salts;* Hermann, Paris, 1936.

[35] E. Helfand. *Theory of homopolymer/binary–polymer mixture interface.* Macromolecules, **25**, 6, 1676–1685, 1992.

[36] T. L. Hill. *Introduction to Statistical Mechanics.* Addison Wesley, Reading, Massachusetts, 1960.

[37] T. L. Hill. *Molecular Clusters in Imperfect Gases.* J. Chem. Phys., **23**, 4, 617–622, 1955.

[38] A. Hoffman, J. Sommer and A. Blumen. *Computers simulations of asymmetric block copolymers.* J. Chem. Phys., **107**, 18, 7559–7570, 1997.

[39] P. M. Holland and D. N. Rubingh. *Mixed Surfactant Systems.* ACS Symposium Series, 501, 1992.

[40] K. M. Hong and J. Noolandi. *Theory of inhomogeneous multicomponent polymer systems.* Macromolecules, **14**, 3, 727–736, 1981.

[41] M. Ito and T. Cosgrove. *Monte Carlo simulation of nonionic surfactants at the oil–water interface.* Molecular Simul., **12**, 3–6, 1994.

[42] J. N. Israelachvili, D. J. Mitchell and B. W. Ninham. *Theory of self–assembly of hydrocarbon amphiphiles into micelles and bilayers.* J. Chem. Soc. Faraday Trans., **12**, 2, 1525, 1976.

[43] J. N. Israelachvili. *Intermolecular and Surface Forces.* Academic Press, San Diego, 1985.

[44] D. Izzo and C. M. Marques. *Formation of micelles of diblock and triblock copolymers in a selective solvent.* Macromolecules, **26**, 26, 7189–7194, 1993.

[45] N. Jan and S. MacLeod. *Large lattice simulation of random site percolation.* Int. J. of Mod. Phys. 1, **9**, 2, 289–294, 1998.

[46] N. Jan and D. Stauffer. *Simulation of membranes, micelles and interfaces with asymmetric surfactants.* J. Phys. I France, **4**, 345–350, 1994.

[47] E. D. Jennings, Y. A. Kuznetsov, E. G. Timoshenko and K. A. Dawson. *Conformational transitions in a lattice model of a three component mixture of solvent, amphiphile and soluble polymers.* J. Chem. Phys., **108**, 4, 1702–1709, 1998.

[48] S. Karaborni, K. Esselink, P. A. J. Hilbers, B. Smit, J. Karthauser, N. M. van Os and R. Zana. *Simulating the self assembly of gemini surfactants.* Science, **206**, 254–256, 1994.

[49] T. Kawakatsu, K. Kawasaki, *et al. Theories and computer simulations of self assembling surfactants systems.* J. Phys. Cond. Matter, **6**, 6385–6408, 1994.

[50] M. Kenward. *Monte Carlo Simulations of surfactants and surfactant aggregation,* B.Sc. Hons. Thesis, Memorial University of Newfoundland, 1998.

[51] M. Kenward and M. D. Whitmore. *Monte Carlo Studies of the Self–Assembly of Amphiphilic Molecules.* High Performance Computing, Systems and Applications. Kluwer Academic Publishers. 481–495, June, 2000.

[52] P. G. Khalatur, A. R. Khokhlov *et al. Aggregation of colloidal particles induced by polymer chains: The RISM integral equation theory.* Physics A., **5**, 1, 205–234, 1997.

[53] P. G. Khalatur, A. R. Khokhlov *et al. Aggregation processes in self–associating polymer systems, computer simulation study of micelles in the super–strong segregation regime.* Macro. Theory Simul., **5**, 1, 713–714, 1996.

[54] P. G. Khalatur, A. R. Khokhlov *et al. Computer simulations of aggregates of associating polymers: influence of low–molecular weight additives solubilizing the aggregates.* Macro. Theory Simul., **7**, 3, 299–316, 1998.

[55] A. R. Khokhlov and I. R. Erukhimovich. *A new class of systems exhibiting microphase separation: Polymer blends with a nonlocal entropy of mixing.* Macromolecules, **26**, 28, 7195–7203, 1993.

[56] M. Laradji, G. Hong and M. J. Zuckermann. *A triangular model for binary and ternary surfactant mixtures containing surfactants.* J. Phys. Cond. Matter, **6**, 2799–2812, 1994.

[57] M. Laradji, O. G. Mouritsen, S. Toxvaerd and M. J. Zuckermann. *Molecular dynamics simulations of phase separation in the presence of surfactants.* Physical Review E, **30**, 2, 1243–1252, 1994.

[58] R. G. Larson. *Simulation of lamellar phase transitions in block copolymers and surfactants.* Mol. Sim., **13**, 321–345, 1994.

[59] R. G. Larson. *Self–assembly of surfactant liquid crystalline phases by Monte Carlo simulation.* J. Chem. Phys., **91**, 4, 2479–2487, 1989.

[60] R. G. Larson. *Monte Carlo simulation of amphiphilic systems in two and three dimensions.* J. Chem. Phys., **89**, 3, 1642–1650, 1988.

[61] R. G. Larson. *Monte Carlo simulation of micro–structural transitions in surfactant system.* J. Chem. Phys., **96**, 11, 7903–7918, 1992.

[62] R. G. Larson, L. Scriven and H. T. Davis. *Monte Carlo simulation of model amphiphile–oil–water systems.* J. Chem. Phys., **83**, 5, 2411–2420, 1985.

[63] R. G. Larson. *Molecular simulation of ordered amphiphilic phases.* Chem. Eng. Sci., **49**, 17, 2833–2850, 1994.

[64] L. Landau and E. M. Lifshitz. *Statistical Physics* 3^{rd} *edition part 1 Volume 5.* Pergamon Press, London, 1980.

[65] L. Landau and E. M. Lifshitz. *Statistical Physics* 3^{rd} *edition part 2 Volume 9.* Pergamon Press, London, 1980.

[66] L. Landau, E. M. Lifshitz and A. I. Akhiezer. *General Physics Mechanics and Molecular Physics.* Pergamon Press, London, 1967.

[67] F. A. M. Leermakers, C. M. Wijmans and G. J. Fleer. *On the structure of polymeric micelles: Self consistent–field theory and universal properties for volume fraction profiles.* Macromolecules, **28**, 3434–3443, 1995.

[68] L. Leibler, H. Orland and J. C. Wheeler. *Theory of critical micelle concentration for solutions of block copolymers.* J. Chem. Phys., **79**, 1, 3550–3556, 1983.

[69] H. Liu and Y. Hu. *Equation of state for systems containing chainlike molecules.* Ind. Eng. Chem. Res., **37**, 8, 3058–3066, 1998.

[70] P. K. Maiti and D. Chowdury. *Micellar aggregates of gemini surfactants: Monte Carlo simulation of microscopic model.* Euro. Phys Letter, **41**, 2, 183–188, 1998.

[71] P. K. Maiti and D. Chowdury. *Numerical Approach to statistical mechanics of surfactants in porous media: A coarse grained description.* Int. J. of Modern Phys., **8**, 6, 1335–1343, 1997.

[72] G. Marangoni. *Personal communication.* 1999.

[73] J. W. McBain and C. S. Salmon. J. of Am. Chemical Society, **42**, 426, 1920.

[74] L. A. Molina and J. J. Freire. *Monte Carlo study of Symmetric diblock copolymers in selective solvents.* Macromolecules, **28**, 8, 2705–2713, 1995.

[75] L. De. Maeyer, C. Trachimow and U. Kaatze. *Entropy–driven micellar aggregation.* J. Phys. Chem. B, **42**, 102, 8480–8491, 1998.

[76] W. L. Mattice, Y. Wang and D. Napper. *Simulations of the self–assembly of symmetric triblock copolymers in dilute solution.* Macromolecules, **25**, 16, 4073–4078, 1992.

[77] W. Mattice and T. Haliloglu. *Monte Carlo lattice simulation of the exchange between micelles of diblock copolymer.* Polymer Preprints, **34**, 2, 460, 1993.

[78] W. L. Mattice and Y. Wang. *Simulation of the formation of micelles by diblock copolymers under weak segregation.* Langmuir, **9**, 1993.

[79] W. L. Mattice and K. Rodrigues. *Micelles and networks formed by symmetric triblock copolymers in dilute solutions that are poor solvents for the terminal block.* Polymer Bulletin, **25**, 1991.

[80] W. Mattice, T. Haliloglu and R. Balaji. *Mobility of free ends and junction points in a lamellar copolymer.* Macromolecules, **27**, 2, 464–465, 1994.

[81] M. W. Matsen and M. Schick. *Stable and unstable phases of a linear multiblock copolymer melt.* Macromolecules, **27**, 24, 7175–7163, 1994.

[82] W. Matties and W. L. Mattice. *In vacuo molecular dynamics simulation of single chain polyethylene and model compounds.* Polymer Preprints, **34**, 2, 456, 1993.

[83] J. E. Mayer and M. G. Mayer. *Statistical Mechanics.* Chapman and Hall, New York, 1954.

[84] J. Melenkevitz, K. S. Schweizer and J. G. Curre. *Self–consistent integral equation theory for the equilibrium properties of polymer solutions.* Macromolecules, **26**, 1993.

[85] F. M. Menger. *Molecular conformations of surfactant micelles.* Nature, **313**, 603–604, 1985.

[86] N. Metropolis, A. W. Rosenbluth, N. M. Rosenbluth, A. H. Teller and E. Teller. *Equation of State Calculations by Fast Computing Machines.* J. Chem. Phys., **21**, 6, 1087–1092, 1953.

[87] S. T. Milner. *Chain architecture and asymmetry in copolymer microphases.* Macromolecules, **27**, 8, 2333–2335, 1994.

[88] M. Moffitt, Y. Yu, *et al. Coronal structure of star–like block ionomer micelles: An investigation by small angle neutron scattering.* Macromolecules, **27**, 7, 2190–2197, 1994.

[89] P. M. Morse and H. Feshbach. *Methods of Theoretical Physics.* McGraw Hill Book Company Inc., New York, 1953.

[90] P. Munk. *Introduction to Macromolecular Science.* Wiley Interscience, New York, 1989.

[91] R. Nagarajan and E. Ruckstein. *Relation Between the Transition Point in the Micellar Size Distribution, the CMC and the Cooperativity of Micellization.* J. Colloidal and Int. Sci., **91**, 2, 500–506, 1983.

[92] R. Nagarajan and E. Ruckstein. *Critical Micelle Concentration: A transition point for micellar size distribution. (A statistical thermodynamic approach).* J. Colloidal and Int. Sci., **60**, 2, 221–231, 1977.

[93] R. Nagarajan and E. Ruckstein. *Aggregation of amphiphiles as micelles or vesicles in aqueous media.* J. Colloidal and Int. Sci., **71**, 3, 580–604, 1979.

[94] R. Nagarajan and E. Ruckstein. *Theory of surfactant self–assembly: A predictive molecular thermodynamic approach.* Langmuir, **12**, 7, 2934–2969, 1991.

[95] P. H. Nelson, G. C. Rutledge and T. A. Hatton. *On the shape and size of self–assembled micelles.* J. Chem. Phys., **107**, 24, 10777–10781, 1997.

[96] P. D. Olmsted and S. T. Milner. *Fluctuation corrections to mean–field theory for homopolymer–copolymer phase separation.* Macromolecules, **27**, 7, 1964–1967, 1994.

[97] B. J. Palmer and J. Liu. *Simulations of micelle self–assembly in surfactant solutions.* Langmuir, **12**, 3, 746–753, 1996.

[98] B. J. Palmer and J. Liu. *Effects of solute interactions on micelle formation in surfactant solutions.* Langmuir, **12**, 25, 6015–6021, 1996.

[99] M. Pépin. *Monte Carlo and mean field studies of polymers in solution.* Ph.D. Thesis, Memorial University of Newfoundland, 1999.

[100] M. Pépin and M. D. Whitmore. *Monte Carlo and mean field study of di–block copolymers micelles.* Macromolecules, **33**, 23, 8644–8653, 2000.

[101] D. C. Poland and H. A. Scheraga. *Hydrophobic bonding and micelle stability; the influence of ionic head groups.* J. Colloidal and Int. Sci., **21**, 273–283, 1966.

[102] D. C. Poland and H. A. Scheraga. *Hydrophobic bonding and micelle stability.* J. Chem. Phys., **69**, 7, 2431–2442, 1965.

[103] L. R. Pratt and S. W. Haan. *A new Monte Carlo method for direct estimation of cluster partition functions. Application to micellar aggregates.* Chem. Phys. Letters, **77**, 2, 436-441, 1982.

[104] L. R. Pratt and B. Owenson. *Molecular statistical thermodynamics of model micellar aggregates.* J. Phys. Chem., **88**, 13, 2905–2915, 1984.

[105] R. Rajagopalan, L. A. Rodriguez and S. K. Talsania. *Lattice Monte Carlo Simulations of Micellar and Microemulsion Systems.* Handbook of Microemulsion Science and Technology, Eds. P. Kumar and K. L. Mittal, Marcel Dekker, 1999.

[106] L. E. Reichl. *A Modern Course in Statistical Mechanics. (First Edition).* University of Texas Press, Austin, Texas, 1980.

[107] F. Reif. *Statistical and Thermal Physics.* McGraw Hill Inc., New York, New York, 1965.

[108] H. S. Robertson. *Statistical Thermophysics.* PTR Prentice Hall Inc., New Jersey, USA, 1993.

[109] K. Rodrigues and W. L. Mattice. *Micelles and networks formed by symmetric triblock copolymers in dilute solutions that are poor solvents for the terminal block.* Polymer Bulletin, **25**, 2, 456–459, 1991.

[110] K. Rodrigues and W. L. Mattice. *Micelles and networks formed by symmetric triblock copolymers in dilute solutions that are poor solvents for the terminal block.* Polymer Bulletin, **25**, 239–243, 1991.

[111] K. Rodrigues and W. L. Mattice. *Segmental distribution functions for a micelle comprised of small symmetric diblock copolymers (short chain amphiphiles).* J. Chem. Phys., **95**, 7, 5341–5347, 1991.

[112] J. F. Rusling and T. F. Kumosinski. *An approximation to hydrophobic attraction for molecular dynamics of self–assembled surfactant aggregates.* J. Phys. Chem., **99**, 22, 9241–9247, 1995.

[113] M. J. Schick. *Nonionic surfactants, physical chemistry.* Marcel Dekker, New York, 1987.

[114] K. Shida, K. Ohno. *Parallelized simulation of complicated polymer structures and its efficiency.* IEICE Trans. Inf. & Sys., **E80–D**, 4, 531–536, 1997.

[115] B. Smit, K. Esselink, *et al. Computer simulations of surfactant self assembly.* Langmuir, **9**, 1, 9–11, 1993.

[116] M. Surridge, D. J. Tildesley *et al. A parallel molecular dynamics simulation code for dialkyl cationic surfactants.* Parallel computing, **22**, 1053–1071, 1996.

[117] E. N. B. Stasiuk and L. L. Schramm. The temperature dependence of the critical micelle concentrations of the foam–forming surfactants. J. Coll. and Int. Sci., **178**. 324–333, 1996.

[118] D. Stauffer, N. Jan and R. B. Pandey. *Simulation of amphiphilic polymer chains in a lattice model for microemulsions.* Physics A **198**, 401–409, 1993.

[119] D. Stauffer and N. Jan *et al. Micelle formation, relaxation time and three–phase coexistence in microemulsion model.* J. Phys. I (France), **4**, 9, 6934–6943, 1994.

[120] M. M. Stecker and G. B. Benedek. *Theory of multicomponent micelles and microemulsions.* J. Phys. Chem., **88**, 26, 6519–6544, 1984.

[121] S. K. Talsania, Y. Wang, R. Rajagopalan and K. K. Kishore. *Monte Carlo simulations for micellar encapsulation.* J. Colloidal and Inter. Sci., **190**, 2, 92–103, 1997.

[122] C. Tanford. *The Hydrophobic Effect.* Wiley Interscience, New York, 1980.

[123] D. Ter Haar. *Elements of Thermostatics.* Holt Reinhart and Winston, New York, New York, 1966.

[124] R. C. Tolman. *The Principles of Statistical Mechanics.* Oxford University Press, New York, New York, 1962.

[125] J. Traube. Ann., **265**, 27, 1891.

[126] T. Wallin and P. Linse. *Monte Carlo simulation of polyelectrolytes at charged micelles 3. Effects of surfactant tail length.* J. Phys. Chem. B, **101**, 28, 5506–5513, 1997.

[127] T. Wallin and P. Linse. *Monte Carlo simulation of polyelectrolytes at charged micelles 1. Effects of chain flexibility.* Langmuir, **12**, 2, 305–314, 1996.

[128] Y. Wang, Y. Li and W. L. Mattice. *Simulation of the adsorption of asymmetric diblock copolymers at the interface between the two monomeric homopolymers.* J. Chem. Phys., **98**, 5, 4068–4075, 1993.

[129] Y. Wang and W. L. Mattice. *Simulation of the adsorption of symmetric diblock copolymers at the interface between the two monomeric homopolymers.* J. Chem. Phys., **12**, 12, 9881–9887, 1993.

[130] Y. Wang and W. L. Mattice. *Simulation of the adsorption of symmetric diblock copolymers at the interface between the two monomeric homopolymers.* Polymer Preprints, **34**, 2, 462, 1993.

[131] WWWebsters Dictionary. *Merriam Websters Online Dictionary.* 2000 by Merriam–Webster, Incorporated, 2000.

[132] H. Wennerström and B. Lindman. *Physical chemistry of surfactant association.* Physics Reports C., 1979.

[133] M. D. Whitmore and T. S. Smith. *Swelling of copolymer micelles by added homopolymer.* Macromolecules., **27**, 17, 4673–4683, 1994.

[134] M. D. Whitmore and J. D. Vavasour. *Self–consistent field theory of block copolymers and block copolymer blends.* Acta Polymer, **46**, 341–360, 1995.

[135] M. D. Whitmore and J. Noolandi. *Theory of Micelle formation in block copolymer–homopolymer blends.* Macromolecules, **18**, 1985.

[136] M. D. Whitmore and T. W. Smith. *Swelling of copolymer micelles by added homopolymer.* Macromolecules, **18**, 17, 4673–4683, 1985.

[137] B. Widom. *Lattice–gas model of amphiphiles and of their orientation at interfaces.* J. Chem. Phys., **88**, 3, 242–251, 1984.

[138] B. Widom. *Theoretical Modeling: An Introduction.* Berichte der Bunsen Gess. fur Phys. Chem., **100**, 3, 1996.

[139] C. M. Wijmans and P. Linse. *Modeling of nonionic micelles.* Langmuir, **11**, 10, 3748–3756, 1995.

[140] C. M. Wijmans and P. Linse. *Surfactant self assembly at a hydrophilic surface. A Monte Carlo study.* J. Phys. Chem. B, **100**, 30, 12583–12591, 1996.

[141] A. Wulf. *Statistical mechanical theory of nonionic micelles.* J. Phys. Chem., **82**, 7, 804–811, 1978.

[142] Y. Zhan and W. L. Mattice. *Conformation and mobility of 1,4–trans–polybutadiene in the crystalline state.* Macromolecules, **20**, 5, 1554–1561, 1992.

[143] Y. Zhan and W. L. Mattice. *Self–assembly and adsorption of diblock copolymers from selective solvents 1. Self assembly.* Macromolecules, **27**, 3, 677–682, 1994.

[144] W. L. Mattice and Y. Zhan. *Self–assembly and adsorption of a copolymers from a selective solvents.* Macromolecules, **27**, 452–453, 1994.

[145] Y. Zhan, W. L. Mattice and D. Napper. *Monte Carlo simulation of the adsorption of diblock copolymers from a non–selective solvent II: Structure of adsorbed layer.* J. Chem. Phys., **98**, 9, 7506–7513, 1993.

[146] Y. Zhan and W. L. Mattice. *Monte Carlo simulation of the adsorption of diblock copolymers from a non–selective solvent 1. Adsorption kinetics and adsorption isotherms.* J. Chem. Phys., **98**, 9, 7502–7509, 1993.

[147] L. Zhang, H. Shen and A. Eisenberg. *Phase separation behaviour and crew–cut micelle formation of polystyrene–b–poly (acrylic acid) copolymers in solutions.* J. Chem. Phys. B, **101**, 24, 4697–4708, 1997.

[148] L. Zhang, H. Shen and A. Eisenberg. *Mesosized crystal like structure of hexagonally packed hollow hoops by solution self–assembly of diblock copolymers,* Phys. Rev. Letters, **79**, 25, 5034–5037, 1997.

Appendix A

A.1 Accompanying CD–ROM

The CD–ROM which accompanies the thesis contains the latest version of the simulation code. The code is contained in **.tar.gz**, **.tar.Z** and **.zip** files . There are also brief instructions for the interested reader on how to compile and run the simulations. There is no example code included in text of this thesis since the shortest single piece of code would occupy at least 10 pages of print. The electronic copy of the code will allow the readers to peruse at their convenience its full functionality and capabilities and will allow them (if so inclined) to run an actual simulation.

Also included on the CD–ROM are electronic copies of the thesis in both **.dvi** and **.ps** formats. These are included for the convenience of the reader.

There are also several time lapse movies from the simulations contained on the CD–ROM in **.mpeg** and **.avi** formats. These are included as they illustrate very succinctly the behaviour of the systems of amphiphiles and their dynamical nature. These movies illustrate many of the important aspects of aggregation including the formation and dissolution of the aggregates.

A.2 Tables of completed simulations

This section contains a complete listing of the simulations which have been carried out in the course of this thesis. Not all of the simulations appear in the text of the thesis. The following tables contain this complete listing along with all other pertinent information about the simulations.

N_s	Z_s	Z_{sh}	L	$-\varepsilon_{hs}/\varepsilon_{ts}$	τ_{max}	Max ε_{ts}
4050	4	2	60	0	100	1.15
2000	5	2	73	1	100	1.10
2000	6	2	49	2	100	0.90
1000	6	3	62	2	100	0.50
500	6	2	50	1	100	0.95
5000	6	2	86	2	60	0.95
1000	6	2	62	2	150	0.90
500	7	2	40	2	100	0.80
1000	8	2	68	2	150	0.70
1000	8	4	56	2	150	1.10
2000	8	2	86	2	100	0.65
1000	8	2	56	1	100	0.40
500	8	2	50	2	60	0.85
2000	9	2	88	2	100	0.65
500	10	2	40	2	100	0.65
500	10	2	55	2	60	0.50
500	10	2	55	2	100	0.60
1000	10	2	60	1	100	0.50
1000	10	5	70	1	150	0.80
2000	10	2	90	2	100	0.65
1000	10	4	74	1	100	0.65

Table A.1: Table of completed Monte Carlo simulations for molecules with lengths $4 \leq Z_s \leq 10$.

N_s	Z_s	Z_{sh}	L	$-\epsilon_{hs}/\epsilon_{ts}$	τ_{max}	Max ϵ_{ts}
1000	10	2	70	3	100	0.55
1000	10	2	70	2	150	0.55
1000	10	2	70	3	100	0.55
1000	10	2	50	1	100	0.55
2000	11	3	70	2	100	0.60
500	12	2	70	1	60	0.45
500	12	2	60	2	100	0.50
1000	12	6	78	1	100	0.40
1000	12	2	70	1	60	0.55
500	12	2	60	1	70	0.55
1000	12	2	70	2	100	0.60
500	12	2	60	2	60	0.55
500	12	2	60	2	100	0.60
2000	12	2	98	2	100	0.55
1000	12	2	80	2	100	0.60
1000	12	2	86	1	150	0.70
500	12	2	60	2	60	0.55
500	12	2	60	2	100	0.60
500	14	2	50	1	60	0.50
500	14	2	50	2	60	0.50
500	14	2	60	3	100	0.50

Table A.2: Table of completed Monte Carlo simulations for molecules with lengths $10 \leq Z_s \leq 14$.

N_s	Z_s	Z_{sh}	L	$-\epsilon_{hs}/\epsilon_{ts}$	τ_{max}	Max ϵ_{ts}
1000	14	4	80	1	100	0.55
1000	14	7	82	1	100	0.45
1000	14	4	80	1	100	0.55
2000	14	2	98	2	150	0.90
500	14	2	62	1	60	0.45
500	14	2	60	3	60	0.50
1000	14	2	60	1	60	0.45
1000	15	5	70	1	60	0.45
500	15	3	70	1	60	0.40
1000	16	4	75	2	100	0.45
500	16	4	70	2	60	0.45
1000	16	4	70	1	100	0.45
1000	16	2	70	3	100	0.45
2000	18	4	90	1	100	0.45
500	20	2	80	1	60	0.45
1000	20	2	92	1	100	0.40
1000	20	5	92	2	100	0.40
2000	22	6	120	1	100	0.375
1000	25	5	100	2	100	0.36

Table A.3: Table of completed Monte Carlo simulations for molecules with lengths $14 \leq Z_s \leq 25$.